Institut für Nutzpflanzenwissenschaften und Ressourcenschutz

Insights into the salt stress adaptation mechanisms of bread wheat genotypes using a systemic approach

Dissertation

Zur Erlangung des Grades

Doktorin der Agrarwissenschaften
(Dr. agr.)

der Landwirtschaftlichen Fakultät
der Rheinischen Friedrich-Wilhelms-Universität Bonn

vorgelegt von

Diana Duarte-Delgado
aus
Bogotá, Kolumbien

Bonn 2020

Referent: Prof. Dr. Jens Léon

Korreferent: Prof. Dr. Heiko Schoof

Tag der mündlichen Prüfung: 25.08.2020

Angefertigt mit Genehmigung der Landwirtschaftlichen Fakultät der Universität Bonn

Acknowledgments

I was a child when I wished to be a scientist one day and I was a teenager at the National University of Colombia when I knew I wanted to continue my studies and become a PhD to follow a career in science. Being a PhD student was a challenge full of emotions, mistakes, some successes and a lot of learning! Besides learning new concepts and methodologies, I also learned a lot about myself, how to increase resilience and never give up. I am grateful for that force beyond me that has given me all the strength, patience and enthusiasm to conclude this research. I also want to thank all the persons that have supported me in several ways along this process.

My **family** has been a great support for me in these years. Being abroad has been a unique opportunity to value my parents, my sisters and my nephew, thanks for being always there for me.

Many thanks to **Prof. Dr. Jens Léon** for the opportunity to work in the Plant Breeding group, for the trust and confidence in my abilities to carry out this research and all his wisdom to face research problems. I am also very grateful to **Dr. Agim Ballvora** for his continuous support, motivation and guidance in my research. It was nice to count on someone who supported my initiatives but also could give new perspectives and ideas to make my research better. Thanks to **Prof. Dr. Heiko Schoof** for being my second advisor and all the useful discussions on bioinformatics issues, it was very helpful. I want to acknowledge **Prof. Dr. Frank Hochholdinger** and **Prof. Dr. Heinrich W. Scherer** who accepted to be part of my defense committee.

I also want to express my gratitude to **Prof. Dr. Teresa Mosquera** because she connected me with great opportunities here in Germany and has always supported me all these years. Thanks for your friendship, it means a lot to me!

I want to thank my friends in Germany Manuel, Alejo, Gina and Franzi. Thanks for all the time and laughs that we have shared, I am happy that I was able to meet you and keep you in my life here. I want to give a special acknowledgment to **Franzi** because I could count on her for the German translation of the abstract of this research. Thank you very much, you have a very kind soul.

I want to thank all the support from my friends and mates in the Plant Breeding group! Especially to Hasina, Patrice, Nur, Asis, Shumaila, Boby, CJ, Salma, Robert, Karin, Karola and Martina. I am happy that I was able to meet people from diverse backgrounds because I could learn many things from you. Very special thanks to **Michael** and **Nazanin** because they took some time to

read my thesis manuscript and give me some feedback. And last but not least to **Said** who also read my thesis and is also mi mejor amigo! Thanks for all your unconditional help and support, they have been very meaningful to me.

I also want to thank all my friends in Colombia! Especially to Cata, Paula, Jose Miguel, Farrel, Esteban, Deissy, Juanito, Pato, Emily, Dolly, Felipe, Linis, Juan Carlos, Lili, Jhady, Frank and Linda. Thanks for remembering me and keep the connection with me in these years. I feel lucky to have such good friends as you that only wish me the best and have been there when I have been happy and not very happy. Also is a good moment to remember all those friends who had the opportunity to visit me here in Germany, I was very happy to see you and had a lot of fun with you.

Many thanks to Inci Vogt who helped me in some experiments while developing her master thesis. Also Neda supported me in the processing of some samples.

Also I want to thank Mr. Josef Bauer who supported my experiments in the growth chamber.

TABLE OF CONTENT

Abstract

Bread wheat is one of the most important crops for the human diet but the increasing soil salinization is causing yield reductions worldwide. The development of appropriate cultivars requires the elucidation of mechanisms of tolerance to salt stress. To study them, physiological, genetic, transcriptomics and bioinformatics analyses were integrated. The dynamic transcriptomic response to salt stress was evaluated using the Massive Analysis of cDNA 3'-Ends (MACE) sequencing protocol in contrasting wheat genotypes from two mapping populations. The leaf transcriptome from Syn86 (salt-susceptible) and Zentos (salt-tolerant) was studied at the photosynthesis turning points identified at the osmotic phase. At the ionic phase, Bobur (salt-susceptible) and Altay2000 (salt-tolerant) were analyzed at 11 days and 24 days after stress exposure. Results revealed that genes involved in calcium-binding and cell wall synthesis were highly expressed in the tolerant genotype at the osmotic phase. On the other hand, the transcriptional suppression of photosynthesis-related and calcium-binding genes in the susceptible genotype was linked with the observed photosynthesis inhibition. At the ionic stage, more ABC transporters and Na^+/Ca^{2+} exchangers were up-regulated in the tolerant genotype, indicating that mechanisms related to Na^+ exclusion and transport may be vital for tissue tolerance at this phase. Moreover, genes involved in mechanisms related to protein synthesis and breakdown were identified at both osmotic and ionic phases. Based on the linkage disequilibrium blocks, the possible salt-responsive genes operating in pathways leading to salt stress tolerance were identified in the QTL intervals. These analyses provided systematic insights into the adaptation mechanisms of salt-tolerant and salt-sensitive wheat genotypes at both salt stress phases.

The over-represented calcium-binding category was analyzed with more detail at the expression and sequence level as the Ca^{2+} signaling events at the early stages of the osmotic phase are crucial for the acclimation response of the plants. Zentos showed primarily the up-regulation of genes at 15 minutes after stress whereas Syn86 displayed the down-regulation at 30 minutes. These results indicated that the distinct timing and the opposite transcriptional regulation of calcium-binding genes during the osmotic phase might represent key factors in the differential salt stress response. The RT-qPCR analysis of two of these genes has confirmed the differential expression in the contrasting genotypes. The comparative phylogenetic analysis revealed that genes that can be involved in the pathway for systemic Reactive Oxygen Species (ROS) production are different and are expressed in different time points in the genotypes studied. The identification of polymorphisms in promoter sequences and 3'-ends of genes provided insights on potential molecular mechanisms controlling the differential expression of these transcripts through differential transcription factor binding affinity or altered mRNA stability. The transcriptional divergences observed in the contrasting genotypes suggest a particular calcium signature in each genotype that can result in the activation or suppression of specific gene networks dependent on Ca^{2+} signaling. Therefore, these transcriptional events might be crucial in triggering either tolerance or susceptibility responses to salt stress in wheat.

Zusammenfassung

Brotweizen ist eine der wichtigsten Nutzpflanzen für die menschliche Ernährung, aber die zunehmende Versalzung der Böden führt weltweit zu Ertragseinbußen. Die Entwicklung geeigneter Sorten erfordert die Aufklärung von Mechanismen der Toleranz gegenüber Salzstress. Um sie zu untersuchen, wurden physiologische, genetische, transkriptomische und bioinformatische Analysen integriert. Die dynamische transkriptomische Reaktion auf Salzstress wurde mit Hilfe des Massive Analysis of cDNA 3'-Ends-Sequenzierungsprotokolls in kontrastierenden Weizengenotypen aus zwei Kartierungspopulationen ausgewertet. Das Blatttranskriptom von Syn86 (salzempfindlich) und Zentos (salztolerant) wurde an den in der osmotischen Phase identifizierten Photosynthesewendepunkten untersucht. In der ionischen Phase wurden Bobur (salzempfindlich) und Altay2000 (salztolerant) nach 11 Tagen und 24 Tagen nach der Stressexposition analysiert. Die Ergebnisse zeigten, dass Gene, die an der Kalzium-Bindung und an der Zellwand-Synthese beteiligt sind, im toleranten Genotyp in der osmotischen Phase hoch exprimiert werden. Andererseits wurde die transkriptionelle Unterdrückung von Photosynthese-bezogenen und Calcium-bindenden Genen im anfälligen Genotyp mit der beobachteten Photosynthese-Hemmung in Verbindung gebracht. Im ionischen Stadium waren im toleranten Genotyp mehr ABC-Transporter und Na^+/Ca^{2+}-Austauscher hochreguliert, was darauf hindeutet, dass Mechanismen, die mit dem Ausschluss und dem Transport von Na^+ zusammenhängen, in dieser Phase für die Gewebetoleranz entscheidend sein könnten. Darüber hinaus wurden Gene identifiziert, die an den Mechanismen der Proteinsynthese und des Proteinabbaus sowohl in der osmotischen als auch in der ionischen Phase beteiligt sind. Auf der Grundlage der Kopplungsungleichgewichtsblöcke wurden die möglichen salzempfindlichen Gene, die in Bahnen arbeiten, die zu Salzstresstoleranz führen, in den QTL-Intervallen identifiziert. Diese Analysen lieferten systematische Einblicke in die Anpassungsmechanismen salztoleranter und salzempfindlicher Weizengenotypen in beiden Salzstressphasen. Die Kategorie der Kalziumbindung wurde auf der Expressions- und auf der Sequenzebene detaillierter analysiert, da die Ca^{2+}-Signalereignisse in frühen Stadien der osmotischen Phase für die Akklimatisierungsreaktion der Pflanzen entscheidend sind. Zentos zeigte in erster Linie die Aufwärtsregulierung der Gene nach 15 Minuten nach dem Stress, während Syn86 die Abwärtsregulierung nach 30 Minuten zeigte.

Diese Ergebnisse deuteten darauf hin, dass das ausgeprägte Timing und die entgegengesetzte transkriptionelle Regulation der Calcium-Bindungsgene während der osmotischen Phase Schlüsselfaktoren für die differentielle Salz-Stress-Reaktion darstellen könnten. Die RT-qPCR-Analyse von zwei dieser Gene hat die differentielle Expression in den kontrastierenden Genotypen bestätigt. Die vergleichende phylogenetische Analyse ergab, dass wesentliche Gene, die am Pfad für die systemische Reaktive Sauerstoffspezies-Produktion (ROS) beteiligt sind, unterschiedlich sind und zu unterschiedlichen Zeitpunkten in den untersuchten Genotypen exprimiert werden. Die Identifizierung von SNPs in Promotorsequenzen und in 3'-Enden lieferte Erkenntnisse über die molekularen Mechanismen, die die differentielle Expression dieser Transkripte durch differentielle Transkriptionsfaktor-Bindungsaffinität oder veränderte mRNA-Stabilität steuern. Die in den kontrastierenden Genotypen beobachteten transkriptionellen Divergenzen lassen auf eine bestimmte Kalziumsignatur in jedem Genotyp schließen, die zur Aktivierung oder Unterdrückung spezifischer Gen-Netzwerke in Abhängigkeit von Ca^{2+}-Signalen führen kann. Daher könnten diese transkriptionellen Ereignisse entscheidend sein, um entweder Toleranz oder Anfälligkeitsreaktionen auszulösen.

1. Introduction

The daily salt-induced degradation of 2000 hectares of arable soil worldwide is a serious threat to global food security (Zaman *et al.*, 2016). Estimations indicate that by 2050 more than 50% of arable land will suffer some degree of salinization (Wang *et al.*, 2003). Soil salinization is progressing mainly in arid and semi-arid regions where generally evapotranspiration is higher than precipitation causing salt accumulation at the soil surface (Pessarakli and Szabolcs, 2019) (Figure 1). The current global climate change is accelerating the soil salinization process as the temperature increment is producing increased evapotranspiration, the alteration of water balance at the land surface, the rise of the sea level and the intensification of tidal waves (Sakadevan and Nguyen, 2010; Dasgupta *et al.*, 2018). Soil salinization describes the condition in which the content of soil soluble salts, such as chlorides of calcium, magnesium, sodium, and sulfates and carbonates reach levels harmful to agricultural production (Rengasamy, 2006). Chlorides and sulfates of sodium, calcium and magnesium are accumulated in saline soils whereas sodium carbonate is the most often in alkaline soils (Abrol *et al.*, 1988). From these salts, NaCl and Na_2SO_4 are the most widespread worldwide (Genc *et al.*, 2016).

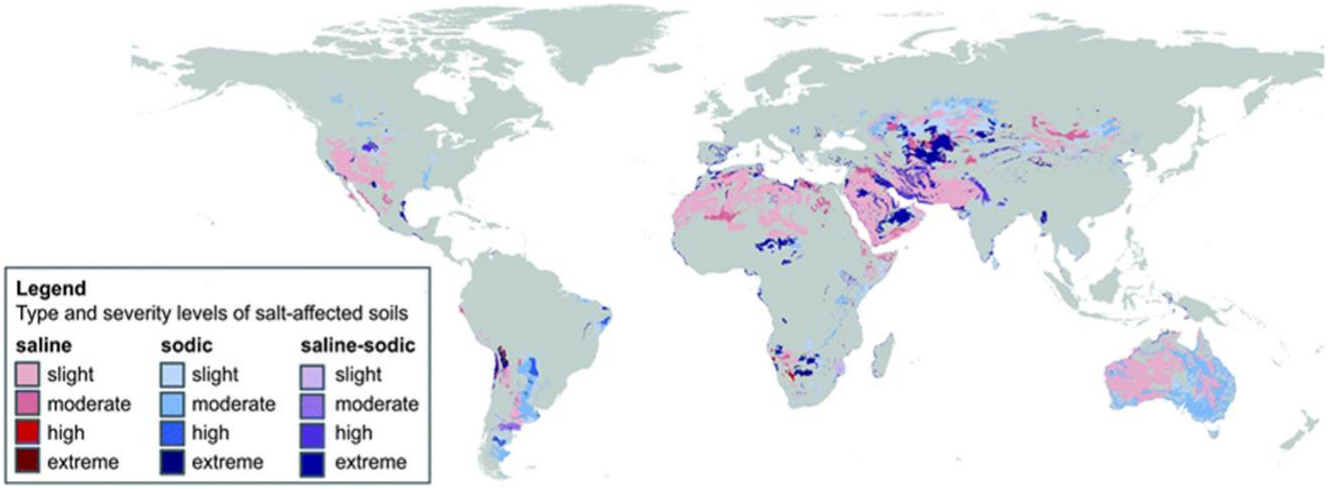

Figure 1. Global distribution of salt-affected soils, classified by type and severity. Reproduced from Wicke *et al.* (2011).

The soil salinization is a major constraint for agriculture since most crops are salt sensitive (i.e. glycophytes) in contrast to halophytes which are species native to saline conditions (Ashraf and Wu, 1994; Keshtehgar *et al.*, 2013). In glycophytes the plant growth rate is reduced which results in a substantial decrease in biomass accumulation and yield (Demetriou *et al.*, 2007; Roy *et al.*, 2014; Silveira and Carvalho, 2016). Salinization management approaches such as salt- leaching or the use of chemical amendments are water- or cost-intensive processes not always practical in the long-term to counteract the problem of salinity in wide extensions (Ashraf and Wu, 1994; Beltrán

and Koo-Oshima, 2006). Consequently, a better understanding of the genetic variation underlying the salt stress adaptation response in crops can facilitate the development of cultivars with increased salinity tolerance which is a more promising strategy to maintain future global food production (Jewell *et al.*, 2010). The salt stress adaptation response is a complex trait since the changes caused in key physiological processes are the effect of the coordinated action of gene networks in several metabolic pathways (Tuteja, 2007; Gupta and Huang, 2014). Hence, it is necessary to implement appropriate strategies for complex trait dissection to assist plant breeders to develop salt-tolerant cultivars. The development of such cultivars may enable the use of saline water sources for irrigation to contribute to the sustainable intensification of agronomic systems (Morton *et al.*, 2019).

Bread wheat (*Triticum aestivum* ssp. *aestivum* L.) is a key staple crop for global food security and its production needs to be increased by 60% to feed the world population by 2050 (Hertel, 2011; Curtis and Halford, 2014). Among all the abiotic stress factors, soil salinity can cause significant yield reductions and decreased grain quality in wheat (Jafari-Shabestari *et al.*, 1995). Thus, breeding programs should emphasize on the genetic improvement to increase yield potential under growth-limiting conditions (Hawkesford *et al.*, 2013). The understanding of the mechanistic basis of the salt stress response from bread wheat can unravel genetic variation useful in breeding strategies.

1.1. Bread wheat genetics

Wheat is the cereal with the broadest range of cultivation worldwide and is the third crop in global production after maize and rice (Shewry and Hey, 2015). The domestication of bread wheat has been essential in feeding humanity throughout history and facilitated the transition from small settlements to large civilizations (Vergauwen and De Smet, 2017). The spread and adaptation of wheat to a wide range of environments in temperate, subtropical and tropical areas are attributed to its high genome plasticity and have created distinct cultivated gene pools (Rasheed and Xia, 2019). This allohexapolyploid (2*n*=6*x*=42, AABBDD) and autogamous species originated from two hybridizations events. The first event between *Triticum urartu* (AA) and an *Aegilops speltoides*-related species (BB) generated the tetraploid wild emmer, *Triticum turgidum* ssp. *diccocoides* about 0.5 million years ago. The latest hybridization of the cultivated emmer *T. turgidum* ssp. *dicoccum* (2*n*=4*x*=28, AABB) with the diploid *Aegilops tauschii* (2*n*=2*x*=14, DD) occurred about 10000 years ago in the Fertile Crescent of the Middle East (Faris, 2014; Gornicki and Faris, 2014; El Baidouri *et al.*, 2017). The genetic studies of complex agronomic traits in this

cereal are challenging because it contains three subgenomes with 85% of repetitive sequences and consequently a large size of 16 Gb (Loginova and Silkova, 2018; IWGSC, 2018). Even though bread wheat is a polyploid species, the pairing of homoeologous chromosomes is prevented by cytological diploidization. This process has led to the elimination, inactivation or neo-functionalization of redundant genes (Feldman *et al.*, 2012; IWGSC, 2014).

A high quality and fully annotated reference genome assembly can contribute to the development of systematic approaches to understand and improve important agronomic traits to achieve future global wheat demand (IWGSC, 2018). Because of the long-term challenges in the sequencing and assembly of the intricate bread wheat genome, the anticipated release of fragmented genome drafts sequences was available for the scientific community (IWGSC, 2014; Clavijo *et al.*, 2017). Efforts from the International Wheat Genome Sequencing Consortium (IWGSC) have allowed the recent publication of a fully annotated and highly contiguous chromosome-level assembly of the Chinese Spring cultivar that represents 94% of the whole genome sequence (Shi and Ling, 2018; IWGSC, 2018; Borrill *et al.*, 2019).

The chromosome-level genome assembly is accelerating the dissection of complex traits as genetic markers can be located in a physical context. Therefore, the identification of quantitative trait genes (QTGs) within chromosome regions detected in genetic mapping studies is facilitated (Borrill *et al.*, 2019). The use of the improved assembly has also allowed the analysis of homeolog-specific expression in RNA-sequencing (RNA-seq) data to better understand gene function. The expVIP expression atlas is a tool available to observe and compare gene expression across diverse tissues, developmental stages and stresses (Borrill *et al.*, 2016, 2019; Ramírez-González *et al.*, 2018). Recently, an Australian initiative released the pangenome of 18 bread wheat cultivars and detected that 39% of genes correspond to the variable pangenome (Montenegro *et al.*, 2017). To overcome the limitation of the low sequencing depth of these assemblies, the IWGSC initiated a pangenome project with the purpose to generate 10 high-quality genome sequences from different worldwide sources. The reference genome assemblies of the diploid progenitors *Ae. tauschii* and *T. urartu* have been also completed which can contribute to establish the origin of genome segments in the hexaploid bread wheat. These genomic and transcriptomic resources can facilitate to uncover signatures of selection, homeologous gene exchange and chromosome structural variations (Rasheed and Xia, 2019).

After centuries of domestication and breeding with emphasis on yield-related traits selected under optimum field and management conditions, genetic variation in modern bread wheat cultivars may

be depleted from alleles with a beneficial effect on growth under abiotic stress conditions (Guzman *et al.*, 2016; Wang *et al.*, 2018*a*). Additionally, the D subgenome has the lowest genetic variability as a result of a bottleneck in the recent spontaneous hybridizations and also due to the limited time for accumulation of mutations (Voss-Fels *et al.*, 2015; Gao *et al.*, 2017; Song *et al.*, 2017). To introduce genetic diversity into modern wheat and to widen the genetic basis for future selection gain, synthetic hexaploid wheat genotypes have been created by artificial hybridization of *T. turgidum* and *Ae. tauschii* (Lange and Jochemsen, 1992). Therefore, synthetic wheat genotypes have been used to mine alleles in D subgenome with an effect on biotic and abiotic stress tolerance (Gao *et al.*, 2017). Greater genetic gains in breeding programs are expected with the accelerated prospection and exploitation of exotic genes that can be obtained through the recent advances in wheat genomics (Rasheed *et al.*, 2018).

1.2. Salt stress adaptation response in plants

The response of plants to salt stress is systemic as it occurs in both roots and shoots and at the organ, tissue, cellular and subcellular levels (Morton *et al.*, 2019). High salinity leads to physiological drought conditions, causes ion toxicity and cell oxidative damage that affect the plant growth (Tuteja, 2007; Gupta and Huang, 2014). The adaptation to saline environments is facilitated by coordinated response mechanisms of the whole plant that are triggered by sensing mechanisms that differ among the different plant tissues and are likely to operate at different time scales (Shabala *et al.*, 2015). Thus, the sensing and transduction of stress signals lead to a transcriptional reprogramming that includes the synthesis of stress-responsive functional proteins (Wan *et al.*, 2018) (Figure 2). The hormone abscisic acid (ABA) is the central regulator of abiotic stress responses in plants and coordinates signaling cascades to promote adaptation to changing environments (Sah *et al.*, 2016) (Figure 2).

According to the time of stress exposure, the plant growth response to salinity comprises the early osmotic and the late ionic phases (Figure 3). The osmotic phase is independent of the sodium accumulation in tissues. The rapid and often transient impact on plant growth in this phase is attributed to the osmotic effect of the salts in the rhizosphere because of reduced water potential (Ismail *et al.*, 2014; Parihar *et al.*, 2015; Julkowska and Testerink, 2015). The primary consequence is the reduction of shoot growth and the production of new leaves because of the stomatal closure and the increase in leaf temperature (Roy *et al.*, 2014). The early signaling events in the osmotic phase that occur within seconds to hours of salt stress exposure are crucial for the acclimation response of the plants (Julkowska and Testerink, 2015). A model proposes that in the

osmotic phase the root senses salt stress and second messengers as Reactive Oxygen Species (ROS) and Ca^{2+} are spread as signals to the aerial parts to trigger adaptive responses to cope with the Na^{+} ions that can reach photosynthetic tissues and cause toxic effects in the following stress phase (Köster *et al.*, 2018). Consequently, the osmotic tolerant plants can adapt to the drought aspect of the stress through the maintenance of the stomatal conductance and the leaf turgor (Carillo *et al.*, 2011). Variation in osmotic tolerance might be due to differences in the initial perception of salt stress or differences in the response to long-distance signals (Roy *et al.*, 2014).

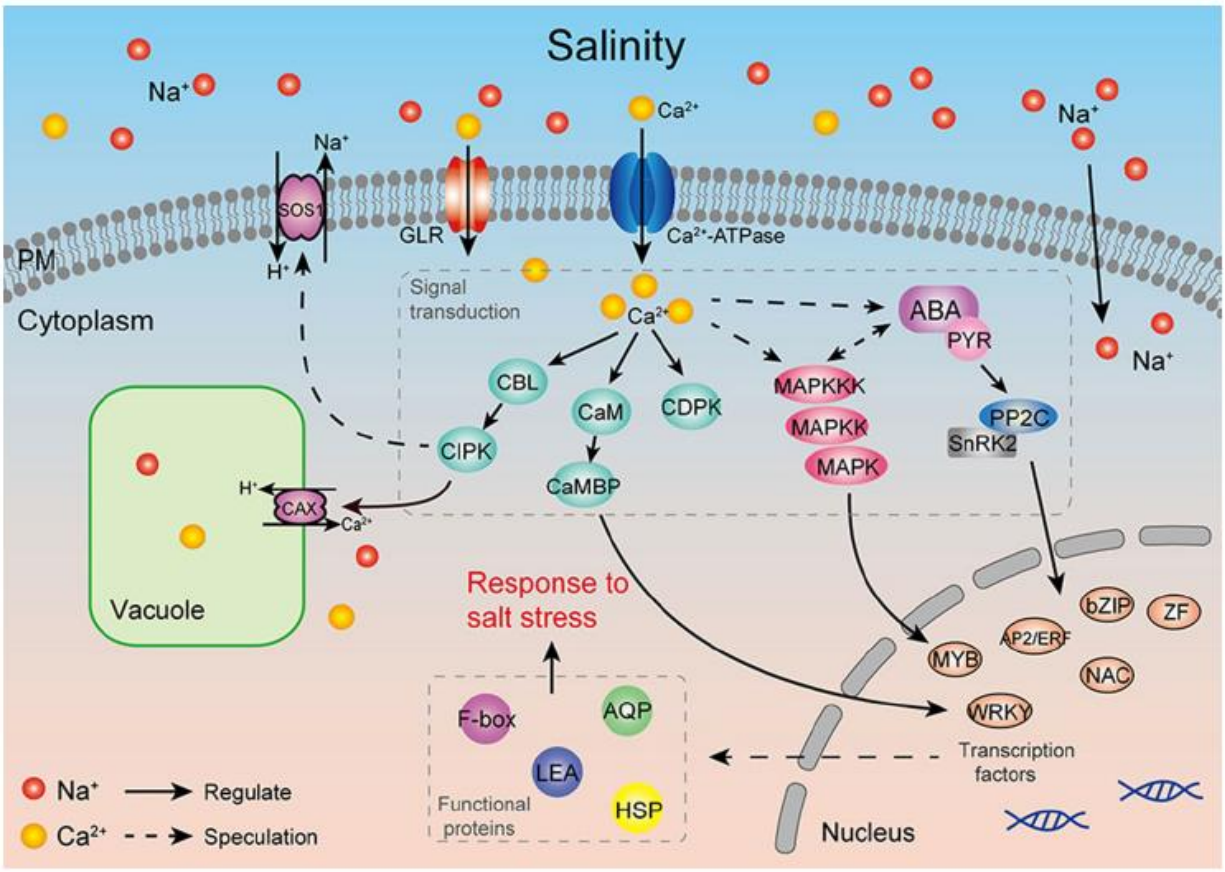

Figure 2. Regulatory model of salt stress sensing and response. When Na^{+} is sensed, secondary messengers as Ca^{2+} and ABA transfer the salt stress signal and activate downstream transcription factors and target genes. Reproduced from Wan *et al.* (2018).

Second, the ionic phase continues as a result of salt accumulation in leaves through transpiration and takes days or even weeks to be manifested. In this phase there is great damage to aerial tissue where the senescence of older leaves is caused by the inability of the plant to tolerate the toxic concentrations of salts in the tissues (Roy *et al.*, 2014; Ismail *et al.*, 2014). To reduce the toxicity effects, tolerant plants can excrete Na^{+} from leaves through the roots or compartmentalize Na^{+} and Cl^{-} in vacuoles to avoid toxic concentrations in the cytoplasm (Munns and Tester, 2008; James *et al.*, 2012). Both of these mechanisms in the ionic phase involve transporters and their regulators at the plasma membrane and tonoplast (Roy *et al.*, 2014).

The limiting effect of salinity on crop productivity in both stress phases is mainly due to its effect on the photosynthetic process which results in a substantial decrease in biomass accumulation (Demetriou *et al.*, 2007; Silveira and Carvalho, 2016). Osmotic tolerance, Na^+ exclusion and Na^+ compartmentalization (tissue tolerance) are the three general salt tolerance mechanisms. The activation of each one of these mechanisms can depend on specific signals sensed by the plant (Roy *et al.*, 2014). Tissue tolerance and osmotic adjustment are very related mechanisms and less is known about their physiological and genetic aspects in comparison to Na^+ exclusion (Genc *et al.*, 2019). These mechanisms that contribute to salt tolerance can vary within a species, throughout the different developmental stages and across diverse environments. These sources of variation should be accounted in the refining of strategies for salt tolerance dissection so that this trait becomes more genetically tractable (Morton *et al.*, 2019).

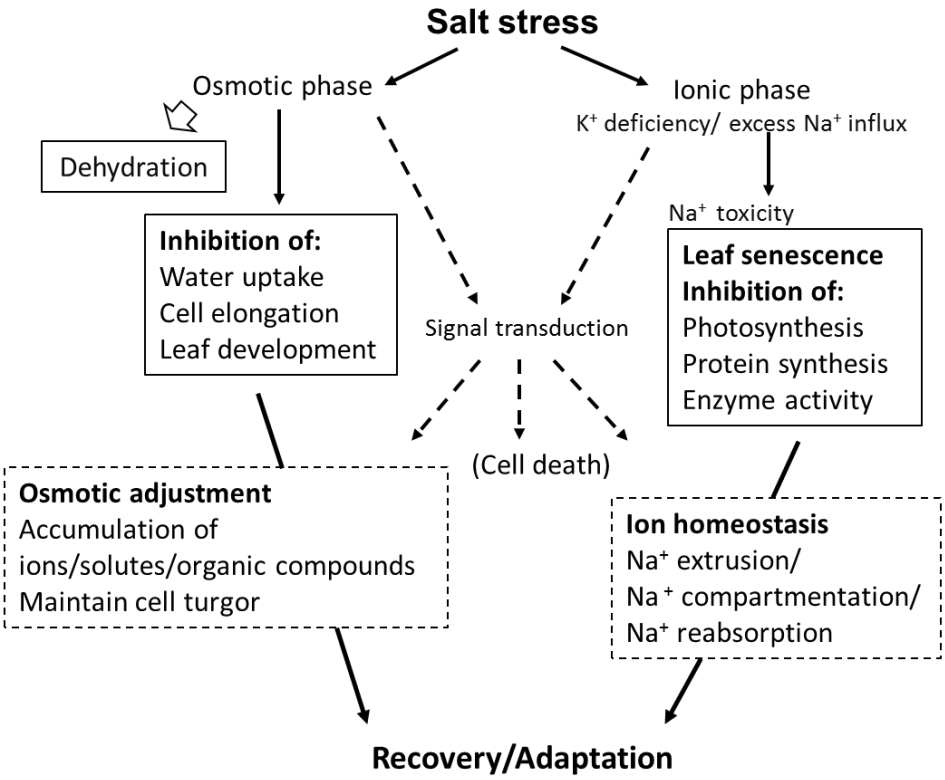

Figure 3. Adaptive responses of plants to the osmotic and ionic phases of salt stress. Modified from Oliveira *et al*. (2013).

1.2.1. Calcium signaling in salt stress response

The calcium signaling has an emerging role in the salt stress reaction because during the chain of events that lead to adaptation there are transient or repetitive elevations of intracellular Ca^{2+} that can be triggered by various stress-related stimuli (Manishankar *et al.*, 2018; Frank *et al.*, 2019).

These intracellular signals can differ in the amplitude, duration, frequency, and spatial distribution thus creating calcium signatures. Different calcium-sensing proteins decode the calcium signatures and specify the activation of a certain type of stress response (Perochon *et al.*, 2011; Zeng *et al.*, 2015). Experimental evidence shows that calcium-ROS waves serve as long-distance messengers through the interaction with electric signals for inducing systemic acquired acclimation (Gaupels *et al.*, 2017). The Ca^{2+} signal wave expansion from roots to leaves has a central role in orchestrating the whole-plant response to salt stress (Manishankar *et al.*, 2018). The activation of downstream effectors by calcium sensors regulates cellular processes that mediate salt adaptation such as gene transcription, osmolyte synthesis, ion channel activity, K^+ uptake and stomatal regulation (Conde *et al.*, 2011; Dixit and Jayabaskaran, 2012; Almeida *et al.*, 2017). The sensor proteins have a diverse affinity for calcium ions. The specific affinity combined with the sub-cellular localization can contribute to defining particular biological roles of these proteins in stress response pathways (Ranty *et al.*, 2016). Calcium-binding proteins are classified as EF-hand domain-containing or as non-EF-hand when other functional domains interact with Ca^{2+} (Mohanta *et al.*, 2019). An overview of the classification of these proteins can be observed in Figure 4.

The EF-hand is a highly conserved helix-loop-helix motif where a central residue of 12 amino acids forms a loop structure for Ca^{2+} binding. The *Arabidopsis* genome consists of approximately 250 genes with an EF-hand domain from which 100 have the role of calcium-sensing. The sensors with EF-hand domain and without any other functional domain correspond to calmodulins (CaMs), calmodulin-like (CMLs) and calcineurin B-like (CBL) (La Verde *et al.*, 2018; Medvedev, 2018). These proteins seem to play a role as sensor relays to regulate downstream targets but do not possess catalytic activity (Mohanta *et al.*, 2019). CaMs are the most studied sensors and contain four conserved EF-hand motifs. CMLs have less than 50% of amino acid sequence identity with CaMs and contain one to six EF-hand domains (La Verde *et al.*, 2018; Sanyal *et al.*, 2019; Mohanta *et al.*, 2019). There are several proteins with binding to CaMs/CMLs such as transporters, channels, metabolic enzymes, transcription factors, myosins, phosphatases and kinases (Bender and Snedden, 2013; Ranty *et al.*, 2016; Bürstenbinder *et al.*, 2017). On the other side, most EF-hands of CBL proteins are non-canonical and therefore their Ca^{2+} affinity is lower. The activation of downstream targets is the result of the interaction with CBL-interacting protein kinases (CIPKs) which contain a catalytic domain for phosphorylation (Sanyal *et al.*, 2019).

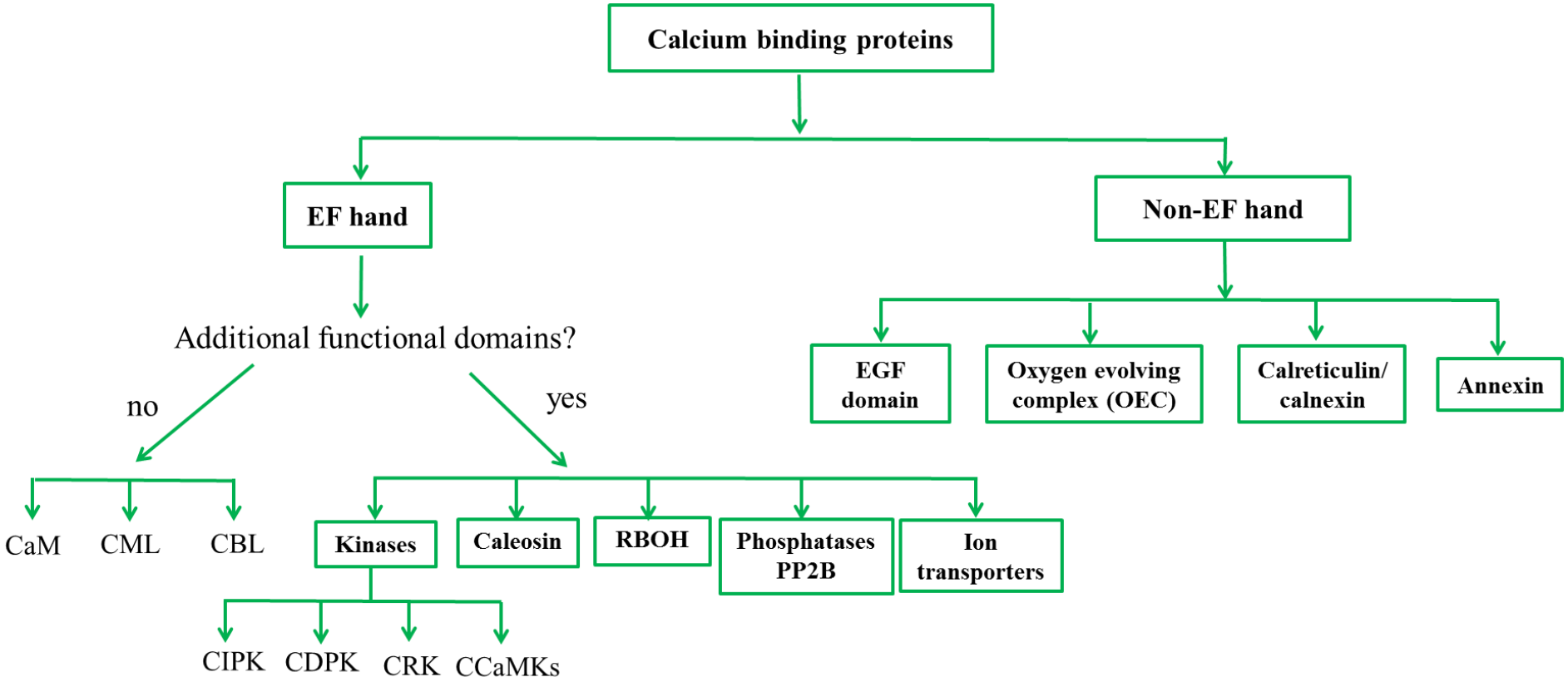

Figure 4. Classification of the calcium-binding proteins found in the current study, based on the calcium-binding domain type.

EF-hand proteins with kinase domain such as calcium-dependent protein kinases (CPKs), CPK-related protein kinases (CRKs), CBL-interacting protein kinases (CIPKs) and calcium and calmodulin-dependent protein kinases (CCaMKs) perform both as sensors and responders through the phosphorylation of stress-related proteins upon calcium sensing (Ho, 2015; Shi *et al.*, 2018; Mohanta *et al.*, 2019). Among the phosphorylated proteins there are heat shock proteins, ABA-responsive transcription factors, protein phosphatases and ion channels (Shi *et al.*, 2018). Phylogenetic analyses have suggested that CPKs and CRKs have a common ancestor that was generated through the fusion of a CaM with a CaM-dependent kinase (Yip-Delormel and Boudsocq, 2019). The CPKs are serine/threonine protein kinases with four EF-hands and myristoylation and palmitoylation sites for sub-cellular targeting at both N- and C-terminal domains (Mohanta *et al.*, 2015). CRKs share similar structural domains with CPKs but often contain degenerate calcium-binding domains and preferentially phosphorylates tyrosine residues in the absence of calcium (Miyamoto *et al.*, 2019; Yip-Delormel and Boudsocq, 2019). Therefore, CRKs might be indirectly regulated by calcium since some of them have shown binding to CaMs (Yip-Delormel and Boudsocq, 2019). CIPKs are the specific downstream targets of CBLs. The C-terminal domain includes a NAF motif required for the binding to CBLs and a domain for phosphatase interaction (Bender *et al.*, 2018). Finally, CCaMKs are highly similar to animal CaMKIIs and contain three visinin-like EF-hand motifs. These kinases require for their functional activity free Ca^{2+} and Ca^{2+} bound to a CaM (Wang *et al.*, 2015).

There are EF-hand-containing proteins with additional functional domains whose main roles differ from calcium-sensing and relay. For instance, NADPH oxidases (RBOHs) produce ROS through the reduction of oxygen to superoxide O_2^- using NADPH as an electron donor. These proteins are integral to the plasma membrane and contain six transmembrane domains. At the N-terminus region they contain two EF-hand motifs and two phosphorylation sites that regulate enzymatic activity (Chapman *et al.*, 2019). Caleosins are calcium-dependent peroxygenases with a single EF-hand and a central hydrophobic domain responsible for the association with oil-bodies (Kim *et al.*, 2011; Blée *et al.*, 2014). These proteins have therefore lipid peroxygenase activity related to epoxy fatty acid biosynthesis which is part of the overall oxylipin metabolism (Rahman *et al.*, 2018). There are Ca^{2+}-activated phosphatases from subgroup PP2B with an EF-hand domain. Phosphatases are characterized for presenting a catalytic subunit for protein dephosphorylation and can perform as positive or negative regulators of abiotic stress responses (Smith and Walker, 1996; Hu *et al.*, 2015; Máthé *et al.*, 2019). Among ion transporters and pumps, there are some sodium/calcium exchangers as well as members from the tandem-pore K^+ (TPK) family from potassium channels which contain EF-hand domains (Sharma *et al.*, 2013; Singh *et al.*, 2015). The previous examples highlight the functional diversity of EF-hand proteins that are subjected to Ca^{2+}-dependent activation during stress responses.

Proteins such as annexins, calnexin/calreticulins (CNX/CRT), from the oxygen-evolving complex (OEC) and with epidermal growth factor (EGF)-like domain are included in the non-EF-hand group (Verica *et al.*, 2003; Wang *et al.*, 2019*a*; Mohanta *et al.*, 2019). Annexins have Ca^{2+} transport activity and are believed to have redox regulatory capacity to control oxidative stress (Yadav *et al.*, 2018). CNX/CRT are proteins from the endoplasmic reticulum with a role in the protein folding machinery and calcium homeostasis. These proteins are up-regulated during oxidative stress in the pathway linked to the activation of the refolding and degradation of unfolded proteins upon stress (Garg *et al.*, 2015). Calcium itself is involved in the photosynthetic reaction as a cofactor of proteins from the OEC which participate in the decomposition of water molecules in the photosystem II (PSII) (Wang *et al.*, 2019*c*). WAKs and WAK-like (WAKL) kinases are a unique class of receptor-like kinases with Ca^{2+} binding EGF and EGF-like domains (Verica *et al.*, 2003). Recently a study in pepper reported the negative modulation of ABA-response under heat stress by a WAKL gene (Wang *et al.*, 2019*a*).

This diversity of calcium signal decoders reflects a wide array of mechanisms to respond to an extensive range of environmental stimuli. The diversification of these mechanisms might be a selective advantage for evolving plants to adapt to changing environments (Edel *et al.*, 2017). The comparison of the calcium-related signaling network in genotypes contrasting in their stress response is of great relevance to identify key proteins and molecular mechanisms that may contribute to greater stress resilience.

1.3. Systemic approaches for complex trait dissection

Over the past years, great efforts have been made towards the identification of genetic factors underlying complex agronomic traits. The reductionist approaches to study these traits have been founded on the hypothesis that genetic additive effects are responsible for the phenotypic variation (Williams and Auwerx, 2015). The genetic mapping is a strategy for complex trait dissection that detects statistical associations of genetic markers with phenotypic values of a quantitative trait to find positions of quantitative trait loci (QTL) in the genome of a given species (Kang *et al.*, 2016; Ishikawa, 2017). This strategy is an intrinsic reductionist approach because it often considers genes as independent functional entities and usually does not account for the regulatory gene networks involved in trait variation (Wang *et al.*, 2014*b*; Lavarenne *et al.*, 2018). Systemic approaches move beyond reductionism and attempt to understand complex traits through the integration of a range of experimental and statistical methods from various disciplines such as genetics, transcriptomics, bioinformatics and stress physiology (Civelek and Lusis, 2014; Baliga *et al.*, 2017).

The data generated by the different -omics methods can be considered as different layers of biological systems (Lavarenne *et al.*, 2018). Many genes that are potential causal QTGs influencing the trait variation are within the detected QTL. The size of the QTL intervals is affected by the marker density, the population size, the mapping resolution and the extent of linkage disequilibrium (LD) and its decay in the mapping populations (Williams and Auwerx, 2015; Otyama *et al.*, 2019). Therefore, a key step to better dissect complex traits is the combination of genetic mapping analyses and transcriptomics layers to provide strong candidate QTGs for the QTL (Gibson *et al.*, 2015; González-Prendes *et al.*, 2017; Ishikawa, 2017). Furthermore, transcriptomics is the most pragmatic choice to track gene regulatory networks involved in complex trait variation, especially when time-series data are obtained. This approach can contribute to pinpoint influent regulators of traits of interest that can be established as breeding targets. These targets are likely to be undetected by traditional forward and reverse genetic approaches and thus provide an added value to systemic analyses in crop species (Lavarenne *et al.*, 2018).

1.4. Genetic mapping studies

The advances made in the high throughput generation of molecular markers as well as in the implementation of statistical methods and computational tools have facilitated the QTL mapping studies in crops. Therefore, these studies are common to understand the genetic architecture of complex traits in crop species (Kulwal, 2018). The precise phenotypic characterization of the mapping populations in diverse environments is essential to obtain reliable variants associated with quantitative traits of interest (Ersoz et al., 2007; Manolio et al., 2009). Linkage or bi-parental mapping and association or LD mapping are the two main strategies used to identify QTLs (Xu et al., 2017). Linkage mapping consists on the analysis of the marker segregation in the progeny of two parents contrasting for the trait of interest. This analysis allows to determine the relative position of markers along the chromosomes and to detect QTL with the phenotypic values scored by the implementation of a suitable statistical method (Semagn et al., 2006; Xu et al., 2017). The genetic mapping using advanced backcross populations (AB-QTL) is a bi-parental mapping alternative useful to identify beneficial QTL alleles of exotic ancestors for introgression into elite cultivars (Kunert et al., 2007).

Association mapping uses populations of diverse individuals to assess the alleles of each locus for statistical association with the phenotype. This method assumes that the associated marker is in LD with the genomic region that is causal of the variation of the trait of interest (Rafalski, 2010). One advantage of association mapping is that a greater record of ancient recombination events can be achieved to reorganize the chromosomes in smaller regions than in a bi-parental mapping study. Therefore, a higher

mapping resolution is obtained to increase the possibility that the marker associated with the phenotype is close to the causal region (Ersoz et al., 2007; Hamblin et al., 2011). This strategy has shown to be a less time-consuming approach for the discovery of marker-trait associations compared with linkage mapping because the construction of a mapping population is not necessary (Álvarez et al., 2014; Saba Rahim et al., 2018). Nevertheless, the main constraint of this approach is population structure as it may produce false positives because markers can be correlated with trait differences among subpopulations. Mixed linear models can be implemented to correct the effect of population structure in association analyses (Xu et al., 2017).

1.5. Analysis of gene expression

Transcription is the process by which the gene information coded in one of the DNA strands is transferred to a messenger RNA (mRNA). The translation process continues when the mRNAs associate with ribosomes for the synthesis of proteins with diverse tasks and roles in the organisms (Klug *et al.*, 2018). A transcriptome is the set of mRNAs produced in a particular tissue under specific environmental conditions (Morozova *et al*., 2009). A fundamental step in the analysis of gene function is the study of expression levels as this is a proxy of protein abundance under certain stimuli. Furthermore, mRNA can be quantified more easily in a high throughput manner by transcriptomic analyses unlike proteins (Pérez-Torres *et al.*, 2009; Gonçalves, 2012; Fassbinder-Orth, 2014). The analysis of gene expression allows the plant breeders to better understand the biological function of genes involved in complex trait variation and contributes to the identification of key targets for the genetic improvement of crops (Pérez-de-Castro *et al.*, 2012). Currently, RNA-seq is the most commonly used strategy for high throughput transcriptome analysis as it leverages the rapid progress of next-generation sequencing (NGS) technologies and the decline in sequencing costs (Teo *et al.*, 2016). On the other side, real-time quantitative PCR (RT-qPCR) has been established as the golden standard for medium-throughput gene expression analysis because of its high accuracy and sensitivity (Derveaux *et al.*, 2010).

1.5.1. Transcriptomic analysis

Before the emergence of NGS technologies, microarrays and Serial Analysis of Gene Expression (SAGE) were common strategies implemented for transcriptomic analyses. The microarray technology allowed the simultaneous inference of expression levels by the hybridization intensity of target transcripts to thousands of known or putative transcripts, while the SAGE approach was based on the Sanger sequencing of short sequence tags (14-21 bp) (Morozova et al., 2009). Since its first description in 2006, RNA-seq has been rapidly adopted by the scientific community as the dominant strategy for

transcriptomics analyses (Lowe et al., 2017). RNA-seq refers to the high throughput sequencing by NGS of transcript cDNAs to capture and quantify the expression of genes in a given RNA sample (Lowe et al., 2017). These experiments may also yield high sequencing depth at highly expressed genes which is suitable for single nucleotide polymorphism (SNP) discovery (Lopez-Maestre et al., 2016).

After RNA isolation for library construction, RNA polyadenylation or ribosomal depletion are performed to select mRNAs from the total RNA extract and discard ribosomal and transfer RNAs from the analysis. Afterward, these mRNAs are chemically or enzymatically fragmented to smaller sizes (300 to 500 bp) to follow reverse transcription to cDNA (Van den Berge et al., 2019). Because of the reduced detection limit of most sequencers, adapters are ligated to cDNA fragments to proceed with PCR amplification of libraries. To correct for PCR amplification biases, the best approach is the use of unique molecular identifiers (UMIs) within the adapter sequences before PCR amplification (Hrdlickova et al., 2017). The cDNA libraries can be sequenced in single-end or paired-end modes. In the first method only one extreme of the fragment is sequenced whereas in the latter both extremes are sequenced producing reads in forward and reverse orientations (Van den Berge et al., 2019).

The Massive Analysis of cDNA 3'-Ends (MACE) sequencing protocol is an alternative to regular RNA-seq to perform transcriptomic analyses in which a transcript is only sequenced once (Hrdlickova et al., 2017; Tzfadia et al., 2018). For the preparation of libraries, polyadenylated mRNA is isolated from total RNA and then cDNA is produced. The population of cDNAs is bound to a streptavidin matrix through 3'-biotinylation and they are shredded to 50-500 bp segments. The bound fragments are sequenced generating tags that can be assembled and annotated (Zawada et al., 2014). The output from this protocol is digital, strand-specific, and the quantification of the expression is simpler and more precise in each library (Asmann et al., 2009; Hrdlickova et al., 2017). Furthermore, this sequencing strategy can contribute to better define gene models towards the 3'-ends (Tzfadia et al., 2018).

The sequenced cDNA fragments can be either aligned to a reference genome or transcriptome or in the case of orphan species a de novo transcriptome assembly can be produced to perform transcript quantification (Fassbinder-Orth, 2014). The main consideration when mapping to a reference genome is the use of spliced aligners as the widely used TopHat, STAR and HISAT2 (Conesa et al., 2016; Sahraeian et al., 2017). Additionally, novel transcripts can be assembled using prediction tools like the one included in the Cufflinks protocol (Roberts et al., 2011; Trapnell et al., 2012). The quantification of gene expression levels is based on the count of reads that map to each transcript sequence with tools as HTSeq-Count and featureCounts (Conesa et al., 2016).

A normalization procedure of read counts is required to perform meaningful comparisons among libraries to detect genes with differential expression. Raw counts are affected by within sample effects as transcript length and between sample effects as the heterogeneous sequencing depth of libraries. Several normalization strategies have been developed and each one relies on particular assumptions that when violated lead to false positives (Evans et al., 2018). The median normalization method implemented in the DESeq Bioconductor package assumes that most genes are not differentially expressed. A scaling factor for each library is calculated based on the median of the ratio of read counts of each gene over its geometric mean across all libraries (Anders and Huber, 2010; Dillies et al., 2013). This normalization method is widely used because it has yielded satisfactory and robust results in the analysis of libraries with heterogeneous compositions (Dillies et al., 2013; Zyprych-Walczak et al., 2015).

The identification of differentially expressed genes across genotypes and treatments is an important goal in many transcriptomics analyses. Count-based methods (e.g. DESeq2, limma and EdgeR), assembly-based methods (e.g. Cuffdiff) and methods specific for alignment-free quantifications (e.g. sleuth) are some of the statistical analyses used to detect genes with differential expression (Sahraeian et al., 2017). After the detection of differentially expressed genes, a gene ontology (GO) enrichment analysis can be performed to identify the over-represented gene categories. The widely used categorizations produced by the Gene Ontology Consortium are the result of a collaborative effort over the past 20 years to make a consistent description of gene products of different origins (The Gene Ontology Consortium, 2019). The results obtained by transcriptomic analysis can therefore provide insights on the molecular and cellular mechanisms triggering adaptation to abiotic stresses (Bashir et al., 2019).

1.5.2. RT-qPCR analysis

RT-qPCR is a sensitive and accurate method for the quantification of gene expression that allows the monitoring of reactions in real-time. This method was first developed in 1996 to overcome the disadvantages of other PCR-based quantification methods and northern blot. The previous PCR-based methods had a limited sample throughput and sometimes required post-PCR manipulations steps that could lead to quantification biases, while in northern blot a complex procedure using radioactivity and large amounts of RNA input were needed (Heid et al., 1996; Morozova et al., 2009). RT-qPCR is characterized by the continuous collection of fluorescent signals over the cycles of multiple PCR reactions and their conversion to a numerical value for each sample (Dorak, 2007). This method is used to demonstrate the accuracy of RNA-seq results due to the multiple sources of biases along the complex

pipeline required for the analysis of sequences and its greater susceptibility to technical artifacts (Busby et al., 2011; Conesa et al., 2016; Klepikova et al., 2017).

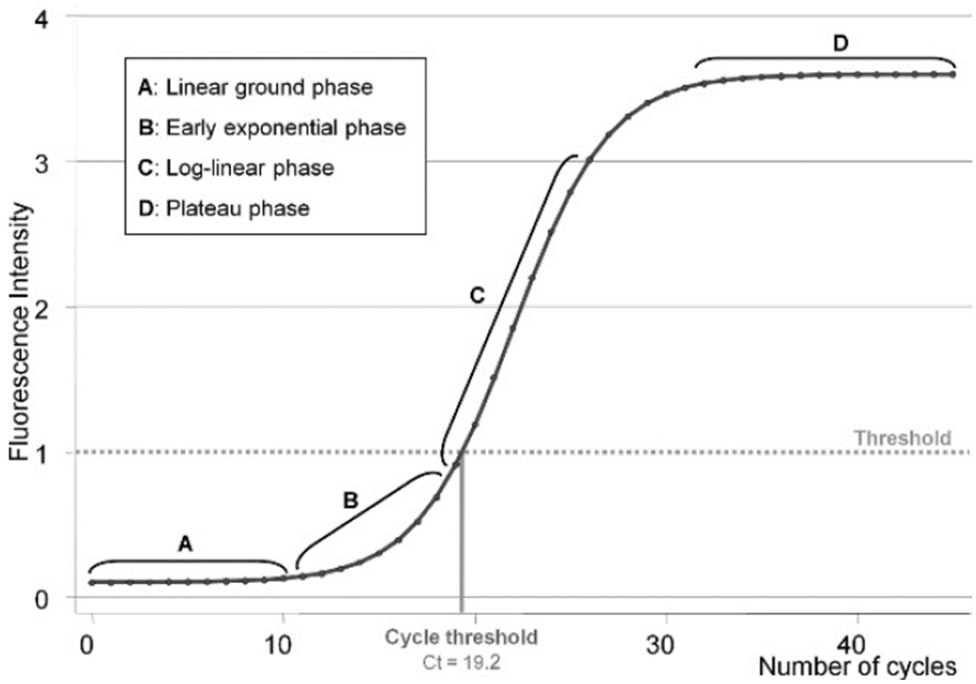

Fig 5. Phases of the real-time amplification curve that represents the fluorescence accumulation across PCR cycles. The cycle threshold (Ct) is highlighted in the initiation of the log-linear phase. Reproduced from Caraguel *et al*. (2011).

The performance of RT-qPCR assays requires suitable detection chemistry for PCR products, an instrument to monitor the reaction in real-time and software for quantitative analysis. The main goal of the assay is to determine the time during cycling when a PCR product is first detected, which will be dependent on the expression levels of the gene. The most widely used detection chemistry recognizes the binding of SYBR Green I to cDNA so that increasing amounts of fluorescence are produced during the polymerization (Bustin and Mueller, 2005). The amplification of a template is defined by four phases as follows: baseline, exponential, linear and plateau. The linear ground or baseline phase includes the cycles below the level of detection of the instrument. The early exponential phase starts at the earliest detectable signal when the amplification continues its maximal amplification rate. The log-linear phase continues when at a certain point the amount of template exceeds the quantity of polymerase. The final plateau phase is reached when the amplification ceases (Dorak, 2007; Jansson and Hedman, 2019) (Figure 5). The threshold cycle (Ct) value represents the cycle at which the fluorescence signal exceeds a defined background threshold (Caraguel et al., 2011) (Figure 5). Ct values therefore reflect the cycle at which a sufficient number of amplicons have accumulated in the reaction and are inversely proportional to the initial cDNA amount of the studied gene. The collection of these data during the

exponential phase produces quantitative information on the expression amount of the studied gene (Caraguel et al., 2011; Ozsolak et al., 2005).

1.5.3. Effect of genetic variation on gene expression

The rationale behind the integration of both genetic mapping and transcriptomic analyses is the assumption that natural genetic variation can underlie complex traits by regulating mechanisms of gene expression (Ackermann *et al.*, 2013; Cai *et al.*, 2019). Regulatory elements of gene expression in plant genomes are classified as *cis*-sequences and *trans*-acting factors. *Cis*-regulatory sequences are nucleotide fragments with various positions in relation to the gene that interact with *trans*-acting factors, such as regulatory proteins (i.e. transcription factors) or microRNAs (miRNAs), to form active complexes that control gene expression levels (Biłas *et al.*, 2016). Among other regulatory mechanisms, gene expression levels can be affected by natural variation in regulatory *cis* sequences. For instance, polymorphisms in transcription factor binding sites located in promoters or miRNA binding sites can influence the expression levels observed in distinct genotypes (Lasky *et al.*, 2014; Võsa *et al.*, 2015).

The transcription factors (TFs) regulate the transcription of genes involved in all cellular functions and play a crucial role in challenging environments by regulating stress-responsive genes. TFs in plants are grouped in more than 50 families and ranges from 1500 to 2000 genes in sequenced genomes. This diversity reflects the complex TF regulatory networks involved in plant physiological and developmental processes (Lehti-Shiu *et al.*, 2017). The TFs can regulate gene transcription through the binding to DNA regions called enhancers or silencers that can exist within the gene, in the promoter region or sometimes thousands of nucleotides away from the gene start (Gonçalves, 2012; Võsa *et al.*, 2015). Therefore, polymorphisms in these regions and the TF sequences control gene expression by affecting the interactions of DNA-regulatory proteins during transcription (Lasky *et al*., 2014).

Additionally, SNPs located in introns, exons or untranslated regions (UTR) may affect the binding of proteins or small RNAs that regulate alternative splicing, mRNA stability or splice-site recognition (Gonçalves, 2012; Mansur *et al.*, 2018). Polymorphisms in 3'-UTR regions or exons can be located in miRNA response elements and either disrupt or create a miRNA binding site thus affecting the allele-specific expression of genes (Ehrenreich and Purugganan, 2008; Võsa *et al.*, 2015). The underlying mechanism is the degradation or the repression of the mRNAs targeted by the binding with the complementary miRNA (Gonçalves, 2012).

Transcriptional regulatory interactions of high quality are usually limited to the model species *Arabidopsis thaliana* (Jin *et al.*, 2017). Based on these known interactions and assuming the conservation of *cis*-regulatory sequences across distant species (Weirauch *et al.*, 2014), some tools have been validated in non-model species to predict TF (Jin *et al.*, 2017) and miRNA (Dai *et al.*, 2018) binding sites in target sequences. This information is useful to create hypotheses on the regulatory effect of polymorphisms in the differential gene expression observed in contrasting genotypes.

1.6. Studies to dissect the mechanisms of salt tolerance in wheat

Ancestral wild relatives from bread wheat and other genetic resources as synthetic genotypes have been used in breeding programs to improve salt tolerance (Colmer et al., 2006; Wang and Xia, 2018) as well as in genetic mapping studies to identify exotic alleles controlling salt stress-related traits (Ismail and Horie, 2017; Dadshani, 2018). Nevertheless, breeding of salt-tolerant varieties has been slow as only a few salt-tolerant varieties adapted to local conditions have been developed and commercialized (Ismail and Horie, 2017). Tetraploid wheat is less salt-tolerant than bread wheat and one major determinant is the ability of bread wheat to maintain a higher K^+/Na^+ ratio in the leaves (Wang and Xia, 2018). This and other genetic mechanisms controlling stress adaptation are often located in the D subgenome which highlights the subgenome functionality (Yang et al., 2014; Zhang et al., 2016; Wang and Xia, 2018). As modern bread wheat has a good Na^+ exclusion ability, further efforts in breeding programs should focus on osmotic adjustment and tissue tolerance mechanisms (Genc et al., 2019).

Several mapping analyses in bread wheat have detected QTL with an effect on salt stress-related traits (Xu et al.; Hussain et al., 2017; Dadshani, 2018; Oyiga et al., 2018, 2019; Asif et al., 2018). The recent studies by Oyiga et al. (2018) and Dadshani (2018) identified QTL for salt stress-related traits at germination, seedling and adult stages in association and AB-QTL mapping populations, respectively. Because of the limited mapping resolution of these studies, the QTL contain many genes that are potential QTGs influencing the trait variation.

Some transcriptomics analyses in bread wheat have reported salt-responsive genes in roots (Goyal et al., 2016; Zhang et al., 2016; Amirbakhtiar et al., 2019), leaves (Mahajan et al., 2017), and both organs (Luo et al., 2019). There are two studies of the salt-stress transcriptome of the widely recognized salt-tolerant landrace Kharchia Local in roots (Goyal et al., 2016) and leaves (Mahajan et al., 2017). Some studies have compared the salt stress transcriptome of tolerant and susceptible genotypes (Zhang et al., 2016; Amirbakhtiar et al., 2019; Luo et al., 2019). These mentioned studies have provided some insights into the molecular mechanisms by which bread wheat responds to salt stress conditions. Nevertheless, a

comprehensive overview and comparison of the mechanisms activated along the stress phases are not available. Furthermore, it is necessary to have a better understanding of the early transcriptional responses in the first minutes and hours after salt stress when relevant transcriptional reprogramming events for stress acclimation may occur (Julkowska and Testerink, 2015).

As only recently a chromosome-level assembly of the wheat genome is available (IWGSC, 2018), few studies have aimed to perform transcriptomics analyses to narrow down the number of genes in QTL intervals. For instance, Oyiga et al. (2019) integrated transcriptomics data at the ionic phase and association mapping to identify the differentially expressed NRAMP-2 and OPAQUE1 as potential QTGs in QTLs in chromosomes 4BL and 6AL. Nevertheless, the transcriptomic analysis performed in this study only focused on few genomic regions, used a fragmented wheat genome assembly (IWGSC, 2014) and implemented a bioinformatics pipeline that was not optimized to reduce false positives in the detection of differentially expressed genes.

This study presents a systemic approach that integrates the dynamic transcriptomic responses of salt-tolerant and salt-sensitive wheat genotypes at osmotic and ionic phases with physiological measurements and genetic mapping studies. The results provided insights into the adaptation response mechanisms of contrasting bread wheat genotypes at both salt stress phases. The over-representation of genes coding calcium-binding proteins was observed in the contrasting genotypes at the osmotic stress response. Therefore, these genes were further analyzed and some of them were validated using RT-qPCR. The genetic variation with a potential effect on the regulation of the expression of calcium-binding genes was also studied.

2. Hypotheses

- The comprehensive understanding of salt stress adaption mechanisms can be facilitated by the implementation of systemic approaches that integrate genetic, physiologic and transcriptomic analyses.
- There are genes regulated at the transcriptional level that can influence salt stress-related physiological traits and operate within QTL to control salt stress response variation.

3. Objectives

3.1. General Objective

To implement a systemic approach to obtain a better understanding of the salt stress adaptation response mechanisms of contrasting bread wheat genotypes.

3.2. Specific Objectives

- To compare the salt-stress transcriptome of contrasting bread wheat genotypes at osmotic and ionic phases through the development of a pipeline for the analysis of MACE-derived sequences and the detection of salt-responsive genes in biological averaged samples.
- To identify salt-responsive genes within selected QTL of salt stress-related traits as potential QTGs operating in the trait variation and link the salt-stress transcriptome with physiological traits measured at the osmotic and ionic phases.
- To validate the expression of selected genes through an RT-qPCR analysis performed in leaves and roots.
- To characterize the functional domain diversity of salt-responsive genes coding calcium-binding proteins and identify putative orthologs of genes with known function on stress response pathways.
- To give some insights into the genetic variation with a potential effect on the differential expression of calcium-binding genes through the analysis of SNPs identified in promoter and gene sequences.

4. Materials and Methods

4.1. Contrasting genotypes from the mapping populations

The elite German winter wheat cultivar Zentos (salt-tolerant) and the synthetic genotype Syn86 (salt-susceptible; Lange and Jochemsen, 1992) were the contrasting parents from an AB-QTL study used to analyze the foliar transcriptome during the osmotic stress response (Kunert et al., 2007; Dadshani, 2018). The AB-QTL analysis revealed some genomic regions with an effect on salt stress-related traits assessed at germination, seedling and adult stages. A differential stress response in these genotypes was revealed at this phase by the measurement of the time course of the photosynthesis rate using a gas exchange system (LI-6400XT; LI-COR Environmental, Lincoln, NE, USA) (Dadshani, 2018). This analysis was performed in a hydroponic system in a growth chamber using five 50 days old plants that were transferred suddenly into a 100 mM NaCl solution. Data were recorded from the third fully expanded leaf in 30 s intervals until 45 min after stress exposure (ASE). Further methodological conditions are described in Dadshani (2018). This study allowed the identification of the turning points of the photosynthesis rate. Turning points referred to the time points with maximum variation response revealed by the change of direction from the curve slope as shown in Figure 6A (Pender et al., 2011). These time points were considered for the transcriptomic analysis.

Altay2000 (salt-tolerant; Altay, 2012) and Bobur (salt-susceptible; Amanov, 2017) were the Turkish and Uzbek winter wheat cultivars used to study the transcriptome during the ionic stress response, respectively. These genotypes were included in an association mapping study that identified QTL from salt stress-related traits measured at three developmental stages (Oyiga et al., 2018). The genotypes were contrasting for shoot accumulation of K^+ and Na^+ measured at the ionic phase among other stress-related traits (Oyiga et al., 2016).

4.2. Hydroponics experiments

The hydroponics experiments were performed in a growth chamber at 20 ± 2 °C with 50 ± 5 % humidity and a 12 h photoperiod. Four hydroponics boxes were distributed under four fluorescent light lamps (600 µmol m-2 s-1). Two hydroponic systems types were used for the transcriptomic analyses at the osmotic (Dadshani, 2018) and ionic phases (Oyiga et al., 2016). The system used at the osmotic phase contemplated the use of dark polypropylene boxes with a capacity of 170 liters (EG 86/42 HG by Auer Packaging, Amerang, Germany) and 54 plants growing on hydrophobic sponges inside holes of styrodur panels (Styrodur 3035 CS; BASF, Ludwigshafen, Germany). First, seeds were germinated in petri boxes (29.0 x 22.5 x 3.0 cm; Licefa GmbH & Co. KG, Bad Salzuflen, Germany) with filter paper (C160; Munktell & Filtrak GmbH; Bärenstein, Germany) and distilled water. After eight days under the growth chamber conditions, healthy seedlings were transferred from the petri boxes to the sponges in hydroponic boxes filled with a nutrient solution prepared as described by Asao (2012). The solution was continually aerated by four air diffusers (Eheim 4002650, Eheim GmbH & Co. KG, Deizisau, Germany), replaced every ten days and the pH adjusted to 6.5 every second day (Dadshani, 2018). Homogeneous seedlings adapted for ten days to hydroponics conditions were used for sampling leaves under control conditions and under a salt stress treatment of 100 mM NaCl applied to the nutrient solution. Samples were collected in the photosynthesis turning time points identified at 8, 15 and 30 min (Figure 6A) and 4 h ASE whereas control conditions were sampled at 0, 30 min and 4 h in plants grown in hydroponic boxes without NaCl. This system type was used for additional hydroponics experiments carried out for RT-qPCR analyses in leaves and roots (Section 4.4.3).

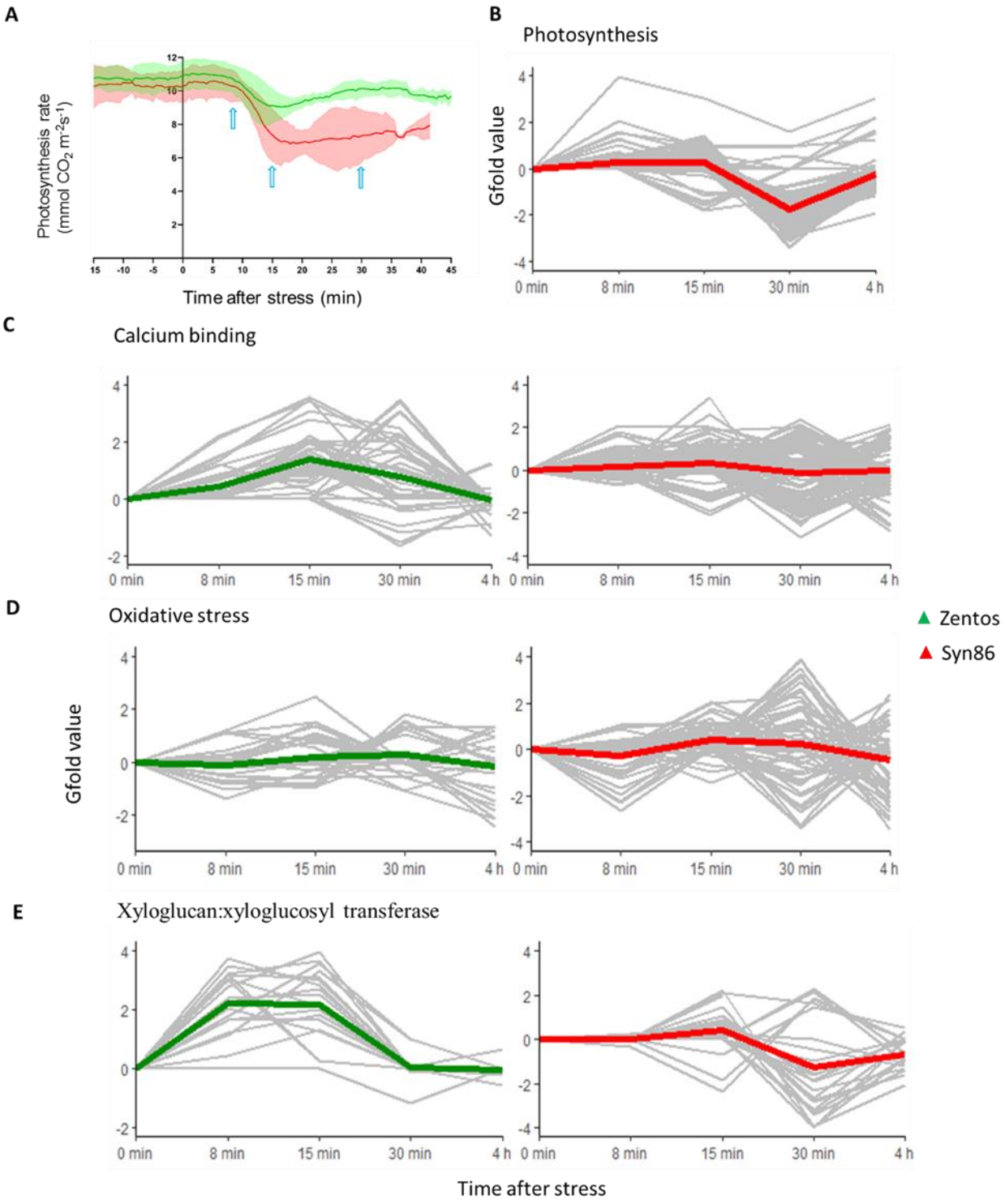

Figure 6. Photosynthesis rate curve (A) and generalized fold change (GFOLD) values of time course relative expression of selected gene ontologies (B, C, D, E). In each expression profile frame, the gray lines show the time course expression pattern of each gene and the red or green lines are locally estimated scatterplot smoothing (LOESS) curves that represent the expression tendency of the clusters of genes. The photosynthesis rate curve was adapted from Dadshani (2018), where the shadows represent the standard deviation of the measurements and the time points selected for the transcriptomic analysis are highlighted with blue arrows.

The system used at the ionic phase considered the use of boxes of 170 L filled with 156 PVC tubes (4.5 cm diameter x 45 cm depth) and 164 L of a nutrient solution prepared as described by Tavakkoli et al. (2010). The seeds in this case were germinated in-situ in the tubes filled with Aquagran filter quartz 2–3.15 mm (Euroquarz GmbH, Dorsten, Germany). Three days after planting, salt was applied gradually during three days until the final concentration was reached. The nutrient solutions were replaced every seven days and the pH adjusted to 6.0 daily (Oyiga et al., 2017). Samples for the ionic stress conditions were collected at 11 days and 24 days in both salt-stressed and control plants.

4.3. Transcriptomic analysis

4.3.1. Reads processing and mapping to the reference genome

The total RNA isolation and the MACE library construction were performed at GenXPro GmbH (Frankfurt, Germany). The analysis of complex experimental designs with several time points and genotypes requires a lot of sequencing data. To test whether important transcriptional changes may occur on some selected time points, RNA pools can be constructed to perform biological averaging. Therefore, an equal amount of leaves from four plants were harvested and homogenized in liquid nitrogen to constitute an RNA pool for each condition. This sampling strategy facilitates analyses with less quantity of sequencing data assuming that most expression measurements from pools are similar to the averages from the individuals that are included in them (Kendziorski et al., 2005; Biswas et al., 2013).

An Illumina NextSeq 500 system was used to sequence fourteen and eight libraries from the osmotic and ionic stress experiments, respectively. The Cutadapt tool was used to remove adapters from reads (Martin, 2011). The quality control (QC) of the prepared libraries was carried out using FastQC (Andrews, 2010) and the short reads with less than 35 bp were removed using Trimmomatic (Bolger et al., 2014). The retained reads were aligned to the reference wheat genome assembly version "RefSeq v1.0" (IWGSC, 2018) using Tophat (Trapnell et al., 2009). Assemblies of novel transcripts were produced with the prediction tool of Cufflinks (Trapnell et al., 2009; Roberts et al., 2011). The markdup tool from SAMtools was employed to produce deduplicated alignment files and to estimate the amount of read duplication (Li et al., 2009).

A new annotation file was elaborated to count reads beyond the predicted 3'-ends of high confidence (HC) and low confidence (LC) gene models with the purpose to contribute to gene model improvement and better estimate gene expression levels. For that, the gene models from the RefSeq v1.1 genome annotation (IWGSC, 2018) were extended by 40 % downstream of the predicted 3'-end in the case of intergenic regions greater than 1000 bp but smaller than three times the gene size. When the intergenic

distance was larger, the elongated target sequence corresponded to the size of the gene. Then, the stranded option from the featureCounts tool (Liao et al., 2014) of the Subread software (Liao et al., 2013) was used to count the unique mapped reads assigned to the elongated HC and LC gene models and novel transcripts. The read count data were normalized to Counts per Million (CPM). An average CPM value of 2.5 across libraries from the same genotype was selected as a threshold to define a transcriptomic background aiming to select the genes adequately represented and to reduce the number of low expressed transcripts that might cause sampling noise (Sha et al., 2015; Lin et al., 2016).

A merged alignment file with all reads from the libraries was generated to compare the number of reads counted using the extended gene models with those counted employing the reference annotation. To exemplify the improvement in transcript quantification with the extended gene models, two windows of 5 Mbp (23 to 28 Mbp coordinates of the chromosomes 5B and 7D) were inspected in the alignment files from two libraries of Altay2000: one at 11 days under control conditions and the other at 24 days ASE. The online web tool GenomeView (Abeel et al., 2012) allowed the visualization of the alignments in the reference genome to observe the coordinates of the reads scored beyond the 3'-end coordinate defined by the gene model.

4.3.2. Identification of salt-responsive genes and GO enrichment analysis

After filtering the low expressed transcripts, salt-responsive genes were identified using the raw count data of fragments as input in the GFOLD (generalized fold change) software (Feng et al., 2012) that implements the DEseq expression normalization approach (Anders and Huber, 2010). The GFOLD value is a reliable estimator of the relative gene expression developed for the analysis of pooled experiments. The method algorithm produces gene rankings that overcome the limitation of the low confidence and often overestimated raw fold changes values calculated from genes with few counts (Feng et al., 2012). Density plots with log10 normalized expression values were used to compare their distributions. Overlapping expression distributions indicate appropriate homogeneity of the sequencing depth and that count normalization is suitable to compare the expression levels of the different libraries (Klaus and Huber, 2016). The 0 min condition was used as a control for both 8 and 15 min ASE, with the assumption that few physiological changes occur in this short time under normal conditions. A high absolute GFOLD value indicated greater up- or down-regulation of the genes. Genes with GFOLD values >1 or < -1 were considered for further analyses as they represent relevant changes in expression levels under stress conditions (Feng et al., 2012).

The GO enrichment tool from the STEM software was implemented to distinguish the categories of genes over-represented by time point in the contrasting genotypes (Ernst et al., 2005; Ernst and Bar-Joseph, 2006). Only the gene categories from the transcriptomic background of each genotype were retained in the analysis (Timmons et al., 2015). A Bonferroni multiple hypothesis correction test was employed, thus GO terms with a corrected p-value < 0.001 were considered as over-represented. The STEM algorithm was used to cluster expression profiles during the osmotic phase and the over-represented GO categories in the clusters were defined (Ernst et al., 2005; Ernst and Bar-Joseph, 2006). Key categories over-represented during the osmotic phase were selected to create graphics of the time-course expression of the corresponding genes. A locally estimated scatterplot smoothing (LOESS) model was fitted to represent the expression tendency of the clusters of genes. The expression levels of transcripts from the transmembrane transport category related to ion homeostasis were compared in the contrasting genotypes at the ionic phase.

4.3.3. Identification of candidate QTGs

QTLs were delimited through the identification of single nucleotide polymorphisms (SNPs) in strong LD ($R^2 \geq 0.8$) with markers with a significant effect on trait variation (Cirilli *et al.*, 2018). QTGs were identified by localizing salt-responsive genes detected with the transcriptomic analysis within the LD blocks determined for the QTL. The positions of the LD blocks in the reference genome sequence RefSeq v1.0 were established according to the IWGSC RefSeq v1.0 BLAST results of the SNPs-flanking sequences (Alaux *et al.*, 2018). The wheat RNA-seq atlas expVIP was used to compare the expression of the QTGs with the expression determined in other abiotic stress experiments in the species (Borrill *et al.*, 2016).

4.4. Expression and sequence analyses of genes coding calcium-binding proteins

The set of salt-responsive genes with a calcium-binding domain identified in Syn86 and Zentos were selected for further expression and sequence analyses. Clusters of time-course expression profiles were identified in each genotype according to the up- or down-regulation patterns observed in the stress time points. SNPs in these transcripts were identified through the examination of the MACE reads collected for the transcriptomic analysis. These polymorphisms contributed to predicting variations in miRNA binding sites that can be linked to the differences in expression observed in the contrasting genotypes (Võsa et al., 2015).

Two of the salt-responsive genes with calcium-binding domain located in the D subgenome were selected to perform time-course RT-qPCR. This analysis was useful to compare with the expression levels obtained from the transcriptomic experiment and to study the gene expression in roots and in additional time points. TraesCS2D02G173600 was only salt-responsive in Zentos and down-regulated while TraesCS5D02G238700 was up-regulated in both genotypes. The first gene in chromosome 2D is located in a QTL with an effect on plant biomass under salt stress conditions detected in the advanced backcross mapping analysis by Dadshani (2018). The salt-responsive gene and the SNP marker Kukri_rep_c72254_186 were separated by 9 kb. The second gene in chromosome 5D was chosen as it showed high relative expression values in Syn86 at 8 and 15 min. The promoter sequence analyses of these two genes were performed to identify SNPs in TF binding sites that can also be linked to the expression differences in Syn86 and Zentos (Lasky et al., 2014).

4.4.1. Classification of calcium-binding genes and phylogenetic analysis of EF-hand proteins

The calcium-binding genes were classified according to the binding domain type (EF-hand or non-EF-hand) and the presence of additional functional domains using the Interpro results available from the RefSeqv1.0 annotation (Alaux *et al.*, 2018). The role in abiotic stress responses of proteins with EF-hand domain has been widely studied in *A. thaliana* and other species (Fuchs *et al.*, 2011; La Verde *et al.*, 2018; Chapman *et al.*, 2019; Sanyal *et al.*, 2019; Yip-Delormel and Boudsocq, 2019). The 79 HC EF-hand proteins from both genotypes were characterized through the comparison with the peptide sequences of the corresponding CaM, CML, CBL, CPK and RBOH proteins of *Arabidopsis*. Therefore, a multiple alignment was performed with MAFFT (Katoh *et al.*, 2019) followed by a phylogenetic tree analysis conducted with MEGA X through the Neighbour-Joining method (Kumar *et al.*, 2018). Consensus trees for salt-responsive CaM/CML, CPK and RBOH of wheat and reference proteins of *A. thaliana* were inferred through a bootstrap analysis with 3000 replicates.

4.4.2. Subgenome specific primer design

Subgenome specific primers were designed for the RT-qPCR analyses and the amplicon sequencing of the pair of genes studied and the corresponding promoter regions. The BLAST tool from the IWGSC RefSeq v1.0 (Alaux *et al.*, 2018) was used to identify the five regions with the highest similarity to the target sequences. These sequences were submitted to the customized multiple sequence tool from the web-based platform GSP to design primers in polyploids (Wang *et al.*, 2016). The multiple alignments performed by the platform facilitated the detection of variants in the target sequence for the design of subgenome specific primers. The amplification conditions were adjusted using foliar DNA isolated with

the Plant DNA mini kit (VWR, Darmstadt, Germany). Thus, 100 ng of DNA template in 25 µl of 1x One Taq Standard Buffer (Biolabs, Ipswich, MA, USA), 0.2 mM dNTPs and 0.2 µM of each primer were amplified with 0.5 units of One Taq DNA polymerase (Biolabs, Ipswich, MA, USA). Cycling conditions were established with an initial denaturation step at 95°C/2 min followed by 40 cycles at 95 °C/45 s, annealing temperature (Ta) for 45 s (specified in Table 1), extension at 72 °C/1 min per kbp, and a final extension step at 72°C/5 min. Designed primers for the two studied genes are shown in Table 1. The amplicons of the tested primers were visualized in 1.5% (w/v) agarose gels stained with peqGreen (0,04 µl/mL; VWR, Darmstadt, Germany). Purified PCR products with Purelink Quick PCR kit (Invitrogen, Waltham, MA, USA) were sequenced at Eurofins Genomics (Ebersberg, Germany) with an ABI 3730xl DNA Analyzer System. Primers were selected for further experiments when the amplicon sequence comparison with the reference sequence confirmed its specificity and the sequence visualization revealed the absence of contamination with unspecific products. The SNAP gel purification kit (Invitrogen, Waltham, MA, USA) was used to purify bands from gels when the presence of additional unspecific fragments was observed.

4.4.3. RT-qPCR analysis

A hydroponic system was implemented following the procedures described in Dadshani (2018) that were summarized in Section 4.2. A salt treatment of 150 mM NaCl was applied to two-weeks-old seedlings for 48 h. Stress conditions were sampled at 8 min, 15 min, 30 min, 4 h, 10 h, 24 h and 48 h ASE. The control conditions corresponded to untreated plants harvested simultaneously with the stressed plants at the same time points. A biological replicate consisted of the whole root or all the leaves from a single plant. Leaves and roots were cut and immediately frozen in liquid nitrogen. Three biological replicates were sampled from each condition. The tissue from each organ was homogenized with liquid nitrogen and 200 mg of the ground tissue was used for total RNA isolation with the RNeasy plant mini kit (Qiagen, Hilden, Germany). RNA was eluted in 30 µl of RNAse free water followed by DNAse I (BioBudget, Krefeld, Germany) digestion using 2 units of the enzyme and 3 µl of the buffer. Enzyme inactivation was performed by incubating RNA at 65°C for 10 min with 3 µl of EDTA 50 mM (BioBudget, Krefeld, Germany). The RNA concentration was measured using a Nanodrop 2000c spectrophotometer (Thermo Scientific, Waltham, MA, USA) and its integrity was assessed in 1.5% (w/v) agarose gels.

The cDNA synthesis was performed with the First Strand cDNA Synthesis Kit (Thermo Scientific) using 5 µg of total RNA from each sample. To discard any genomic DNA contamination during RNA isolation, a pair of primers were used to amplify a region of the Actin gene that included an intron (5'-

CCATCATGAAGTGTGACGTGG-3', 5'-TCCAAGGATGAGTACGACGAG-3', Ta= 58°C, provided by A. Bungartz). The SDS-7500 Sequence Detection System (Applied Biosystems, Waltham, MA, USA) was used for the RT-qPCR with cycling conditions of 95 °C/7 min followed by 40 cycles at 95 °C/10 s, 60 °C/30 s, 72 °C/30 s, and 82 °C/30 s (fluorescence acquisition). The RT-qPCR reaction of 20 µl consisted on 0.25 µM of each primer (Table 1), 10.12 µl of DyNamo Color Flash SYBR Green 2X-master mix with ROX (Thermo Scientific, Waltham, MA, USA) and 1:20 diluted cDNA template (2 µl leaves, 3µl roots).

A cycle of 95 °C for 10 s, 60 °C for 30 s and 95 °C for 15 s was applied to PCR products for melting curve analysis. These curves were analyzed to discard contamination, unspecific amplification or primer dimers that might affect the results of the quantification. The average Ct values of three technical replicates were calculated and used as input for the quantification of the relative expression of the selected genes under stress conditions using the 2^(-ΔΔCt) method where ΔΔCt= (Ct,target - Ct, Ct,reference)treatment - (Ct,target - Ct, Ct,reference)control. The main assumption for this method to be valid is that the amplification efficiencies of both target and reference genes are approximately equal (Livak and Schmittgen, 2001).

Reference genes with stable expression levels across different tissues and stimuli are used to normalize the cDNA levels of the genes of interest to facilitate the comparison of their expression in the different samples (Rebouças et al., 2013). The reference gene primers TaEf-1.1 and TaEf-1.1 used in previous studies of salt stress in bread wheat (Oyiga et al., 2018; 2019) were tested in this study. The comparisons of primer efficiencies were performed in serial dilutions made from a pool of cDNA from all samples (Pfaffl, 2004). Therefore, the amplification efficiencies of the reference and target genes were compared to select the control gene that provided the greatest similarity. A linear regression model based on the ΔCt values of the two primers versus the cDNA input in the dilutions was analyzed. Slopes of linear regressions < 0.1 indicated a similar efficiency of both target and reference gene primers (Li et al., 2012).

A one-sample single-tailed t-test ($p < 0.05$) was implemented in the $2^{-\Delta\Delta Ct}$ values of each genotype per time point to assess whether the mean was > 2.0 or < 1.0 to define when the transcripts were up-regulated or down-regulated upon stress, respectively. A two-sample two-tailed t-test ($p < 0.05$) was used to compare the $2^{-\Delta\Delta Ct}$ values from the two genotypes to determine if the mean relative expression values were significantly different in each time point. Finally, the ΔΔCt values calculated from RT-qPCR experiments and the GFOLD values obtained from the transcriptomic analysis were compared.

Table 1. Primer sequences for the amplification of gene and promoter sequences of *CML-2D* (*TraesCS2D02G173600*) and *CML47-5D* (*TraesCS5D02G238700*) with their corresponding annealing temperatures (Ta).

Gene	Forward 5'-3'	Reverse 5'-3'	Size (bp)	Ta (°C)	Objective
CML-2D	TCTGCTGTGCTATGCTCGAC	TCCCGTTCTGTCCGAATTCTA	250	60-62[a]	RT-qPCR
	AACTTTCAGCATTCTTGGGCA	CGTCCTGAGCTTGCGAACG	591	60	Gene
	TCGCCCTCCACCAAGAAGAA	TCCGTTTGAGTCAGCCAAAAG	784	56	Gene
	AATAGGGTATTAGGAATGTCAC	GAATCTCGTCCCTTTTTGTTC	1485	58	Promoter
	TGGAATGGAGTCAAAGATATCG	GGTTGGCATTCTTGAGGGAA			Internal[b] for promoter
		TAGATCTACGCCCTGATTGAG[c]			Internal for promoter
		GAGCTGTGACGATGAAACATG[d]			Internal for promoter
CML47-5D	GTATAAAGAATAGGATTGGATACA	CAAACGAACAAACGAACAAACGA	110	60	RT-qPCR
	CTTGGAGTTAGCGTTAGATGA	TTCCCAGCAAATTTCCAATCTA	1684	60	Gene + promoter
	GGAAAAAGGACAAGGAGAACA	CTTCTGCGACTGAATTTTGATT			Internal for gene + promoter
		TGTGAGAGCGATGGAATTGT			Internal for gene + promoter
	GGTGCTTGCTTCTTGATCGT	GCTAATTATGTGTGCGAGCG	1454	60	Promoter

[a] Ta of 62ºC was used for expression analysis of roots

[b] Primers used for completing the sequencing of amplicons

[c] Specific for Zentos

[d] Specific for Syn86

4.4.4. Study of genetic variation with potential effect on stress-induced differential expression

4.4.4.1 Promoter and gene sequence analyses

The analysis of the gene and promoter sequence of the two selected genes was carried out by amplicon sequencing. Primer design and sample preparation for sequencing were described in Section 4.4.2. The primers used for amplification and sequencing are shown in Table 1. Polymorphisms in the contrasting genotypes were visually identified using the pairwise alignment tool from Bioedit version 7.2.5 (Hall et al., 1999). The PlantTFDB (v 5.0) database allowed the prediction of TF families with recognition motifs in the promoter sequence through the projection of experimentally validated motifs to the genome of 156 sequenced plant species including wheat (Jin et al., 2017). TF families binding to motifs containing polymorphic sites were recognized as putative regulators of gene expression when q-value < 0.05.

4.4.4.2 MACE-based SNP identification and miRNA binding site analysis

The alignments from the MACE libraries described in Section 4.3.1 were merged by genotype for SNP identification using SAMtools (Li, 2011). The following conditions were considered to retain high-confidence SNP calls: the minimum Phred base quality in the variant site was 25, the minimum mapping quality from the read was 20 and variants were represented in at least 10 reads from the same genotype. The psRNAtarget tool allowed the prediction of miRNA binding sites in the regions adjacent to the polymorphisms (Dai *et al.*, 2018).

5. Results

5.1. Sequence processing and reference genome mapping

The sequenced MACE libraries were processed and the reads aligned to the reference genome. An overview of the reads processing and reference genome mapping is presented in Table 2. The libraries from Altay2000 and Bobur contained on average greater number of total and duplicated reads than the libraries from the genotypes studied in the osmotic phase (Table 2). The exclusion of a fewer number of reads after the quality control filtering and a greater average mapping efficiency were observed in the ionic stress libraries compared to those from the osmotic stress experiment (Table 2; see details in Appendix 1). The use of the reference annotation scored 86% of the total number of unique mapped reads while with the extended gene models 91% of the reads were counted. Therefore, with the extended annotation ca. 6 million of additional reads were detected in 12019 genes which accounted for 4.5 % of the gene models predicted in the RefSeq v1.1 genome annotation. Five of these genes are shown as examples and revealed elongations from 186 to 470 bp (Table 3).

Table 2. Summary of MACE libraries processing and reference genome mapping (mean ± standard deviation).

	Osmotic phase	Ionic phase
Libraries	14	8
Total millions of reads	5.0 ± 0.7	9.0 ± 2.4
Reads excluded after QC[a] (%)	7.8 ± 1.6	2.6 ± 0.3
Mapping efficiency (%)	83.6 ± 1.2	93.0 ± 0.3
Millions of mapped reads	3.8 ± 0.5	8.2 ± 2.2
Multiple aligned reads (%)	21.7 ± 3.3	19.7 ± 1.7
Millions of unique mapped reads	3.0 ± 0.4	6.6 ± 1.8
Reads after deduplication (%)	62.2 ± 3.7	53.9 ± 3.2

[a]QC: Quality control

Table 3. Comparison of the reads scored with the reference annotation (R) and with extended gene models (E).

Gene[a]	Reads scored (R/E)		Extension size (bp)
	Library 1[b]	Library 2	
TraesCS5B02G027100	1/9	2/3	242
TraesCS5B02G028200	27/28	23/27	196
TraesCS7D02G049200	1/2	5/16	186
TraesCS7D02G062000LC	5/17	4/9	368
TraesCS7D02G051200	4/107	8/268	470

[a] Genes in bold letters also show a prolonged 3'-end according to RNA-seq data from Pingault *et al.* (2015)

[b] Library 1 is from Altay2000 at 11 days under control and Library 2 is from Altay2000 at 24 days of stress without deduplication.

5.2. Identification of salt-responsive genes

To compare the level of expression of genes in response to salt stress in the osmotic and ionic phases, the GFOLD tool was used to identify salt-responsive genes in the two tolerant and two susceptible genotypes studied. The libraries from Syn86 and Zentos were comparable as evidenced by their

overlapping expression densities (Appendix 2). Differently, a greater mean of the expression values was observed at 24 days ASE when compared to the mean in the other time points (Appendix 2). This type of distribution of the expression is an indicator of high levels of PCR duplication of reads and therefore the deduplicated alignment files were used for the differential expression analysis at the ionic phase. After deduplication, the density plots revealed a better homogeneity of Altay2000 and Bobur samples (Appendix 2). The removal of low expressed transcripts led to the reduction of the number of reads for the differential expression analysis on average by 3.1% and 3.6% in the osmotic and ionic stress experiments, respectively (Appendix 1).

The differential expression analysis showed a reduced variability among genotypes (mean ± standard deviation) concerning the percentage of identified novel transcripts (4.5 ± 0.4%) (see genome coordinates in Appendix 3), LC (5.0 ± 0.8%) and HC (90.5 ± 1.1%) gene models. The D subgenome contained the greatest percentage of salt-responsive genes (35.8 ± 1.7%) followed by subgenomes B (31.4 ± 1.1%) and A (31.3 ± 1.5%) and unplaced superscafolds (1.5 ± 0.3%).

5.3. Comparative analysis of the osmotic stress response

To better understand the early plant reaction to salt exposure, a comparative transcription profiling at the osmotic stress phase was performed. The greatest number of salt-responsive genes was observed at 15 min ASE in Zentos and at 30 min in Syn86, whereas the lowest number was identified at 8 min ASE in both genotypes (Figure 7B, C). Thirty-eight and 14 genes were differentially expressed simultaneously across all the time points in Syn86 and Zentos, respectively (Figure 7B, C). The distribution of up and down-regulated genes revealed that Zentos had the highest number of up- and down-regulated genes at 15 min and 4 h ASE, respectively (Figure 8A). In contrast, Syn86 had the highest number of up-regulated genes at 4 h and of down-regulated at 30 min. In total, Zentos showed 75% of up-regulated genes while Syn86 had 60%.

Highlighted in the heatmaps are the 24 and 18 over-represented ontology terms that were exclusively up- and down-regulated, respectively (Figure 9A, B). Among the up-regulated categories, the over-representation of response to wounding genes and tryptophan synthase activity were recognized in the susceptible genotype whereas in Zentos the calcium-binding category was identified. Defense response to fungus and bacterium, transcription factor activity and protein kinase coding genes were over-represented and up-regulated in both genotypes (Figure 9A). The over-representation of spermine and spermidine biosynthesis and antioxidant activity genes was recognized in the down-regulated categories from Syn86 (Figure 9B).

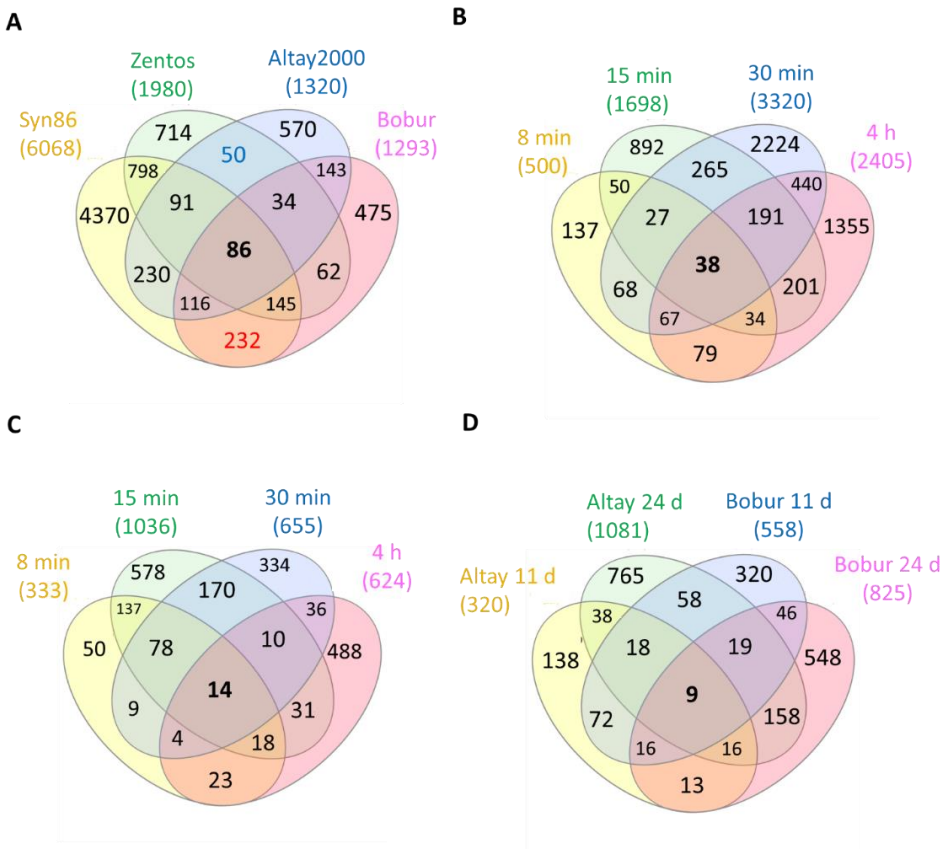

Figure 7. Venn diagrams of the salt-responsive genes in the contrasting genotypes studied. The total number of genes in each genotype and/or time point are shown above each diagram. (A) Diagram with the four genotypes. The blue number represents the genes shared by the tolerant genotypes while the red number indicates the genes shared by the salt-susceptible; (B) diagram of the salt-responsive genes in Syn86 by time point; (C) diagram of the salt-responsive genes in Zentos by time point; (D) diagram of the salt-responsive genes in the two sampled days from the ionic stress phase.

Five clusters with particular expression profiles included 96% of the salt-responsive genes from each genotype (see Appendix 4). According to the expression tendency, the main cluster of Zentos contained genes up-regulated at 15 min followed by a cluster of genes up-regulated at 30 min. The main cluster of Syn86 consisted of genes down-regulated at 30 min while the second cluster included genes up-regulated at this time point. The GO terms over-represented in the clusters (see Appendix 5) coincided mostly with the categories over-represented in the time points that showed greater expression magnitude as revealed by the expression tendency (Figure 9). The expression profiles of some over-represented gene categories relevant to the osmotic phase showed crucial differences in the two genotypes. These categories were compared with further detail in the next section. Moreover,

the link of their time course expression and the photosynthetic response at the osmotic phase was analyzed.

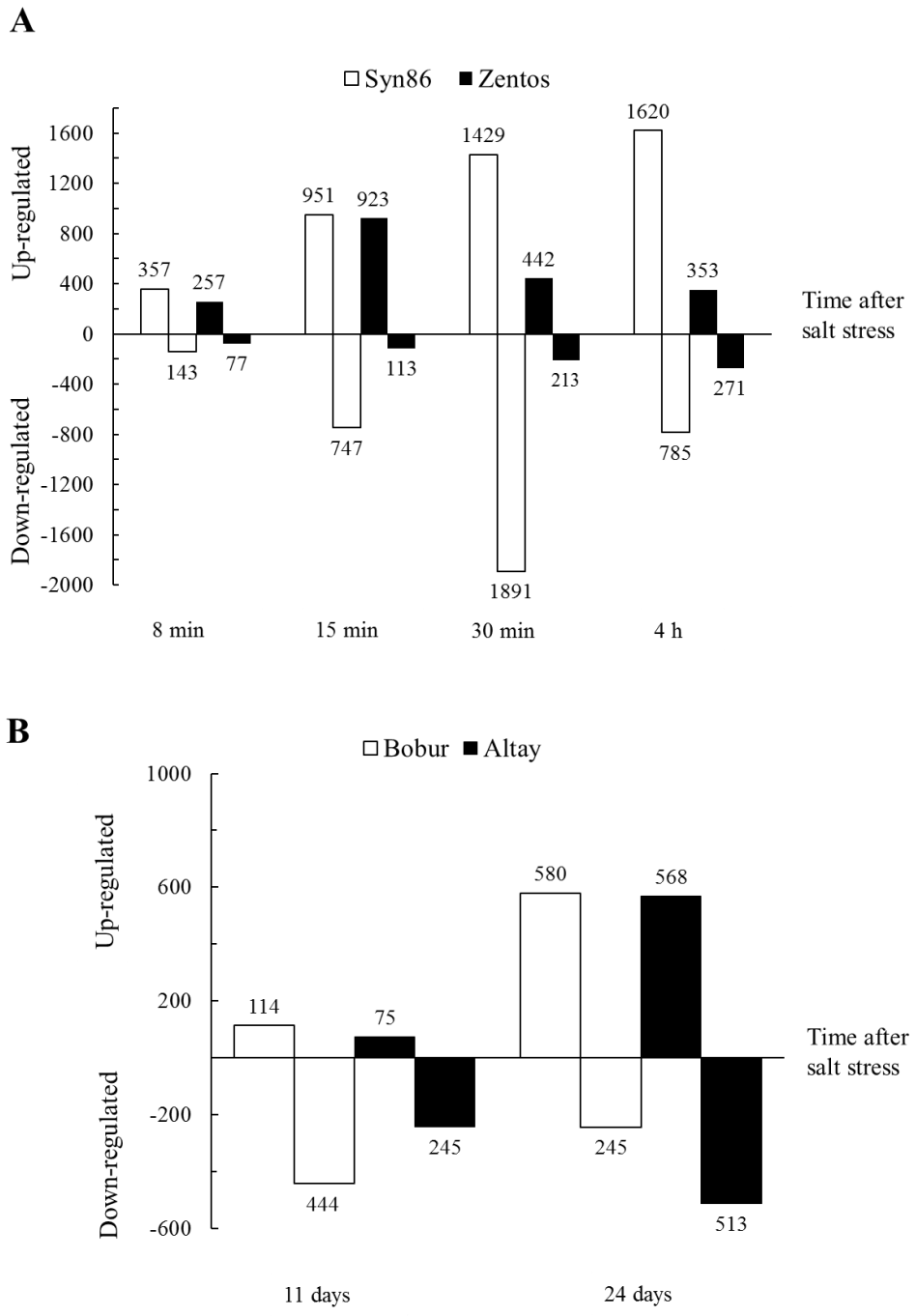

Figure 8. Distribution of up- and down-regulated salt-responsive genes across stress time points. (A) Osmotic phase and (B) ionic phase time points.

5.3.1. Time course of gene expression and photosynthesis rate during the osmotic phase

A comparison of the expression profiles of the salt-responsive photosynthesis-related, calcium-binding, oxidative stress response and xyloglucan:xyloglucosyl transferase activity genes was

performed in the contrasting genotypes (Figure 6). The expression of 101 photosynthesis-related genes is only shown in the susceptible genotype (Figure 6B) since these genes were not over-represented in the tolerant genotype. The up-regulation of eight genes related to electron transport in PSII was observed at 8 min ASE when the photosynthesis rate starts to decrease in Syn86 (Figure 6A). When the photosynthesis rate showed recovery but was still inhibited (Figure 6A), 91 transcripts from photosystems I and II categories were down-regulated at 30 min with relative expression values ranging from -1.1 to -3.4 (Figure 6B).

The LOESS curve from the 50 salt-responsive calcium-binding genes of the tolerant genotype revealed a gene up-regulation tendency at 15 min. Thirty-four transcripts were identified in this time point with relative expression values ranging from 1.0 to 3.4 (Figure 6C). From these genes, 32 contained an EF-hand calcium-binding domain. This term was not over-represented in Syn86 (p-value > 0.05) even though more genes showed differential expression than in Zentos. Thus, Syn86 presented heterogeneous expression patterns of 129 calcium-binding genes. Most of these genes (40) were down-regulated at 30 min with GFOLD values ranging from -1.0 to -3.1 (Figure 6C). The majority of them (29 genes) were components of the OEC from the PSII (Wang et al., 2019c). This result was also in line with the suppressed photosynthesis rate of Syn86 at this time point (Figure 6A). Other genes from this category were up-regulated in this genotype, 35 at 30 min and 21 at 15 min ASE.

On the other hand, 33 salt-responsive genes from the oxidative stress response category were identified in Zentos. Eight and 10 of them were up-regulated and showed relative expression values lower than 2.5 at 15 and 30 min ASE, respectively. The down-regulation of eight genes was observed at 4 h with expression values ranging from -1.0 to -2.4 (Figure 6D). In contrast, 59 genes in Syn86 displayed heterogeneous expression patterns with greater relative expression values than Zentos (Figure 6D). The expression values from the down-regulated transcripts fluctuated from -1.0 to -3.5 and the up-regulated genes revealed a GFOLD value range from 1.0 to 4.2. The greatest number of salt-responsive oxidative stress genes was observed at 30 min (38 transcripts) with both up- and down-regulated transcripts included. These greater transcriptional variations in the susceptible genotype were congruent with the inhibited photosynthetic activity observed in this time point (Figure 6A).

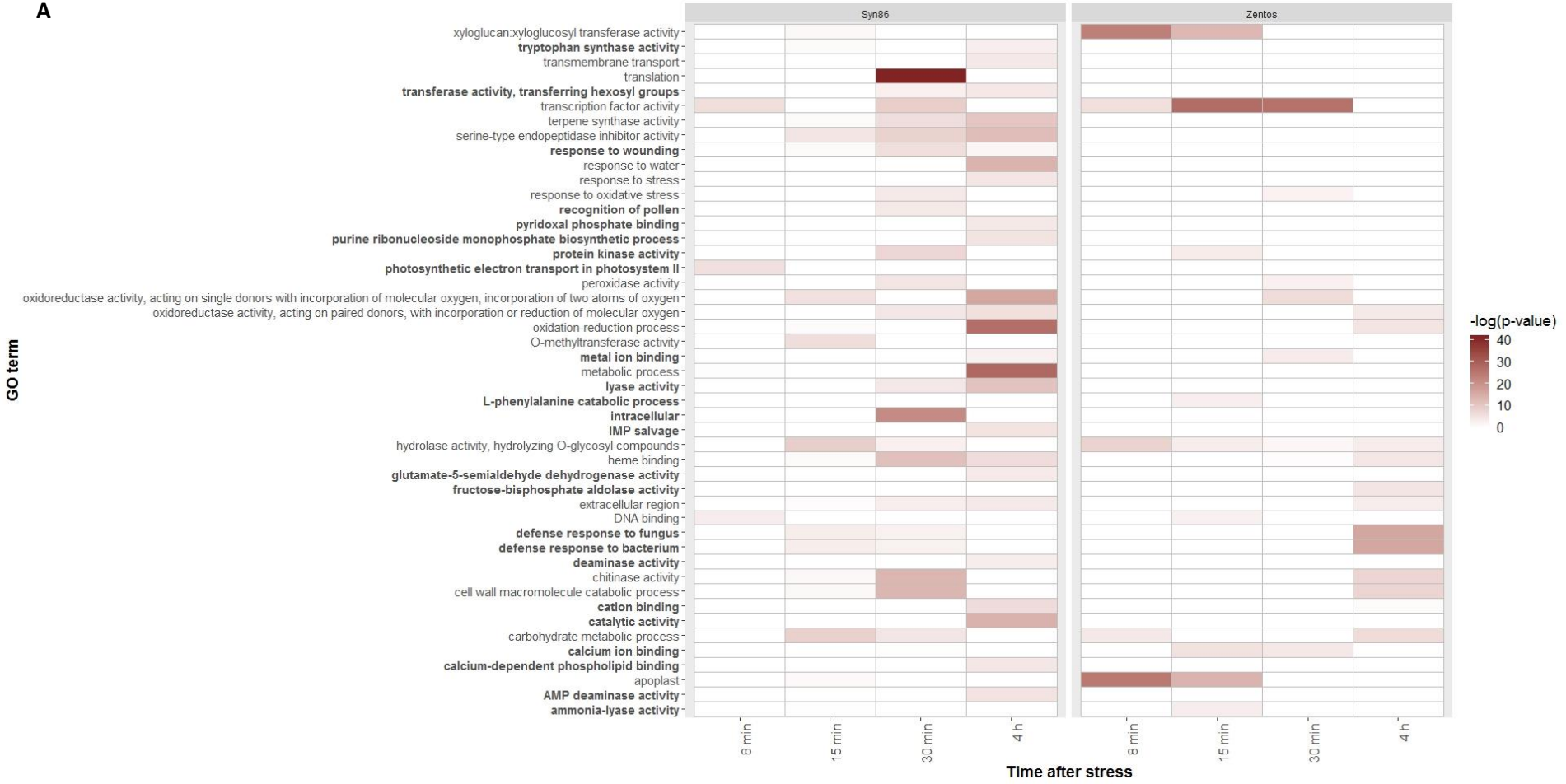
A
Syn86
Zentos
xyloglucan:xyloglucosyl transferase activity
tryptophan synthase activity
transmembrane transport
translation
transferase activity, transferring hexosyl groups
transcription factor activity
terpene synthase activity
serine-type endopeptidase inhibitor activity
response to wounding
response to water
response to stress
response to oxidative stress
recognition of pollen
pyridoxal phosphate binding
purine ribonucleoside monophosphate biosynthetic process
protein kinase activity
photosynthetic electron transport in photosystem II
peroxidase activity
oxidoreductase activity, acting on single donors with incorporation of molecular oxygen, incorporation of two atoms of oxygen
oxidoreductase activity, acting on paired donors, with incorporation or reduction of molecular oxygen
oxidation-reduction process
O-methyltransferase activity
metal ion binding
metabolic process
lyase activity
L-phenylalanine catabolic process
intracellular
IMP salvage
hydrolase activity, hydrolyzing O-glycosyl compounds
heme binding
glutamate-5-semialdehyde dehydrogenase activity
fructose-bisphosphate aldolase activity
extracellular region
DNA binding
defense response to fungus
defense response to bacterium
deaminase activity
chitinase activity
cell wall macromolecule catabolic process
cation binding
catalytic activity
carbohydrate metabolic process
calcium ion binding
calcium-dependent phospholipid binding
apoplast
AMP deaminase activity
ammonia-lyase activity
GO term
8 min
15 min
30 min
4 h
8 min
15 min
30 min
4 h
Time after stress
-log(p-value)
40
30
20
10
0

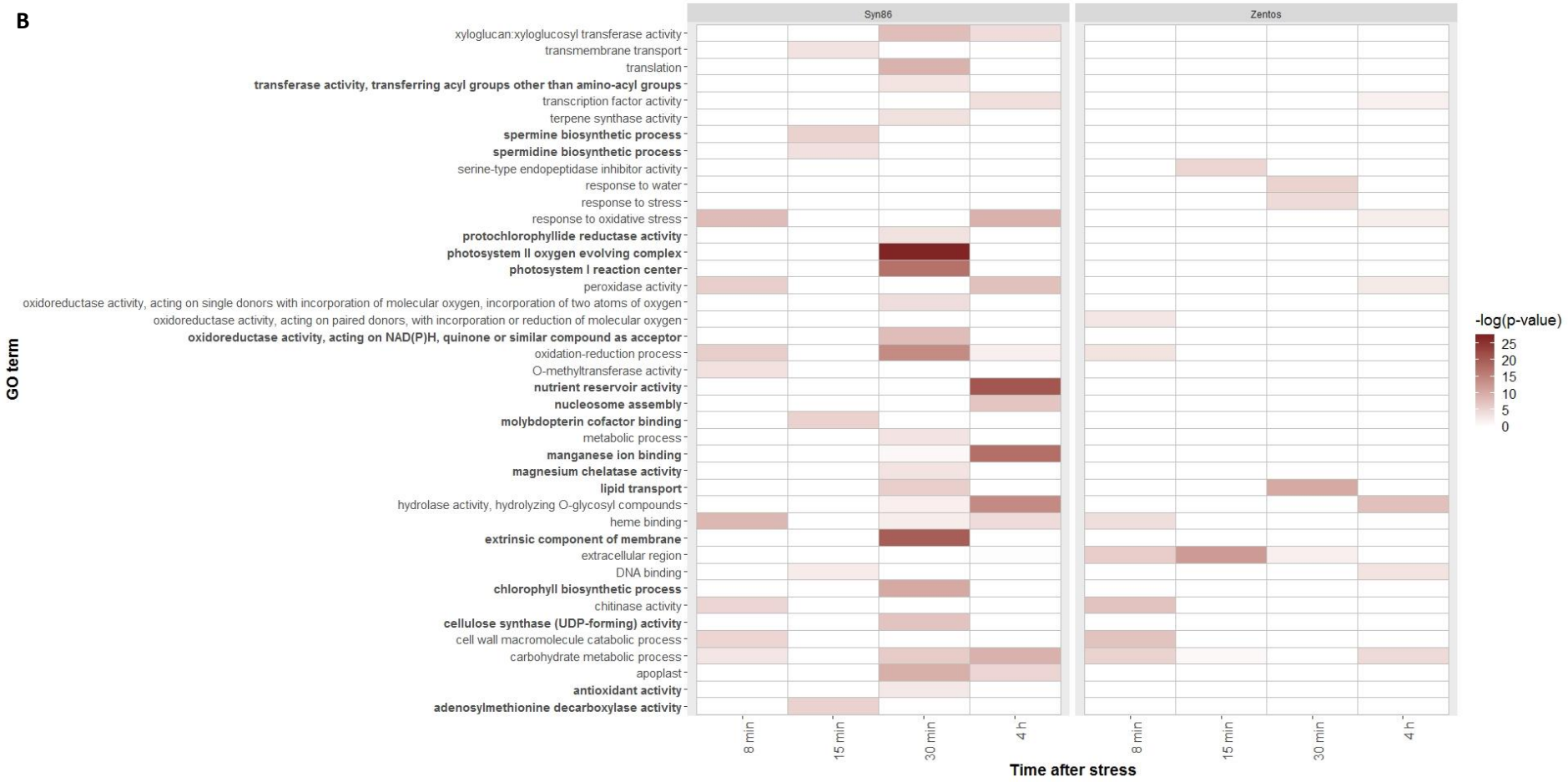
B
Syn86
Zentos
xyloglucan:xyloglucosyl transferase activity
transmembrane transport
translation
transferase activity, transferring acyl groups other than amino-acyl groups
transcription factor activity
terpene synthase activity
spermine biosynthetic process
spermidine biosynthetic process
serine-type endopeptidase inhibitor activity
response to water
response to stress
response to oxidative stress
protochlorophyllide reductase activity
photosystem II oxygen evolving complex
photosystem I reaction center
peroxidase activity
oxidoreductase activity, acting on single donors with incorporation of molecular oxygen, incorporation of two atoms of oxygen
oxidoreductase activity, acting on paired donors, with incorporation or reduction of molecular oxygen
oxidoreductase activity, acting on NAD(P)H, quinone or similar compound as acceptor
oxidation-reduction process
O-methyltransferase activity
nutrient reservoir activity
nucleosome assembly
molybdopterin cofactor binding
metabolic process
manganese ion binding
magnesium chelatase activity
lipid transport
hydrolase activity, hydrolyzing O-glycosyl compounds
heme binding
extrinsic component of membrane
extracellular region
DNA binding
chlorophyll biosynthetic process
chitinase activity
cellulose synthase (UDP-forming) activity
cell wall macromolecule catabolic process
carbohydrate metabolic process
apoplast
antioxidant activity
adenosylmethionine decarboxylase activity
GO term
8 min
15 min
30 min
4 h
Time after stress
-log(p-value)
25
20
15
10
5
0

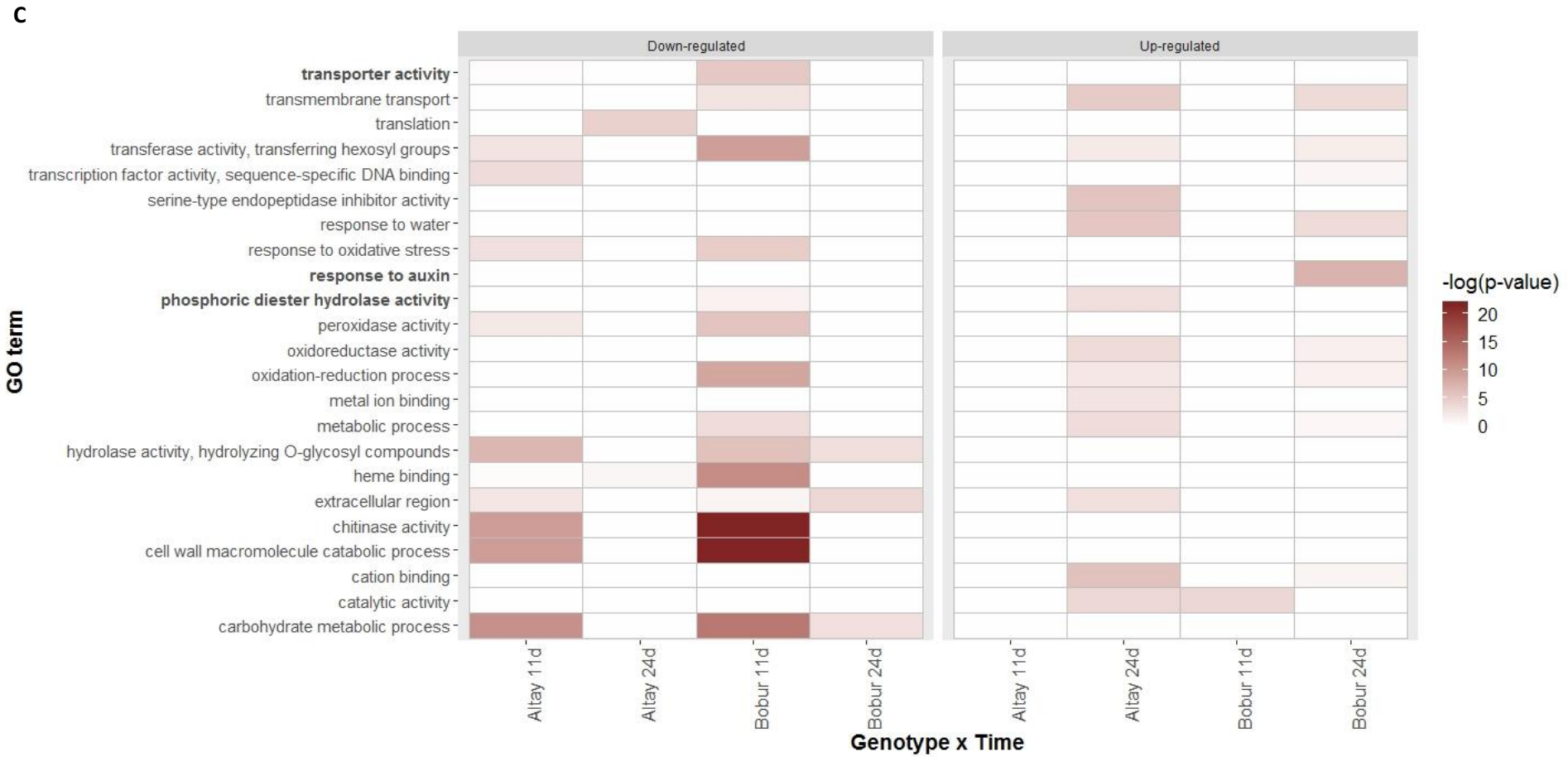

Figure 9. GO terms over-represented during the salt stress response. (A) Up-regulated and (B) down-regulated categories identified in the four stress time points sampled during the osmotic phase; (C) up- and down-regulated categories observed in the two stress time points from the ionic phase. Bold ontologies are categories specific for each heatmap. The $-\log_{10}$ transformation of the corrected p-values highlights the categories with greater significance that are therefore better over-represented.

Finally, all the salt-responsive cell wall genes corresponded to the xyloglucan:xyloglucosyl transferase activity category. Eighteen genes were identified in Zentos from which 14 showed up-regulation both at 8 and 15 min with GFOLD values ranging from 1.1 to 4.0 (Figure 6E). On the other hand, 24 genes from this category were observed in Syn86. The LOESS curve highlighted the down-regulation of 16 transcripts at 30 min (Figure 6E). The relative expression values of these transcripts ranged from -1.0 to -4.3.

5.3.2. Expression patterns of salt-responsive transcription factors during the osmotic phase

The analysis of TF families revealed the salt stress effect on the expression of AP2/ERF, WRKY, bZip, GATA and HSF families in the two genotypes. The additional families HD-Zip, Sigma Factor Like (SFL) and MADS were down-regulated in Syn86. In general, most TFs were up-regulated in Zentos at 15 min and presented greater relative expression values than Syn86 (Fig 10). AP2/ERF and WRKY were the most commonly expressed families in the two genotypes (Fig 10). The expression profiles from the AP2/ERF family in Syn86 showed two peaks with up-regulated genes at 8 and 30 min. On the other side, the members of this family were up-regulated at 15 min with greater relative expression values in Zentos (Fig 10). The WRKY type TFs presented the greatest up-regulation at 30 min in both genotypes. Zentos had greater relative expression values and Syn86 presented down-regulation of genes at 4 h ASE (Fig 10). The members of the GATA family were up-regulated at 15 min in Zentos and later at 30 min in Syn86. The LOESS curves evidenced the up-regulation in both genotypes of members of the bZip family at 4 h with greater relative expression values in the tolerant. Finally, the HSF family revealed opposite expression values in the contrasting genotypes as the corresponding transcripts were down-regulated in Syn86 and up-regulated in Zentos (Fig 10).

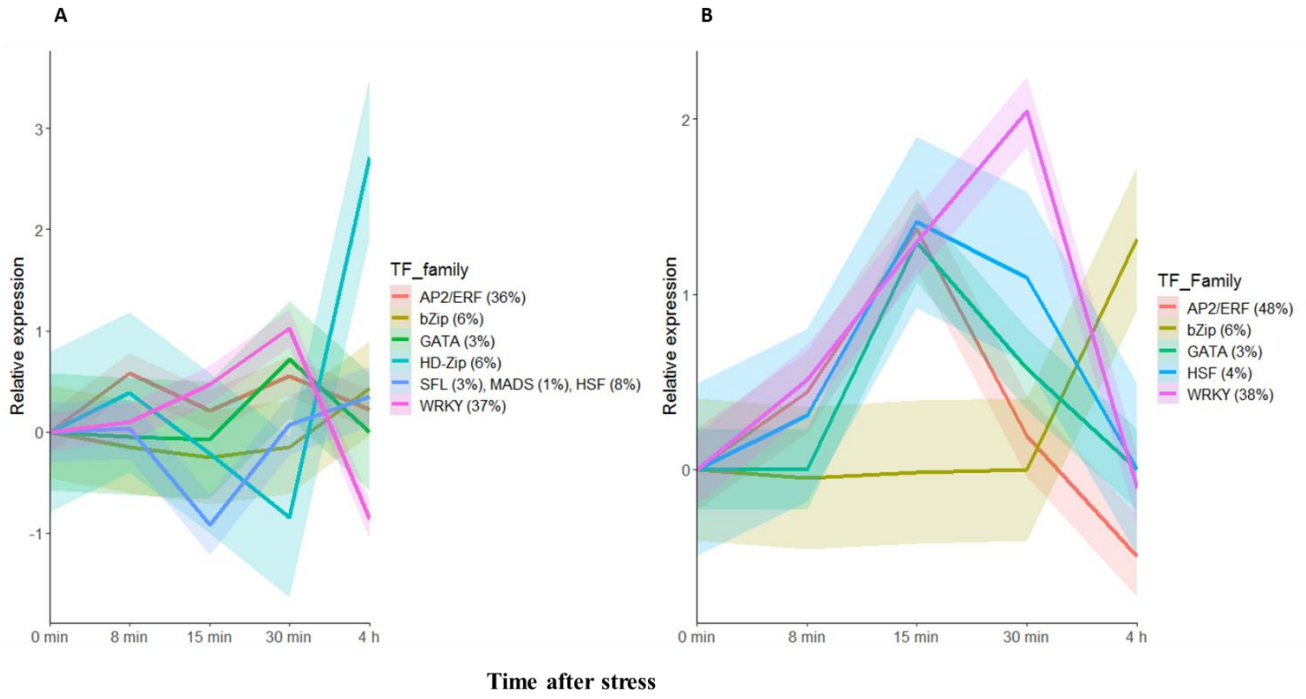

Figure 10. Expression patterns of salt-responsive transcription factor (TF) families in Syn86 (A) and Zentos (B) during the osmotic phase. A LOESS (locally estimated scatterplot smoothing) curve was fitted to represent the expression tendency of the members of each TF family and the shadows indicate the standard error of the relative expression values.

5.4. Comparative analysis of the ionic stress response

To better understand the later phase of plant reaction to salt exposure, a comparative transcription profiling at the ionic stress phase was performed. This analysis revealed the fewest transcriptional changes in Altay at 11 days (Figure 7D). The simultaneous differential expression of nine genes was identified across genotypes and time points (Figure 7D). At 24 days ASE more genes were up- than down-regulated, whereas the opposite pattern with more down-regulated genes was found at 11 days ASE in both genotypes (Figure 8B). In total, Altay2000 and Bobur contained 54% and 50% of down-regulated genes, respectively.

Three GO terms specific for this stress phase were identified and 11 from 23 categories shared the same stress effect in the two genotypes (Figure 9C). For instance, chitinase activity and response to oxidative stress were down-regulated in both genotypes while the response to water and transmembrane transport were up-regulated (Figure 9C). Up-regulated transcripts at 24 days ASE from the transmembrane transport category with potential roles on ion homeostasis were identified (Figure 11). This analysis revealed a greater number of ABC transporters and Na^{+}/Ca^{2+} exchangers

expressed in the tolerant genotype but greater relative expression values in the genes expressed in the susceptible genotype. On the other hand, translation was down-regulated in the tolerant genotype while metal ion binding was up-regulated. The up-regulation of the response to auxin category was observed in the susceptible genotype (Figure 9C).

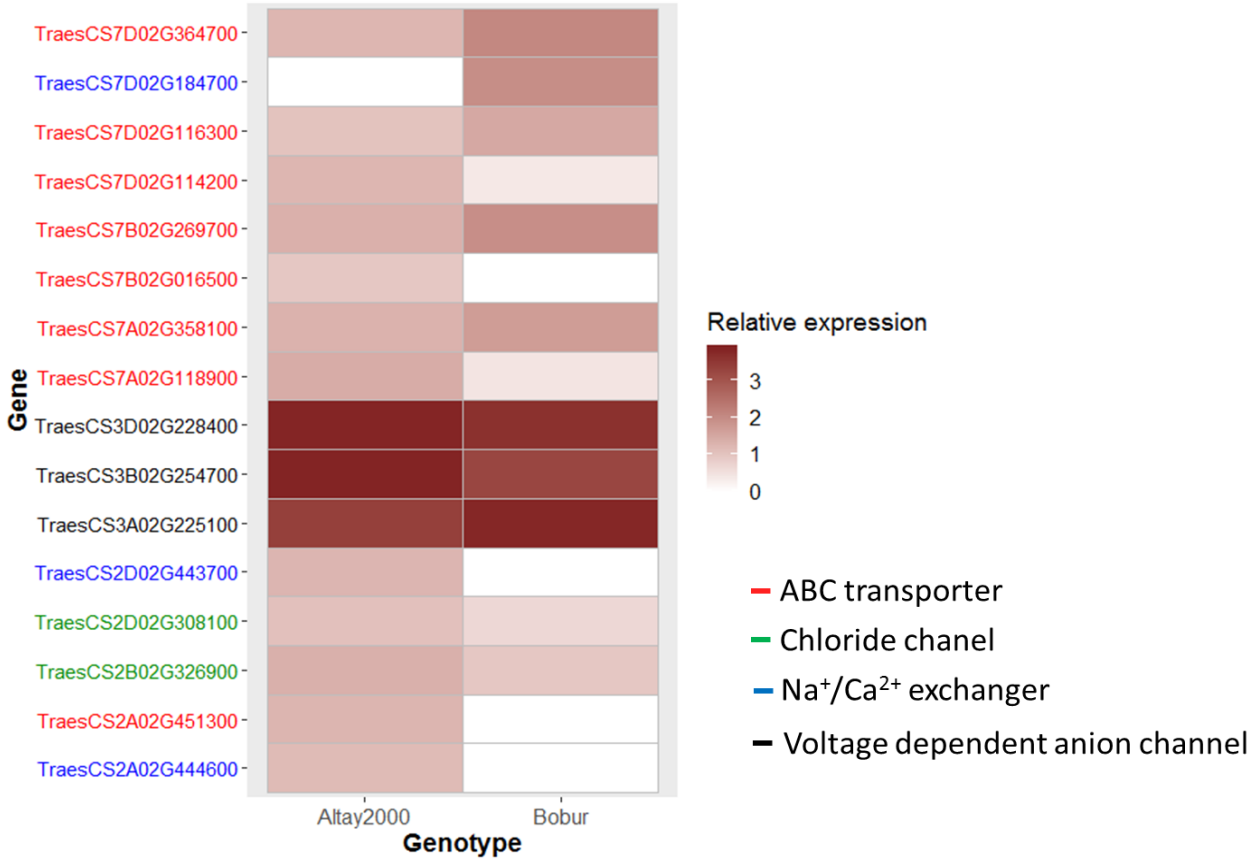

Figure 11. Relative expression (GFOLD value) of transcripts from the transmembrane transport category with role on ion homeostasis at 24 days after stress.

5.5. Comparative analysis of osmotic and ionic stress responses

The implementation of a transcriptomic approach allowed the comparison of the salt stress response during the osmotic and ionic phases in the four analyzed genotypes. Syn86 was the genotype presenting the highest number of salt-responsive genes, from three to five times more genes than the three cultivars. From all the differentially expressed genes, 86 were stress-responsive in the four genotypes while 50 and 232 transcripts were found in both tolerant and both sensitive genotypes, respectively (Figure 7A).

A total of 20 GO terms were over-represented in both the osmotic and ionic phases (Figure 9). The translation category was down-regulated in the salt-sensitive Syn86 at the osmotic phase and the tolerant Altay2000 at the ionic phase. The term serine-type endopeptidase inhibitor activity presented opposite relative expression values in the tolerant genotypes of both salt stress phases. These genes were down-regulated in the tolerant genotype and up-regulated in the salt-sensitive one during the osmotic phase. On the contrary, this category showed up-regulation in the salt-tolerant genotype at the ionic stress phase. The response to oxidative stress category was both up- and down-regulated in the contrasting genotypes from the osmotic stress phase while it was only down-regulated in both genotypes studied during the ionic phase.

5.6. Identification of candidate QTGs

To unravel candidate QTGs that might contain alleles controlling salt stress-related traits, salt-responsive transcripts within QTL intervals were identified. Figure 12 and Table 4 present the candidate QTGs from two QTL identified in an association panel (Oyiga et al., 2018) and an AB-QTL mapping population (Dadshani, 2018) on the chromosome 2A. A 36 Mbp LD block was covered by the QTL interval detected by the marker RAC875_c38018_278. This marker showed an effect on shoot fresh weight after salt stress in the association mapping panel. Three differentially expressed genes were found in this region, one salt-responsive in the sensitive genotype and two in the tolerant (Table 4, Figure 12). Among them, TraesCS2A02G395000 showed the strongest stress response since the gene coding an oxoglutarate/iron-dependent dioxygenase was suppressed in the salt-susceptible genotype with an expression value of -2.4. On the AB-QTL mapping population, a 9 Mbp LD block constituted the QTL interval from the marker BS00041707_51. A marker-trait association with kernel weight under stress was discovered with this SNP. This region included two up-regulated genes in Syn86 with similar expression levels that coded for an amino acid transporter and a copper amine oxidase. The five candidate QTGs were stress-responsive in other studies (Table 4).

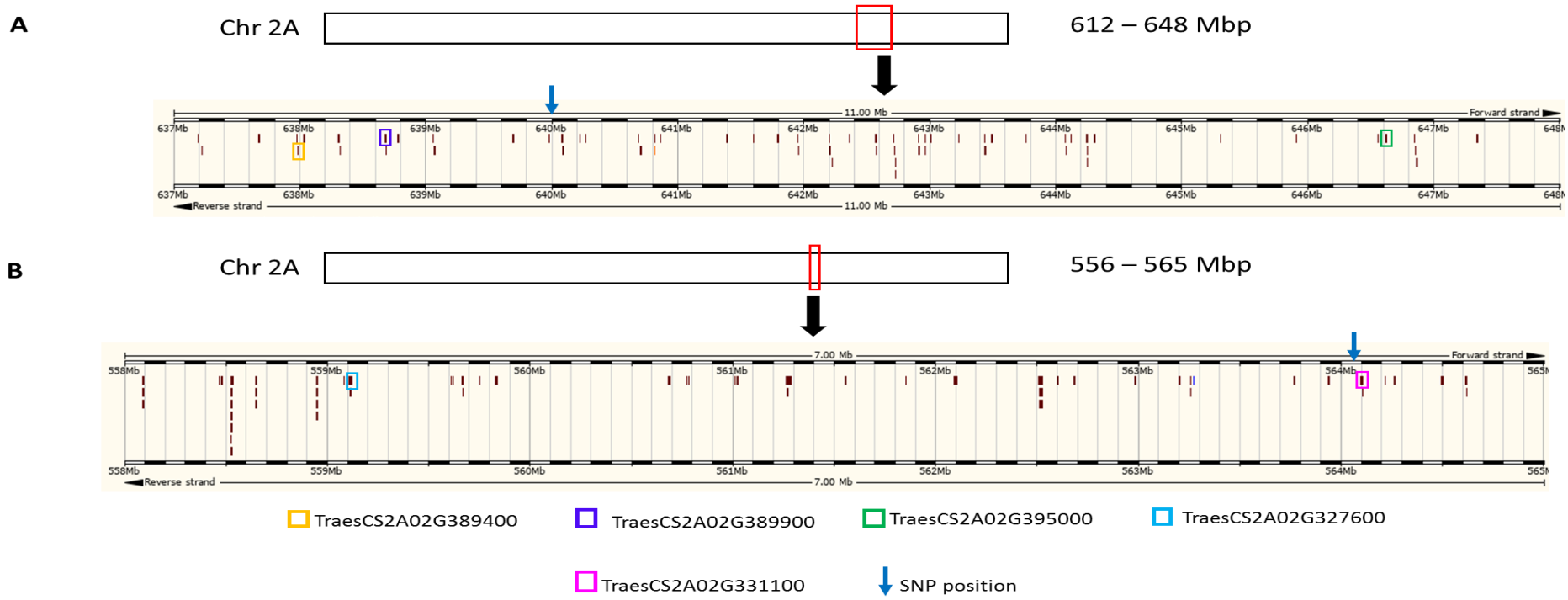

Figure 12. Overview of salt-responsive genes in QTL intervals in chromosome 2A. (A) Marker RAC875_c38018_278 detected by association mapping (Oyiga *et al*., 2018) and (B) marker BS00041707_51 detected by AB-QTL mapping (Dadshani, 2018). Salt-responsive genes are marked with colors. The chromosome regions were retrieved from Ensembl plants release 46 (Howe *et al*., 2020).

Table 4. Differentially expressed genes in LD blocks of markers with effect on salt stress-related traits in the Chr 2A.

Marker[a] R^2 (%)	**Gene relative expression[d]**	**Annotation[e]**	**Abiotic stress effect[f]**
RAC875_c38018_278[b]	*TraesCS2A02G389400*: **1.5**	Leucine zipper, homeobox-associated	1) ↑, 2) ↑
	TraesCS2A02G389900: **1.0**	Glutamate dehydrogenase	1) ↑, 2) ↑
12.98	*TraesCS2A02G395000*: *-2.4*	Oxoglutarate/iron-dependent dioxygenase	1) ↓
BS00041707_51[c]	*TraesCS2A02G327600*: *2.1*	Copper amine oxidase	1) ↑, 2) ↑
12.5	*TraesCS2A02G331100*: *1.8*	Amino acid transporter	1) ↑

[a] Marker names according to Wang *et al.* (2014*b*)

[b] From the mapping study by Oyiga *et al.* (2018)

[c] From the mapping study by Dadshani (2018)

[d] GFOLD values from tolerant genotypes are bold and from the susceptible are in italics.

[e] Based on the Interpro results from the RefSeqv1.0 annotation (Alaux *et al.*, 2018).

[f] Abiotic stress response based on studies deposited in the wheat expression atlas expVIP (Borrill *et al.*, 2016). 1) Drought and heat (Liu *et al.*, 2015) and 2) cold (Li *et al.*, 2015). The direction of the arrows indicates the stress effect on expression, ↑ when the gene is up-regulated and ↓ when is down-regulated.

5.7. Expression and sequence analysis of calcium-binding genes

5.7.1. Comparison of the expression profiles of salt-responsive genes from the calcium-binding category

Clusters of expression patterns were determined for the salt-responsive calcium-binding genes in Syn86 and Zentos (Figure 13). The tolerant genotype showed five clusters, the main one with genes up-regulated at 15 min followed by a group of transcripts up-regulated both at 15 and 30 min (Fig 13A). Seven clusters were defined in the susceptible genotype. Clusters I and II grouped the greatest number of genes with down- and up-regulated transcripts at 30 min, respectively (Figure 13B). The cluster I contained mainly OEC proteins (29) and annexins (5) while the cluster II included EF-hand domain (14), EGF-like (9) and CNX/CRT (4) proteins. There were 27 common salt-responsive genes from this category in the two genotypes (Figure 13C). Most of these transcripts were up-regulated until 30 min with greater relative expression values in Zentos compared to Syn86. Some of them were down-regulated in the susceptible genotype at 4 h ASE (Figure 13C). Twenty-two of these genes corresponded to the CML type.

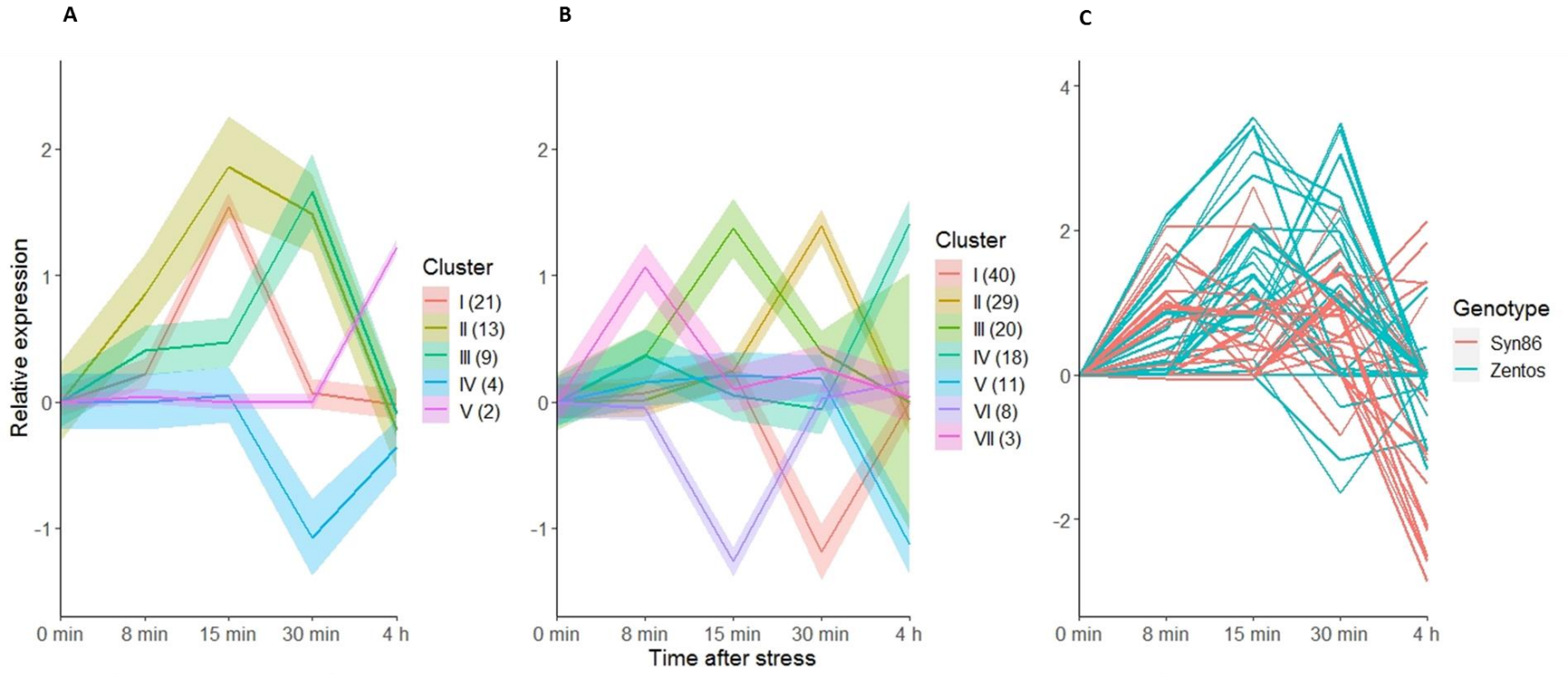

Figure 13. Expression profiles of salt-responsive genes with a calcium-binding domain at the osmotic phase. Clusters from Zentos (A) and Syn86 (B) in which a LOESS (locally estimated scatterplot smoothing) curve was fitted to represent the expression tendency of the transcripts from each group and the shadows indicate the standard error of the relative expression values. Expression profiles of 27 transcripts identified in both genotypes (C).

5.7.2. Salt-responsive calcium-binding genes classification and phylogenetic analysis of EF-hand containing proteins

The proportion of salt-responsive genes coding EF-hand and non-EF-hand domains was determined in Syn86 and Zentos (Figure 14). The tolerant genotype showed 92% of calcium-binding genes containing EF-hands domains from which 76% was without any other functional domain. The non-EF-hand group was a minority (8%) and only contained genes coding EGF-like domains (Figure 14). A greater percentage of genes coding non-EF-hand domains was observed in Syn86 (53%) which also presented greater diversity of categories within the two groups of calcium-binding proteins (Figure 14). Most of the non-EF-hand type genes coded for OEC proteins (24%) followed by EGF-like domain proteins (13%). The EF-hand group consisted mainly of proteins that lacked any other functional domain (33%) followed by EF-hand proteins with other additional domains (5.5%). In this group, proteins as caleosins (1.5%) and phosphoglycolate phosphatases (2%) were included.

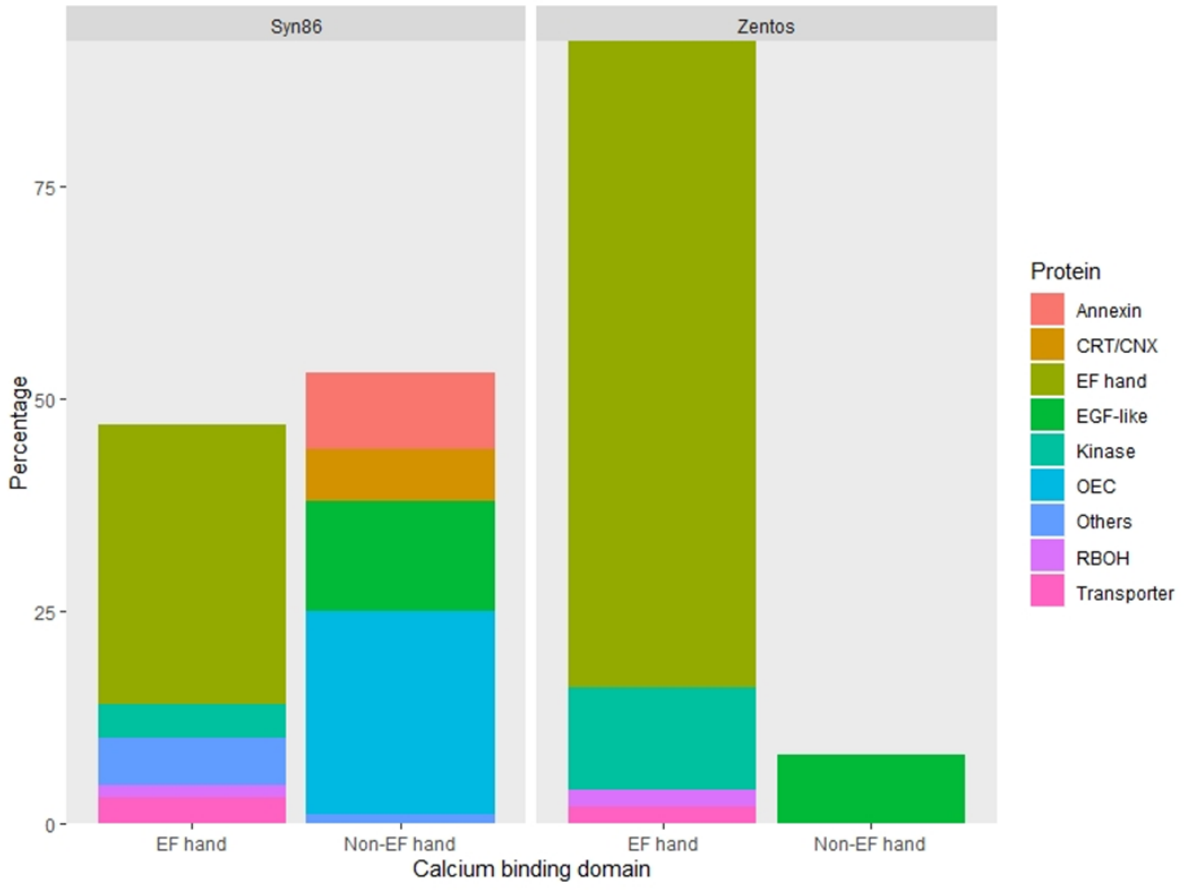

Figure 14. Distribution of protein types with EF-hand or non-EF-hand domains coded by the salt-responsive calcium-binding genes identified in the contrasting genotypes studied at the osmotic phase.

The phylogenetic analysis with EF-hand domain proteins revealed the homologies and the clustering with related CaM/CML, CBL, CPK and RBOHs from *A. thaliana.* The subgroup of CaM proteins was with the highest statistical support (98%) in the CaM/CML analysis (Figure 15). Five salt-responsive genes from Syn86 were in the CaM cluster with similarity to CaM1, CaM4 and CaM7 (Figure 15). From all genes containing an EF-hand domain, 57 (72%) corresponded to the CML type and were distributed across several clusters with *Arabidopsis* proteins presenting mostly low bootstrap values (<50%) (Figure 15). This analysis therefore revealed few clear CaM and CML orthologs in *Arabidopsis*. The salt-responsive *TraesCS1B02G370900* from Syn86 was the only transcript from the CBL type and was ortholog from CBL8.

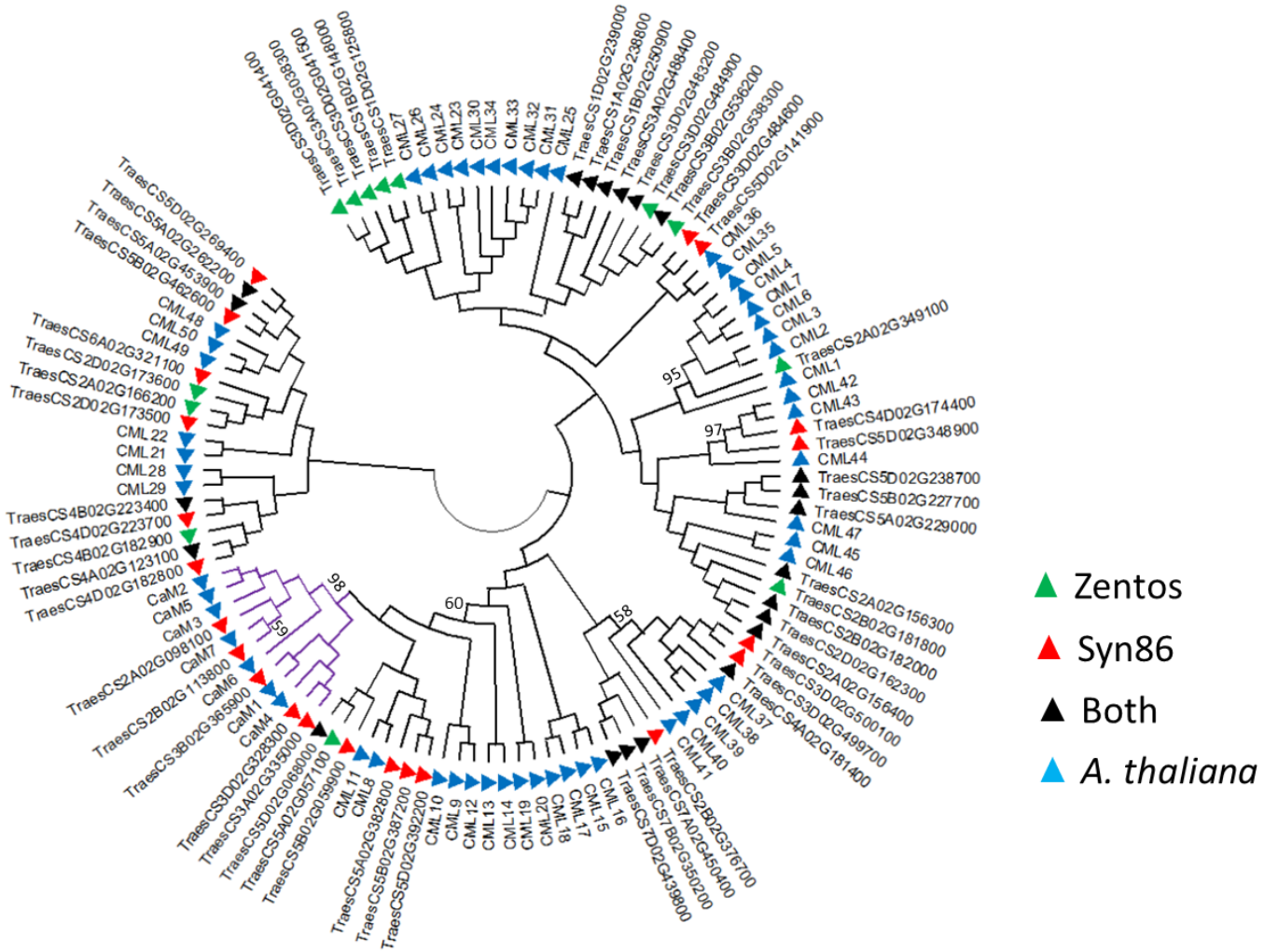

Figure 15. Dendrogram of CaMs (purple) and CMLs (black) amino acid sequences from *Arabidopsis thaliana* and coded by the corresponding salt-responsive genes from Zentos and Syn86. The consensus phylogenetic tree was constructed with MEGA X (Kumar *et al.*, 2018) using the Neighbour-Joining method and through a bootstrap analysis of 3000 replicates. Clusters of wheat and *Arabidopsis* proteins with bootstrap values > 50 are shown.

All the differentially expressed genes coding EF-hand proteins with kinase domain were from the CPK type and clustered with good statistical support in subgroups I, III and IV from the classification proposed by Yip-Delormel and Boudsocq (2019) (Fig 16). Three wheat genes were found in the subgroup I. From these, two homeologous genes located in the chromosomes 5A and 5B were up-regulated in Zentos at 15 min and were included in a cluster with CPK1, CPK2 and CPK20. The subgroup III contained two wheat genes and three where observed in the subgroup IV. From three RBOH proteins of wheat, two clustered with RBOHD and the third presented similarity with RBOHB from *A. thaliana* forming groups with good statistical support (Figure 17). The wheat RBOHD orthologs were up-regulated, one in Zentos at 15 min and the other in Syn86 at 30 min.

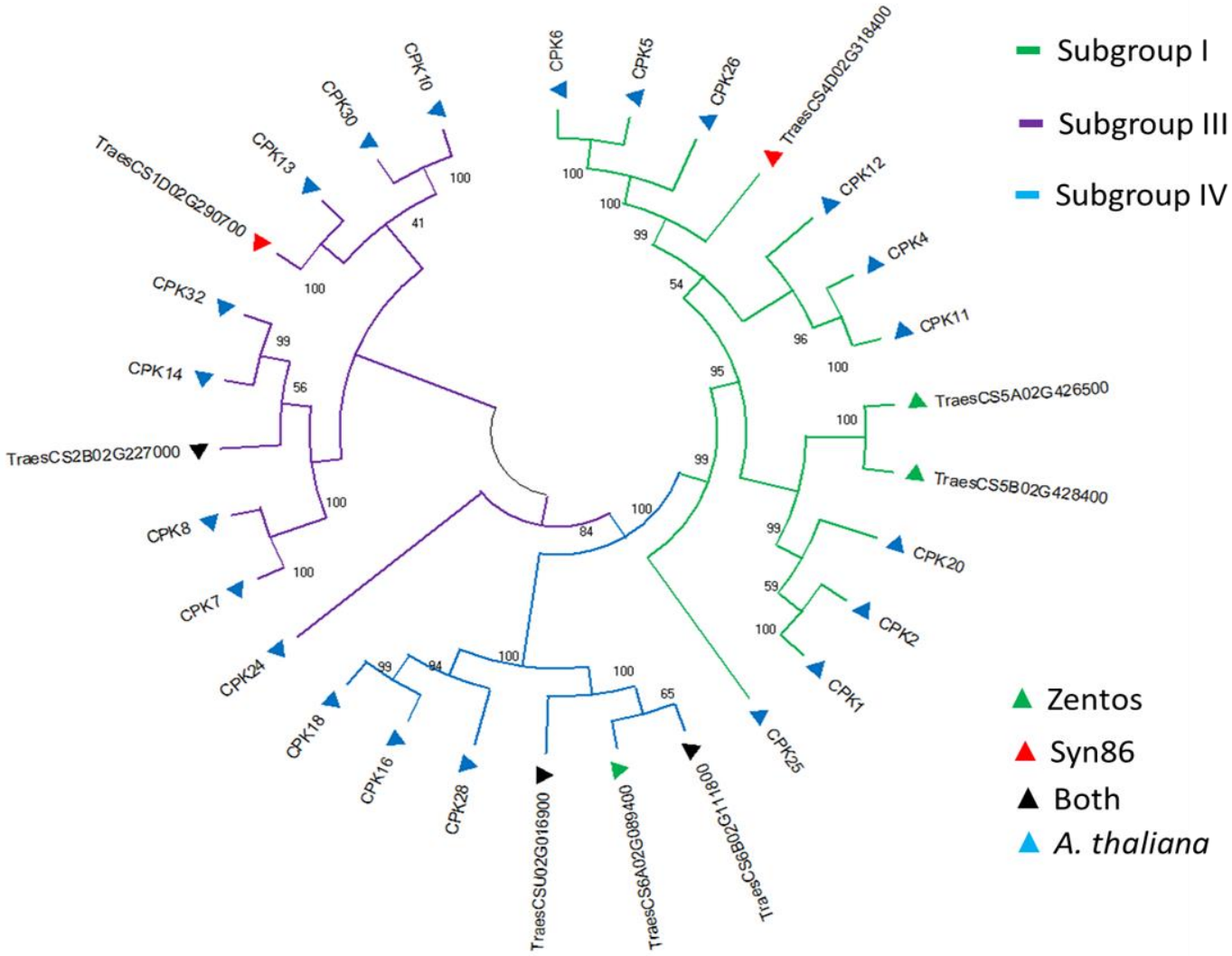

Figure 16. Dendrogram of CPKs amino acid sequences from *Arabidopsis thaliana* and coded by the corresponding salt-responsive genes from Zentos and Syn86. The consensus phylogenetic tree was constructed with MEGA X (Kumar *et al.*, 2018) using the Neighbour-Joining method and through a bootstrap analysis of 3000 replicates.

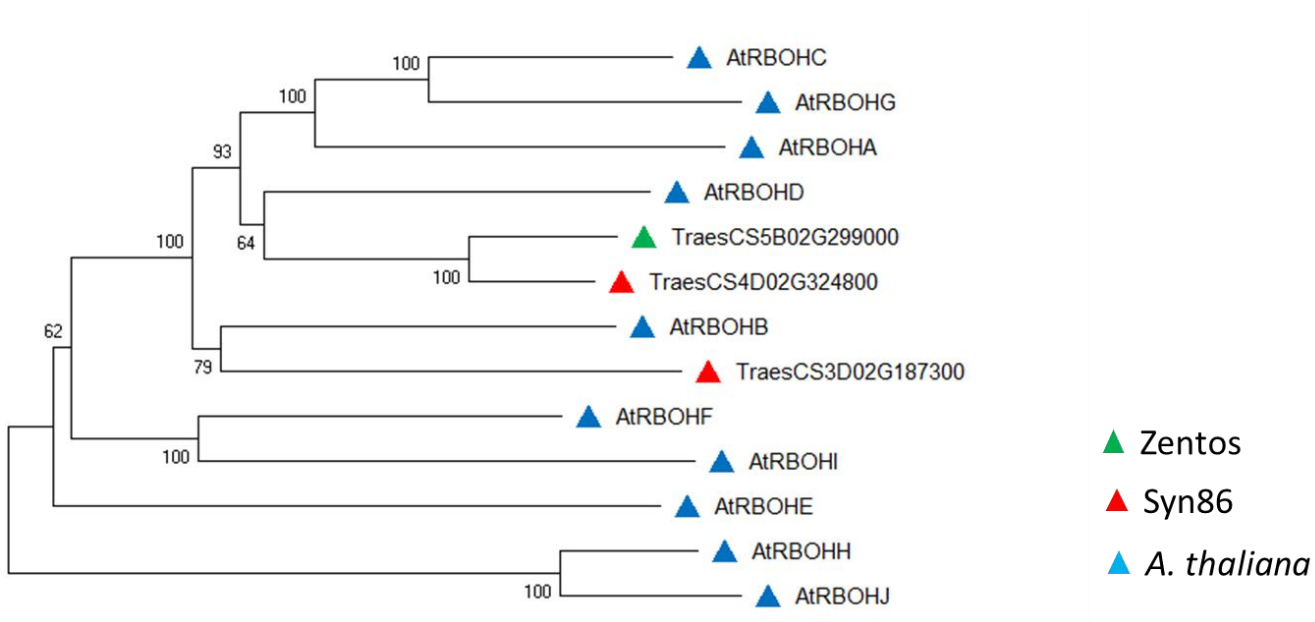

Figure 17. Dendrogram of RBOHs amino acid sequences from *Arabidopsis thaliana* and coded by the corresponding salt-responsive genes from Zentos and Syn86. The consensus phylogenetic tree was constructed with MEGA X (Kumar *et al.*, 2018) using the Neighbour-Joining method and through a bootstrap analysis of 3000 replicates.

5.7.3. RT-qPCR analyses in roots and leaves

The two genes studied by RT-qPCR corresponded to the CML type; TraesCS2D02G173600 was in a cluster with CML48, CML49, CML50 while TraesCS5D02G238700 was in a cluster with CML47 (Figure 15). These genes will be referred as CML-2D and CML47-5D, respectively. Based on the amplification efficiency comparison of the primers through the slope values (Appendix 6), TaEf-1.1 was the reference gene selected for the analysis of CML47-5D and the analysis of CML-2D expression in roots. The reference gene TaEf-1.2 was selected for the study of CML-2D expression in leaves. The melting curves of the PCR products revealed single peaks that indicated specific amplification and absence of primer dimers (Appendix 7).

The time-course expression of CML-2D and CML47-5D in leaves and roots of Syn86 and Zentos is shown in Figure 18. CML-2D was down-regulated at 4 h in leaves from Syn86 and in the other time points it was not stress-responsive (Figure 18A). This gene was up-regulated in Zentos in all time points except at 10 h; especially at 24 and 48 h the relative expression values were high (Figure 18A). The assessment of the expression of this gene in roots indicated that it was not salt stress-responsive

in this organ (Figure 18B). In this case, the RT-qPCR and transcriptomic relative expression values showed few concordance as the latter analysis detected down-regulation in Zentos (Appendix 8).

CML47-5D was mostly up-regulated in both organs and revealed greater relative expression values in leaves than in roots (Figure 18C, D). The relative expression values of this gene were greater than those measured in CML-2D and it was up-regulated until 30 min in leaves and until 4h ASE in roots. When compared to Zentos, Syn86 presented the greater mean relative expression values across all time points except at 8 min in roots. Syn86 showed the greater relative expression values at 15 min in both organs whereas in the tolerant genotype the greater values were observed at 15 min in leaves and 8 min in roots (Figure 18C, D). The RT-qPCR analysis of this transcript confirmed the up-regulation detected in the transcriptomic analysis at 8 and 15 min in Syn86 (Appendix 8).

5.7.4. Transcription factor binding site analysis

The analysis of the gene sequence of CML-2D and CML47-5D did not reveal polymorphisms in the contrasting genotypes. A deletion of seven nucleotides in Syn86 and three SNPs were found in the promoter sequence of CML2D (Appendix 9) while a single nucleotide insertion in Zentos and two SNPs were identified in the promoter of CML5D (Appendix 9). The TF binding site analysis revealed 11 TF families with potential binding in regions adjacent to polymorphisms. From these families, six were common in both promoters (Figure 19). The identification of bZip, GATA and ERF binding sites in the promoters (Figure 19) coincided with the identification of members from these families up-regulated under salt stress conditions in the transcriptomics analysis (Figure 10).

5.7.5. SNPs identification in MACE reads and miRNA binding analysis

A total of 82 SNPs in 47 genes were scored in the MACE reads of the salt-responsive calcium-binding genes studied (Appendix 10). Most of the SNPs were located in 3'-UTR regions (52) followed by exons (21), unpredicted 3'-UTR (6) and introns (3). There are eight SNPs in six genes that contain potential miRNA binding sites in their surrounding regions (Table 5). From these genes, three are salt-responsive in Syn86, two are in Zentos and one is in both genotypes. The possible effects of the SNP alternative allele in the miRNA affinity are the creation/loss of binding sites or the increased/reduced binding (Table 5). Five of these potential miRNA have been reported under biotic or abiotic stress stimuli in other studies. For instance, responsive to salt and drought stresses in wheat is reported miR171a (Table 5). This miRNA seems to bind to the Zentos gene sequence to regulate the expression of TraesCS5B02G428400.

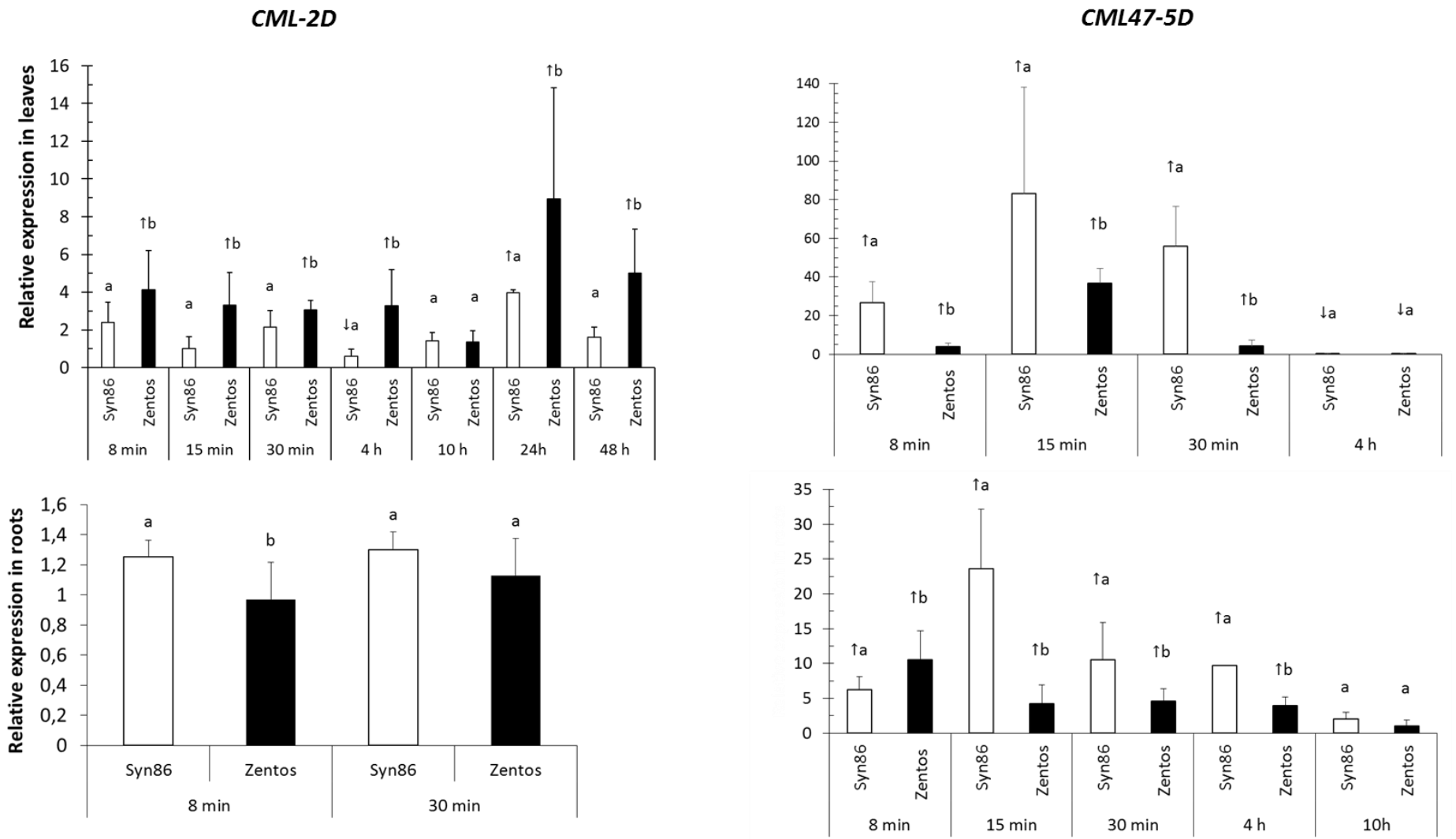

Figure 18. Relative expression values from *CML-2D* (left column) and *CML47-5D* (right column) calculated with the ΔΔCt method (Livak & Schmittgen, 2001) in leaves and roots. Different letters show significant differences in mean values from the two genotypes ($p < 0.05$). Mean relative expression values > 2.0 or < 1.0 ($p < 0.05$) indicated up-regulation (↑) or down-regulation (↓) of genes, respectively.

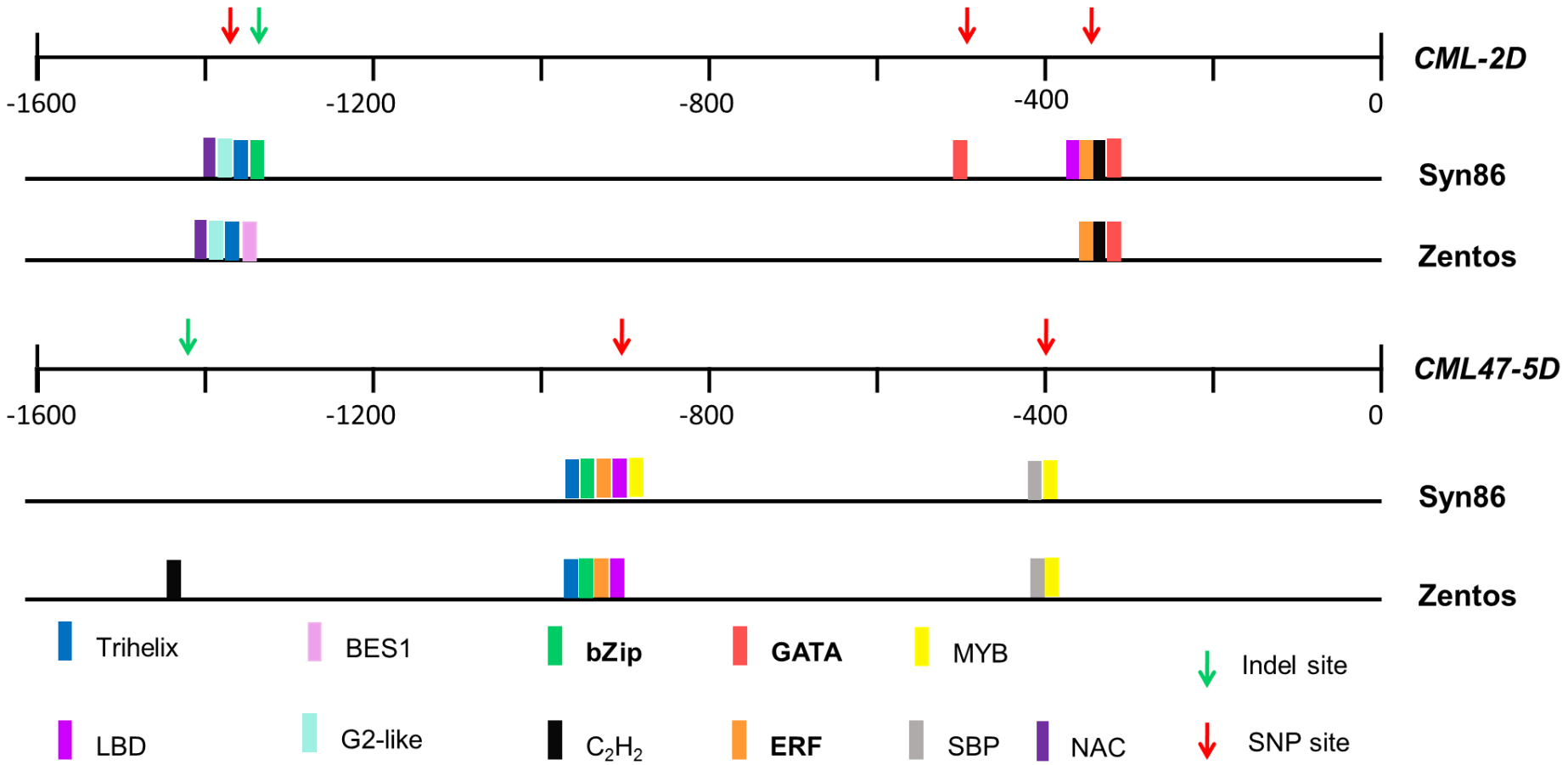

Figure 19. Transcription factor families with predicted binding to the adjacent regions of the polymorphisms identified in the promoters of the two calcium-binding genes studied by RT-qPCR. Families with bold letters are salt stress-responsive as indicated in Figure 10. The binding prediction was performed with the PlantTFDB (v 5.0) database (Jin *et al.*, 2017).

Table 5. Overview of the SNPs identified in salt-responsive calcium-binding genes with potential miRNA binding in the adjacent sequence to the polymorphisms predicted with the psRNAtarget tool (Dai et al., 2018).

Gene	SNP Position	Alternative Allele[a]	Location in gene	Salt-responsive	miRNA binding[b]	Effect alternative allele	Stimulus
TraesCS1A02G239600	426881024 426881030	**T** A	3'-UTR	Syn86 ↓ ↑	ath-miR861-5p	loss of binding site	Nitrogen starvation (Liang *et al*., 2012)
TraesCS1B02G251900	444688564	T	3'-UTR	Syn86 ↓↑	ath-miR472-5p ath-miR851-3p	loss of binding site increased binding	Insect and bacteria (Barah *et al.*, 2013) Nitrogen starvation (Liang *et al.*, 2012)
TraesCS6B02G227900	354955972	G	intron	Syn86 ↓	ath-miR3933	creation of binding site	Not reported
TraesCS2A02G166200	118488650	**G**	3'-UTR	Zentos ↓↑	ath-miR5649a ath-miR5649b	creation of binding site	Not reported
TraesCS5B02G428400	604067974	G	3'-UTR	Zentos ↑	tae-miR5050	reduced binding	Not reported
	604068120	A	3'-UTR		tae-miR171a ath-miR171a-3p	loss of binding site	Drought (Alptekin *et al*., 2017), salt (Wang *et al*., 2015)
TraesCS7B02G350200	607529797	**G**	exon	Both ↓↑	ath-miR861-3p	reduced binding	Not reported
					ath-miR775	creation of binding site	Hypoxia (Moldovan *et al.*, 2010)

[a] Bold nucleotides were found in Zentos

[b] ath: *A. thaliana*, tae: *T. aestivum*

6. Discussion

This study revealed a wide diversity of transcriptional changes resulting from the salt stress application during the osmotic and ionic phases in the genotypes studied. The GO categories from these salt-responsive genes and their suppression or over-expression were in line with the physiological measurements performed in the contrasting genotypes at both stress phases. Furthermore, this transcriptomics analysis facilitated the identification of potential QTGs within QTL intervals detected in two mapping studies to dissect salt stress-related traits. The second part of this study focused on the analysis of the transcriptional changes in the calcium-binding category during the osmotic phase. Crucial differences in the expression patterns and the types of calcium-binding domains were observed in the contrasting genotypes. Some polymorphisms were identified in promoter sequences and in 3'-ends of the genes providing indications on plausible genetic mechanisms that might influence the observed transcriptional differences.

6.1. Detection of novel regions with transcription in bread wheat

Besides uncovering the dynamic transcriptomic response during salt stress, the MACE-derived sequence analysis conferred evidence of two types of novel regions with transcription in wheat. Firstly, the differential expression analysis assigned a putative role in the salt stress response to in silico predicted novel transcripts. These novel salt-responsive transcripts might enrich the wheat variable pangenome that represents 39% of the pangenome according to the analysis of the whole genome of 18 cultivars (Montenegro et al., 2017). Secondly, the detection of reads beyond predicted 3'-ends of genes might indicate longer transcription and can contribute to the improvement of the current gene models (IWGSC, 2018). The discovery of these reads suggests that some current gene model predictions were based on transcripts with incomplete read coverage in the region possibly due to low expression levels in previous transcriptomic experiments (Roberts et al., 2011). The genes identified with extended transcription can be included in computational prediction approaches to better define gene structures (Inatsuki et al., 2016; Tzfadia et al., 2018). The RT-qPCR validation of both novel transcripts and 3'-ends is necessary to confirm the transcription of these regions.

6.2. Gene categories linked to the differential photosynthesis rate during the osmotic phase

The overlapping expression densities from Syn86 and Zentos indicated an adequate expression normalization of the libraries to perform the detection of salt-responsive transcripts (Klaus and Huber, 2016). The osmotic stress experiment revealed the early up-regulation and the posterior down-regulation of photosynthesis-related transcripts in the susceptible genotype. The up-regulation at 8

min of the electron transport in the PSII category can be linked to the over-excitation of this system which leads to an increase in the generation of ROS (Parihar et al., 2015; Foyer, 2018). The down-regulation of photosynthesis-related genes at 30 min ASE might be a consequence of excessive ROS accumulation that inhibits the repair of photodamaged PSII at both transcriptional and translational levels (Allakhverdiev et al., 2002; Murata et al., 2007; Saibo et al., 2009; Queval and Foyer, 2012). Nevertheless, the results indicate that plants can recover the expression levels of photosynthesis-related genes as the transcriptional suppression of photosynthesis was not observed at 4 h ASE (Figure 1B).

The reduced oxidative stress response of Zentos can be attributed to a restrained ROS production which might stimulate the growth under stressful conditions (Queval and Foyer, 2012). The reduced photosynthesis inhibition of this genotype can therefore be linked to lower oxidative damage of the photosynthetic apparatus. On the other side, the susceptible genotype revealed the down- and up-regulation of genes implicated in oxidative damage protection with greater relative expression values than the tolerant genotype (Figure 1E, F). These results indicate that salt stress exerted a stronger effect on the oxidative damage protection system of Syn86 at the transcriptional level which supports its greater photosynthesis inhibition (Queval and Foyer, 2012). Additional studies of ROS contents under stress would be beneficial to link them with the observed transcriptional changes in the contrasting genotypes.

The over-representation of genes coding for calcium-binding proteins at 15 min in Zentos agrees with earlier timing of calcium and ROS signaling proposed for salt-tolerant genotypes (Ismail et al., 2014). These molecules interact in signaling pathways to regulate salt stress response and to trigger systemic responses (Ismail et al., 2014; Parihar et al., 2015; Choudhury et al., 2017; Köster et al., 2018). Delayed Ca2+/ROS signaling will lead to the activation of the jasmonic acid signaling pathway that will culminate in cell death. Differently, an earlier activation of calcium- and ROS-dependent signaling induces a constraint on jasmonic acid (JA) signaling through the activation of the ABA signaling pathway (Ismail et al., 2014). We can infer that the calcium-binding genes that exhibited an early up-regulation in Zentos may play a role in activating the signaling pathway leading to ABA accumulation to stimulate growth under stress conditions (Ergen et al., 2009). In contrast, in the susceptible genotype the calcium-binding up-regulation was delayed and occurred at 30 min ASE which is consistent with the described model (Ismail et al., 2014). In addition to a delayed calcium-binding up-regulation, the salt-driven suppression of calcium-binding genes related to photosynthesis

(OEC genes) was observed as well. This result is also linked to the photosynthesis inhibition observed in Syn86.

The present study revealed as well the differential response of the xyloglucan:xyloglucosyl transferase activity term in the contrasting genotypes. The greater transcription observed in the tolerant genotype might enable plant growth under stress and might be beneficial for cell wall strengthening, the prevention of excessive water loss and to maintain turgor pressure due to the biosynthesis of xyloglucan in the cell wall (Eckardt, 2008; Le Gall et al., 2015). On the other hand, the down-regulation of these genes in the salt-sensitive genotype might be linked to the inhibition of cell expansion and cell wall synthesis that limit plant growth under stress conditions (Wang et al., 2018b). The synergy of the described transcriptional events might be crucial for the contrasting salt stress response of Syn86 and Zentos during the osmotic phase.

6.3. Greater number of genes with role in ion homeostasis are salt-responsive in the tolerant genotype during the ionic phase

The distribution of the expression values at the ionic phase insinuated a high amount of PCR duplication in the libraries at 24 days ASE which coincided with the higher number of reads sequenced in this time point in both genotypes. The use of deduplicated read alignments was therefore chosen to reduce false positives in the identification of differentially expressed genes and to allow better comparability among libraries. PCR duplication leads to the overestimation of transcript abundance because the number of reads is biased in the libraries (Klepikova et al., 2017).

The similar stress response of some GO terms observed in the contrasting genotypes at the ionic stress phase suggests that some earlier transcriptional responses might present stronger differences and might cause a greater impact in the contrasting acclimation response of the genotypes to long-term salt stress (Julkowska and Testerink, 2015). Nevertheless, it is also possible that when similar categories are salt-responsive in both genotypes the difference might lie in the specific genes and their levels of expression to affect the differential stress response. For instance, the transmembrane transport category was up-regulated in both genotypes. This category contained a greater number of ABC transporters and $Na^+/Ca2^+$ exchangers expressed in the tolerant genotype. ABC transporters are proposed to be involved in sodium exclusion (Kang et al., 2011; Kim et al., 2011). Further experiments are needed to confirm the link of the stress-induced expression of these genes and the reduced Na^+ accumulation discovered in the tolerant genotype at the ionic phase (Oyiga et al., 2016).

6.4. Protein synthesis and breakdown is differentially regulated at both stress phases

The D subgenome showed the greatest transcriptional response across genotypes and stress phases which agrees with greater involvement of this subgenome in stress adaptive pathways (Yang et al., 2014). A greater number of hotspots containing tandemly arrayed salt-responsive genes have been identified in this subgenome (Zhang et al., 2016). Most of the GO terms over-represented in the ionic phase were also found in the osmotic phase which indicated a set of common transcriptional responses in both stress phases. There is an opposite regulation of the translation and the serine-type endopeptidase inhibitor categories across both stress phases that suggests that the control of these mechanisms is stress stage-specific. The accumulation of aberrant proteins in cells can result from stress-related ROS damage which can lead to the transient suppression of the de novo synthesis of proteins and the intracellular protein degradation by proteases (Kidrič et al., 2014; Zhu, 2016; Robles and Quesada, 2019.

6.5. Recognition of salt-responsive genes in QTL intervals as putative QTGs

From the three salt-responsive genes observed in the QTL interval from the association mapping analysis, the oxoglutarate/iron-dependent dioxygenase showed the strongest down-regulation in the susceptible genotype. This gene superfamily might be involved in the biosynthesis of several specialized secondary metabolites responsive to biotic and abiotic stresses (Farrow and Facchini, 2014; Xu and Song, 2017). Therefore, this gene is a strong candidate that can be prioritized for further validation analyses. The AB-QTL mapping interval contained two salt-responsive genes including a copper amine oxidase and an amino acid transporter with similar magnitudes of relative expression. The up-regulation of both genes in the sensitive genotype can be linked to the positive phenotypic effect of the allele from Syn86 in the variation of kernel weight under salt stress (Dadshani, 2018). Studies in Arabidopsis have shown the involvement of copper amine oxidases in the biosynthesis of nitric oxide which is a signaling molecule that participates in adaptive responses to biotic or abiotic stresses (Neill et al., 2002; Wimalasekera et al., 2011; Groß et al., 2017). On the other hand, there are salt-responsive amino acid transporters that are involved in the transport of amino acids as proline which accumulates under stress to act as an osmolyte for osmotic adjustment (Hayat et al., 2012; Wan et al., 2017). The differential expression of the genes in the interval may contribute concomitantly to the phenotypic variation (González-Prendes et al., 2017). Only the implementation of a higher resolution mapping approach and functional studies could help to confirm the causality of the selected candidate genes on the trait of interest.

The above-mentioned results validate the use of the recent genome assembly to facilitate the integration of genomic and transcriptomic resources to resolve QTL and advance in the understanding of the genetic variation underlying agronomic complex traits in bread wheat (Adamski et al., 2018; IWGSC, 2018). This screening approach to target potential functional candidate genes is relevant since the mapping resolution of the studies is limited and the average gene density considering solely HC models is of approximately seven genes per Mbp (IWGSC, 2018). Nevertheless, this strategy can be more robust when expression data of other tissues under salt stress and different time points can be also included.

6.6. Differential calcium-binding-related transcriptional landscape in the contrasting genotypes

The propagation of calcium waves is an initial reaction to stress to mediate rapid systemic responses. This study evidenced a wide diversity of genes containing distinct types of calcium-binding domains that can interact with this ion to trigger different stress responses in systemic tissues (Gilroy et al., 2016). The domain analysis from the salt-responsive calcium-binding genes indicated that there is a different composition of domain types in the two genotypes. Zentos contained mainly genes corresponding to the EF-hand type and therefore was less diverse than Syn86. There is a core of common genes coding EF-hand domains with distinct expression profiles in the contrasting genotypes. The activation or suppression of specific gene networks dependent on Ca^{2+} observed in the contrasting genotypes represent a differential execution of calcium signal transduction and suggest a particular calcium signature in each genotype (Sanyal et al., 2019; Mohanta et al., 2019). The variation of signaling events can be involved in either tolerance or susceptibility responses in the genotypes.

In addition to the OEC transcripts that were previously discussed (see Sections 5.3.1 and 6.2), annexins were observed among the non-EF-hand type genes down-regulated at 30 min ASE in Syn86. These proteins are proposed to have a role as H2O2 sensors, modulate cytosolic calcium signatures and can function in the plasma membrane to transport Ca^{2+} (Liao et al., 2017; Sanyal et al., 2019). Therefore, it can be inferred that the down-regulation of these transcripts can have a role in altering the [Ca^{2+}]cytosolic signals to be decoded by intracellular Ca^{2+} sensors such as CaMs, CMLs and CPKs from Syn86 (Liao et al., 2019). The up-regulation in this genotype of an additional non-EF-hand type corresponding to CNX/CRT can be linked to the greater oxidative stress response that was observed at the transcriptional level. This non-EF-hand category is characterized by its increased activity during oxidative stress in the pathway from the endoplasmic reticulum to refold and degrade

stress-damaged proteins (Garg et al., 2015). Proteins with transmembrane EGF-like domain identified in both genotypes can recognize oligogalacturonides which are cell wall fragments that trigger cell wall damage signaling (Saijo and Loo, 2020).

Besides the common EF-hand protein types in both genotypes, Syn 86 contained caleosins and phosphoglycolate phosphatases. The up-regulation of caleosins in the susceptible genotype can be linked to its lipid peroxygenase activity and its role in oxylipin metabolism in which is included JA biosynthesis (Wasternack and Feussner, 2018). This event can lead to benefit JA signaling that is proposed as preferential for salt susceptible genotypes over the activation of the ABA pathway as discussed earlier (Section 6.2) (Ismail et al., 2014). Phosphoglycolate phosphatases are involved in photorespiration metabolism (Schwarte and Bauwe, 2007). The up-regulation of these genes in Syn86 at 15 min is linked with the role of photorespiration in stress protection by preventing the over-reduction of the electron transport chain of photosynthesis and alleviating photoinhibition (Wingler et al., 2000). The calcium-binding domain-types and the calcium-binding-related transcriptional changes observed in Syn86 are consistent with the susceptibility response.

Calcium is involved in several pathways in plant cells including photosynthesis. Besides participating as co-factor of proteins from the PSII, calcium can regulate the transcription and translation of genes encoding proteins and enzymes involved in the photosynthesis reaction (Wang et al., 2019). Our study suggests that salt tolerance- and salt susceptibility-related pathways converge with Ca^{2+} signals that can be related to the differential photosynthesis rate curves observed under salt stress (Seifikalhor et al., 2019).

6.7. The phylogenetic analysis of EF-hand proteins reveals genes involved in rapid systemic ROS production

Proteins with an EF-hand domain have evolved to detect transient increases of cytosolic Ca^{2+} and activate proper stress responses (Sanyal et al., 2019). The involvement in the initial Ca^{2+}-dependent signaling network during stress responses is postulated for the high diversity of salt stress-responsive genes coding EF-hand proteins identified in the contrasting genotypes (Seifikalhor et al., 2019). The phylogenetic analysis allowed to classify them as CaM, CML, CBL, CPKs or RBOHs based on the comparisons with Arabidopsis. Wheat CPKs and RBOHs showed clear orthologous relationships with the corresponding Arabidopsis proteins. The lack of clear orthologs of CaM and CML in Arabidopsis indicates a greater sequence divergence along evolutionary time and therefore gene function might be less conserved in distant taxa (Eisman and Kaufman, 2013). The sequence

similarity relatedness among the two species contributed to infer some stress response pathways in which the salt-responsive genes from Syn86 and Zentos might be involved.

CaM and CML are widely characterized EF-hand sensors that during stress signaling interact with target proteins to cause gene expression reprogramming (Virdi et al., 2015). While stress-responsive CaM and CML transcripts were identified in Syn86, the tolerant genotype presented only transcripts from the CML type. Most of them were also salt-responsive in the susceptible genotype. The EF-hand number and the domain sequence variation among these proteins provide differences in ion binding affinity which underlies the sensing of various stimuli and the activation of several targets (Zhang et al., 2017; Nie et al., 2017). Therefore, we can infer that the genotypes can activate a set of common and also differential targets involved in stress pathways. For instance, there was a cluster with good statistical support of CML42 and CML43 and two salt-responsive CMLs up-regulated in Syn86. The up-regulation observed in the susceptible genotype can be linked to the negative effect of CML42 in ABA biosynthesis upon drought stress (Vadassery et al., 2012).

The RBOH family members are EF-hand containing proteins that produce localized signaling ROS bursts to regulate growth, developmental processes and stress responses (Choudhury et al., 2017; Chapman et al., 2019). The clustering with high statistical support of two wheat proteins with RBOHD from Arabidopsis is consistent with its role in salt stress response, systemic acquired acclimation by abiotic stress and regulation of ABA-mediated stomatal closure (Chapman et al., 2019; Kaya et al., 2019). The earlier expression of the RBOHD ortholog from Zentos at 15 min coincided with a faster calcium and ROS signaling that is proposed as a crucial mechanism to trigger salt tolerance (Ismail et al., 2014). In a previous phylogenetic analysis of this family in wheat (Hu et al., 2018), these RBOHD orthologs clustered with other RBOHs from A. thaliana. According to the nomenclature of the study, the up-regulated in Syn86 corresponded to TaNox9-4D and the up-regulated in Zentos to TaNox10-5BL. The different clustering can be due to the use of different gene models available in prior reference genome assemblies from wheat (IWGSC, 2014; Hu et al., 2018). Opposite to our results, the earlier study reported as well the down-regulation of TaNox10-5BL with NaCl and ABA treatments at 12 and 24 h ASE and its up-regulation by an oxidative stress treatment (Hu et al., 2018). Further studies of these RBOHD orthologs are necessary to reveal their specific roles in tolerance and susceptibility.

Among the EF-hand proteins with kinase domain, this study discovered that CPKs from subgroups I, III and IV were salt stress-responsive in wheat during the osmotic phase. Several members of

subgroup I (CPK1, CPK3, CPK4, CPK5, CPK6 and CPK11) are reported to have RBOHD as substrate (Yip-Delormel and Boudsocq, 2019). This reported kinase-substrate interaction agrees with the co-expression of the RBOHD ortholog and the two CPKs of subgroup I from Zentos at 15 min. The co-expression of the homeologs coding CPKs might suggest a functional redundancy or a dosage effect on the phosphorylation performed by the two proteins (Borrill et al., 2015) that can generate a more efficient operation of the RBOH-dependent ROS-Ca^{2+} hub. In the case of Syn86, one CPK from this subgroup was up-regulated at a later time point (4 h) than the RBOHD homolog (30 min). Studies at the expression and protein level are necessary to validate the phosphorylation of the RBOHD homologs by these kinases. On the other hand, an ortholog of CPK13 from the subgroup III was identified in Syn86. This gene has a proposed role as a negative regulator of light-induced stomatal opening during drought stress (Yip-Delormel and Boudsocq, 2019; Atif et al., 2019). Therefore, this gene can be involved in networks related to the genotype susceptibility to salt stress.

6.8. Co-expression of some TF families and calcium-binding genes

Transcription factors control the transcription of stress-inducible genes and therefore are critical in the activation of downstream mechanisms for stress adaptation (Banerjee and Roychoudhury, 2015). Genes from AP2/ERF and WRKY families were the most abundant among the transcription factor families up-regulated at the osmotic phase. This result suggests an important role of these families on the salt stress response. Genes from the AP2/ERF family showed greater relative expression values in the tolerant genotype. This versatile family is involved in different types of abiotic stress responses and often affect the crosstalk between different signaling cascades (Dey and Corina Vlot, 2015). The proteins coded by these genes can bind to the promoters of stress-responsive genes that can confer stress tolerance (Licausi et al., 2013).

The immediate early expression of WRKY genes following stress contributes to the transcriptional activation of abiotic stress adaptation mechanisms. For instance, these TFs can activate ABA signaling or regulate the production of some secondary metabolites with relevance on stress response (Banerjee and Roychoudhury, 2015; Phukan et al., 2016). The co-expression of WRKY, CaM and CML genes found in this study can be related to a protein-protein interaction through a CaM-binding domain that has been observed in Group IId WRKY TFs. This interaction can be favored during abiotic stresses by high calcium concentrations in the cells (Banerjee and Roychoudhury, 2015; Seifikalhor et al., 2019). The greater expression levels of WRKY genes identified in the tolerant genotype can be associated with increased transcription of WRKY-dependent genes with important contributions to salt tolerance. The co-expression of WRKY and GATA transcription factors

identified in our study agrees with the type of ROS/Ca^{2+} wave-associated transcripts identified in Arabidopsis after few minutes of light stress (Zandalinas et al., 2019).

Regarding other salt-responsive TFs, the HSF family presented different expression patterns in the contrasting genotypes. The up-regulation of members of this family in the tolerant genotype at 15 and 30 min ASE coincides with the role of conferring salt stress tolerance found for some of these TFs in Arabidopsis (Pérez-Salamó et al., 2014; Zang et al., 2019). The observed down-regulation in Syn86 of members of this TF family might be a transcriptional event that condition the genotype susceptibility. On the other hand, some types of bZip proteins have essential roles in several salt stress adaptation responses. For instance, they can participate in ABA signaling or the endoplasmic reticulum stress signaling cascade (Wang et al., 2019b). The greater expression levels of these TFs in the tolerant genotype also support the activation of adaptation mechanisms leading to salt tolerance. Some bZip proteins from A. thaliana with a calmodulin-binding domain are activated by calcium signaling and stress stimuli (Galon et al., 2010; Reddy et al., 2011; Tsugama et al., 2018). The potential protein-protein interactions of co-expressed TFs and calcium biding genes can be further studied with additional methodological approaches.

6.9. *CML-2D* and *CML47-5D* show different expression patterns in leaves and roots

The RT-qPCR analysis of two genes indicated different expression patterns in leaves and roots. Even though both genes are functionally equivalent, they revealed organ-specific and temporal variations in their transcriptional regulation. They might be involved in different gene networks and signaling pathways under salt stress as one gene is more expressed in the tolerant while the other is more expressed in the susceptible genotype (Kirik et al., 2005).

CML-2D expression seems to be specific for salt stress response in the leaves and is mainly up-regulated in the tolerant genotype. Therefore, we can infer that the greater expression of this gene under stress conditions leads to the activation of target genes involved in pathways and cellular processes for salt tolerance in leaves. CML37 and CML38 are examples of genes with tissue-specific expression in Arabidopsis under salt stress. These genes are responsive to osmotic stress in leaves while in roots there are time points without expression or with reduced expression levels (Vanderbeld and Snedden, 2007). Nevertheless, it cannot be discarded that the expression in roots can be at an earlier stage of the osmotic phase as other studies in this organ have reported the up-regulation of calcium-binding genes after 1-2 min of stress and the posterior decrease in expression levels at 10 min ASE (Choi et al., 2014).

CML-2D is a potential QTG as is the differentially expressed gene closest to the marker Kukri_rep_c72254_186. This marker has an effect on plant biomass under salt stress in the AB-QTL study (Dadshani, 2018). In this case the LD delimitation of a QTL interval was not possible as the D subgenome has the lowest SNP density. The reduced genetic variability of this subgenome complicates the dissection of complex traits (Voss-Fels et al., 2015; Gao et al., 2017; Dadshani, 2018). Additionally, other CML gene (i.e. TraesCS2D01G173500) was down-regulated in Syn86 and is 28 kb away from the significant marker. Expression and functional studies of these genes can validate if they have a concomitant effect on the salt stress response.

On the other hand, CML47-5D show greater expression levels in the susceptible genotype in both leaves and roots. The over-expression in roots was maintained for a longer time after stress compared to leaves. These results suggest that this gene activates targets involved in pathways that trigger stress susceptibility. This gene was included in a cluster with CML45, CML46 and CML47 in the phylogenetic analysis, but lacks a clear ortholog. Nevertheless, functional analysis have demonstrated the negative regulation on salicylic acid accumulation and the consequent detrimental effect on plant immunity and likely on abiotic stress caused by CML46 and CML47 (Khan et al., 2015; Lu et al., 2018). The homeologs from CML47-5D were expressed in both genotypes and the homeolog-specific role of them in the salt stress response can be explored with more detail.

The up-regulation of CML47-5D at the osmotic phase was confirmed by the RT-qPCR analysis at 8 and 15 min. The greater relative expression values measured by RT-qPCR can be influenced by the increased salt concentration used in the corresponding hydroponic experiment. The poor concordance of the expression of CML-2D in the two platforms might result from the high frequency of multiple aligned reads in some genomic regions that can lead to expression quantification biases in the transcriptomics analyses (Everaert et al., 2017). More salt-responsive transcripts should be analyzed by RT-qPCR to have a better idea of the proportion of non-concordant genes resulting from the transcriptomic approach implemented.

6.10. Genetic variation with potential influence on expression levels of calcium-binding genes

The analysis of the promoter sequences from two calcium-binding genes revealed polymorphisms in the genotypes studied. Several families showed potential binding sites adjacent to the identified polymorphisms, but only the families GATA, bZip and ERF were identified as salt-responsive in the transcriptomic analysis. Therefore, the variation on the sequence of the corresponding transcription

factor binding sites is likely to influence the differential expression of CML2D and CML47-5D in the contrasting genotypes. There is evidence of genes with calcium-binding domains regulated by these TF families. For instance, the drought inducible OsERF48 from rice binds to the promoter of OsCML16 in a pathway to enhance drought tolerance (Jung et al., 2017). Furthermore, the binding of a bZip type TF was observed in the promoter of CaM3 (Reddy et al., 2011). These examples support the potential regulation of the expression of calcium-binding genes by TFs of these families. As the transcriptomic analysis was performed until 4 h ASE, the other TF families identified with binding sites in the promoters might influence gene expression at later time points of the stress response.

The identification of SNPs in calcium-binding genes was possible through the analysis of MACE reads. Considering that SNPs were identified in sites covered with at least 10 reads, it is not likely that the polymorphisms identified in reads mapping to intronic regions were derived from technical artifacts. On the contrary, these reads can derive from unknown exons as there is evidence that they can be a proxy of nascent transcription and splicing events (Gaidatzis et al., 2015).

The study of the effect of miRNA binding on expression levels under stress is emerging in the last years as there is increasing evidence indicating that plants can respond to environmental stresses by altering gene expression through the activity of miRNAs (Khraiwesh et al., 2012; Asefpour Vakilian, 2020). Therefore, more information on the interactions of miRNA and mRNA sequences have been experimentally validated and collected in databases of model organisms (Chou et al., 2018). The prediction database from wheat contained only few information to infer interactions with mRNA sequences of interest (Dai et al., 2018). As miRNA binding sites can be conserved across distant taxa (Floyd and Bowman, 2018), the Arabidopsis database was used as it included the greatest number of experimentally validated interactions. Some polymorphisms that can regulate the expression levels of some calcium-binding genes by differential miRNA binding were identified. The potential interaction of TraesCS5B02G428400 and tae-miR171a might be the most promising to study and validate as this miRNA is salt- and drought-responsive in wheat and other species from Triticeae (Wang et al., 2014a; Alptekin et al., 2017). The calcium-binding gene corresponded to the CPK from the subgroup I that was up-regulated at 15 min in Zentos (also discussed in Section 6.7). This potential interaction can repress the expression of the CPK gene. This gene seems to be stress-responsive for a short period of time which can be related to tissue- and time-specific expression of miRNAs towards stress (Asefpour Vakilian, 2020).

7. Conclusions and perspectives

The pipeline developed and implemented for the processing and analysis of MACE-reads was useful to detect variation in the expression of salt stress-responsive genes. The categories from these genes were related to some physiological variations observed at the osmotic and ionic phases. Transcripts with high relative expression values within QTL intervals can be prioritized for further studies. The analysis of MACE-reads provided as well evidence of regions with novel transcription in wheat as some genes were found with elongated 3'-ends and novel salt-responsive transcripts were discovered. Some of the extended gene models and novel transcripts found in this study might coincide with some of the gene models revised in the annotation RefSeq v2.0 that has not been released yet. The wheat pangenome resource will contribute also to recognize if the novel transcripts identified here might be expressed in other genetic backgrounds.

This is one of the first studies to combine transcriptomics, genetics and stress physiology analyses in a systemic approach and a more comprehensive understanding of the salt stress adaptation response in bread wheat at both osmotic and ionic phases was obtained. This analysis leads to a better QTL dissection to finally shed light on novel genes controlling regulatory pathways for salt stress-related traits in wheat. The use of the chromosome-level assembly of the wheat genome facilitated in this case the integration of transcriptomics and genetic mapping analyses to identify candidate QTGs. This resource is relevant in wheat genetic studies due to the large number of genes contained by the QTL intervals. A greater mapping resolution and transcriptomics studies considering more tissues and time points would be useful to gain more precision on the identification of candidate QTGs.

The time points selected for the transcriptomic analysis at the osmotic phase were valuable to detect the earlier transcriptional reaction to stress from the tolerant genotype. These results supported the design of a pooled transcriptomic experiment as important transcriptional changes occurred in the first minutes after stress exposure which were linked to photosynthesis response. The transcriptional differences observed in key gene categories coincided with the photosynthesis stability of the tolerant genotype and the photosynthesis inhibition observed in the susceptible genotype. Some of the genes categories involved can be studied with further detail to have a greater understanding of the mechanisms that can trigger salt tolerance and greater photosynthesis stability in wheat.

The over-represented calcium-binding category was therefore analyzed with more detail at the expression and sequence level. A differential execution of calcium signal transduction was revealed during the osmotic phase by the diverse expression profiles and the different composition of calcium-

binding protein types observed in the contrasting genotypes. The identification of polymorphisms in the genes and some promoter sequences provided indications of mechanisms with a potential effect on the differential expression levels observed in the genotypes. Furthermore, some early transcriptional changes linked to the ROS/Ca^{2+} wave were identified. The results from this study evidenced that genes with a putative role in the pathway for systemic ROS production are time- and genotype-specific. This aspect highlights the usefulness of the systemic approach implemented to pinpoint influent regulators of salt stress response pathways. A transcriptomic study in roots can clarify which genes are involved first in the salt stress sensing and in the calcium propagated signaling. The analysis of ROS contents is also required to observe if there are temporal and quantitative variations on this molecule that can be related to the differences detected in the expression of relevant genes.

The transmembrane transport category was over-represented at the ionic phase in both genotypes. More ABC transporters and Na^+/Ca^{2+} exchangers with a potential role in Na^+ and K^+ homeostasis were identified in the tolerant genotype. Additional studies can validate the contribution of the expression of these genes in the greater tolerance of Altay2000 and confirm their role in ion homeostasis. Based on the results of this study, the wheat research community can perform functional analyses of some prioritized stress-responsive genes.

References

Abeel T, Van Parys T, Saeys Y, Galagan J, Van de Peer Y. 2012. GenomeView: a next-generation genome browser. Nucleic Acids Research 40, e12.

Abrol IP, Yadav JSP, Massoud FI. 1988. *Salt-affected soils and their management*. Rome: Food and Agriculture Organization of the United Nations. http://www.fao.org/3/x5871e/x5871e00.htm.

Ackermann M, Sikora-Wohlfeld W, Beyer A. 2013. Impact of natural genetic variation on gene expression dynamics. PloS Genetics 9, e1003514.

Adamski NM, Borrill P, Brinton J, Harrington S, Marchal C, Uauy C. 2018. A roadmap for gene functional characterisation in wheat. PeerJ Preprints 6, e26877v1.

Alaux M, Rogers J, Letellier T, *et al.* 2018. Linking the International Wheat Genome Sequencing Consortium bread wheat reference genome sequence to wheat genetic and phenomic data. Genome Biology 19, 111.

Allakhverdiev SI, Nishiyama Y, Miyairi S, Yamamoto H, Inagaki N, Kanesaki Y, Murata N. 2002. Salt stress inhibits the repair of photodamaged photosystem II by suppressing the transcription and translation of *psbA* genes in *Synechocystis*. Plant Physiology 130, 1443–1453.

Almeida DM, Oliveira MM, Saibo NJM. 2017. Regulation of Na^+ and K^+ homeostasis in plants: towards improved salt stress tolerance in crop plants. Genetics and Molecular Biology 40, 326–345.

Alptekin B, Langridge P, Budak H. 2017. Abiotic stress miRNomes in the *Triticeae*. Functional & Integrative Genomics 17, 145–170.

Altay F. 2012. Yield stability of some Turkish winter wheat (*Triticum aestivum* L.) genotypes in the western transitional zone of Turkey. Turkish Journal of Field Crops 17, 129–134.

Álvarez MF, Mosquera T, Blair MW. 2014. The use of association genetics approaches in plant breeding. In: Janick J, ed. *Plant Breeding Reviews: Volume 38*. New Jersey: John Wiley & Sons, 17–68.

Amanov A. 2017. Wheat breeding in Uzbequistan. Research Institute of Plant Industry, Kibray. http://www.iwwip.org/images/dosya/636220600428830708.pdf.

Amirbakhtiar N, Ismaili A, Ghaffari MR, Nazarian Firouzabadi F, Shobbar Z-S. 2019. Transcriptome response of roots to salt stress in a salinity-tolerant bread wheat cultivar. PloS One 14, e0213305.

Anders S, Huber W. 2010. Differential expression analysis for sequence count data. Genome Biology 11, R106.

Andrews S. 2010. FastQC a quality control tool for high throughput sequence data. https://www.bioinformatics.babraham.ac.uk/projects/fastqc/

Asao T. 2012. *Hydroponics - A Standard Methodology for Plant Biological Researches*. Rijeka, Croatia: IntechOpen, doi: 10.5772/2215.

Asefpour Vakilian K. 2020. Machine learning improves our knowledge about miRNA functions towards plant abiotic stresses. Scientific Reports 10, 1–10.

Ashraf M, Wu DL. 1994. Breeding for salinity tolerance in plants. Critical Reviews in Plant Sciences 13, 17–42.

Asif MA, Schilling RK, Tilbrook J, *et al.* 2018. Mapping of novel salt tolerance QTL in an Excalibur × Kukri doubled haploid wheat population. Theoretical and Applied Genetics 131, 2179–2196.

Asmann YW, Klee EW, Thompson EA, *et al.* 2009. 3' tag digital gene expression profiling of human brain and universal reference RNA using Illumina Genome Analyzer. BMC Genomics 10, 531.

Atif RM, Shahid L, Waqas M, Ali B, Rashid MAR, Azeem F, Nawaz MA, Wani SH, Chung G. 2019. Insights on Calcium-Dependent Protein Kinases (CPKs) signaling for abiotic stress tolerance in plants. International Journal of Molecular Sciences 20, 5298.

Baliga NS, Björkegren JLM, Boeke JD, *et al.* 2017. The State of Systems Genetics in 2017. Cell Systems 4, 7–15.

Banerjee A, Roychoudhury A. 2015. WRKY proteins: signaling and regulation of expression during abiotic stress responses. The Scientific World Journal 2015, 807560.

Barah P, Winge P, Kusnierczyk A, Tran DH, Bones AM. 2013. Molecular signatures in *Arabidopsis thaliana* in response to insect attack and bacterial infection. PloS One 8, e58987.

Bashir K, Matsui A, Rasheed S, Seki M. 2019. Recent advances in the characterization of plant transcriptomes in response to drought, salinity, heat, and cold stress. F1000Research 8, 658.

Beltrán JMM, Koo-Oshima S. 2006. Water desalination for agricultural applications. *Proceedings of the FAO Expert Consultation on Water Desalination for Agricultural Applications*. Rome: Food and Agriculture Organization of the United Nations.

Bender KW, Snedden WA. 2013. Calmodulin-related proteins step out from the shadow of their namesake. Plant Physiology 163, 486–495.

Bender KW, Zielinski RE, Huber SC. 2018. Revisiting paradigms of Ca^{2+} signaling protein kinase regulation in plants. The Biochemical Journal 475, 207–223.

Biłas R, Szafran K, Hnatuszko-Konka K, Kononowicz AK. 2016. *Cis*-regulatory elements used to control gene expression in plants. Plant Cell, Tissue and Organ Culture 127, 269–287.

Biswas S, Agrawal YN, Mucyn TS, Dangl JL, Jones CD. 2013. Biological averaging in RNA-Seq. arXiv, 1309.0670v2 [q-bio.QM].

Blée E, Boachon B, Burcklen M, Le Guédard M, Hanano A, Heintz D, Ehlting J, Herrfurth C, Feussner I, Bessoule J-J. 2014. The reductase activity of the Arabidopsis caleosin RESPONSIVE TO DESSICATION20 mediates gibberellin-dependent flowering time, abscisic acid sensitivity, and tolerance to oxidative stress. Plant Physiology 166, 109–124.

Bolger AM, Lohse M, Usadel B. 2014. Trimmomatic: a flexible trimmer for Illumina sequence data. Bioinformatics 30, 2114–2120.

Borrill P, Adamski N, Uauy C. 2015. Genomics as the key to unlocking the polyploid potential of wheat. The New Phytologist 208, 1008–1022.

Borrill P, Harrington SA, Uauy C. 2019. Applying the latest advances in genomics and phenomics for trait discovery in polyploid wheat. The Plant Journal 97, 56–72.

Borrill P, Ramirez-Gonzalez R, Uauy C. 2016. expVIP: a customizable RNA-seq data analysis and visualization platform. Plant Physiology 170, 2172–2186.

Bürstenbinder K, Möller B, Plötner R, Stamm G, Hause G, Mitra D, Abel S. 2017. The IQD Family of calmodulin-binding proteins links calcium signaling to microtubules, membrane subdomains, and the nucleus. Plant Physiology 173, 1692–1708.

Busby MA, Gray JM, Costa AM, Stewart C, Stromberg MP, Barnett D, Chuang JH, Springer M, Marth GT. 2011. Expression divergence measured by transcriptome sequencing of four yeast species. BMC Genomics 12, 635.

Bustin SA, Mueller R. 2005. Real-time reverse transcription PCR (qRT-PCR) and its potential use in clinical diagnosis. Clinical Science 109, 365–379.

Cai M, Chen L, Liu J, Yang C. 2019. Quantifying the impact of genetically regulated expression on complex traits and diseases. bioRxiv, 546580.

Caraguel CGB, Stryhn H, Gagné N, Dohoo IR, Hammell KL. 2011. Selection of a cutoff value for real-time polymerase chain reaction results to fit a diagnostic purpose: analytical and epidemiologic approaches. Journal of Veterinary Diagnostic Investigation 23, 2–15.

Carillo P, Annunziata MG, Pontecorvo G, Fuggi A, Woodrow P. 2011. Salinity stress and salt tolerance. In: Shanker A, Venkateswarlu B, eds. *Abiotic stress in plants - Mechanisms and adaptations*. Rijeka, Croatia: IntechOpen, doi: 10.5772/22331.

Chapman JM, Muhlemann JK, Gayomba SR, Muday GK. 2019. RBOH-dependent ROS synthesis and ROS Scavenging by plant specialized metabolites to modulate plant development and stress responses. Chemical Research in Toxicology 32, 370–396.

Choi W-G, Toyota M, Kim S-H, Hilleary R, Gilroy S. 2014. Salt stress-induced Ca^{2+} waves are associated with rapid, long-distance root-to-shoot signaling in plants. Proceedings of the National Academy of Sciences of the United States of America 111, 6497–6502.

Chou C-H, Shrestha S, Yang C-D, *et al.* 2018. miRTarBase update 2018: a resource for experimentally validated microRNA-target interactions. Nucleic Acids Research 46, D296–D302.

Choudhury FK, Rivero RM, Blumwald E, Mittler R. 2017. Reactive oxygen species, abiotic stress and stress combination. The Plant Journal 90, 856–867.

Cirilli M, Giovannini D, Ciacciulli A, Chiozzotto R, Gattolin S, Rossini L, Liverani A, Bassi D. 2018. Integrative genomics approaches validate *PpYUC11-like* as candidate gene for the stony hard trait in peach (*P. persica* L. Batsch). BMC Plant Biology 18, 88.

Civelek M, Lusis AJ. 2014. Systems genetics approaches to understand complex traits. Nature reviews. Genetics 15, 34–48.

Clavijo BJ, Venturini L, Schudoma C, *et al.* 2017. An improved assembly and annotation of the allohexaploid wheat genome identifies complete families of agronomic genes and provides genomic evidence for chromosomal translocations. Genome Research 27, 885–896.

Colmer TD, Flowers TJ, Munns R. 2006. Use of wild relatives to improve salt tolerance in wheat. Journal of Experimental Botany 57, 1059–1078.

Conde A, Chaves MM, Gerós H. 2011. Membrane transport, sensing and signaling in plant adaptation to environmental stress. Plant & Cell Physiology 52, 1583–1602.

Conesa A, Madrigal P, Tarazona S, *et al.* 2016. A survey of best practices for RNA-seq data analysis. Genome Biology 17, 13.

Curtis T, Halford NG. 2014. Food security: the challenge of increasing wheat yield and the importance of not compromising food safety. The Annals of Applied Biology 164, 354–372.

Dadshani S. 2018. Genetic and physiological characterization of traits related to salinity tolerance in an advanced backcross population of wheat. PhD thesis, University of Bonn

Dai X, Zhuang Z, Zhao PX. 2018. psRNATarget: a plant small RNA target analysis server (2017 release). Nucleic Acids Research 46, W49–W54.

Dasgupta S, Hossain MM, Huq M, Wheeler D. 2018. Climate change, salinization and high-yield rice production in coastal Bangladesh. Agricultural and Resource Economics Review 47, 66–89.

Demetriou G, Neonaki C, Navakoudis E, Kotzabasis K. 2007. Salt stress impact on the molecular structure and function of the photosynthetic apparatus - The protective role of polyamines. Biochimica Et Biophysica Acta 1767, 272–280.

Derveaux S, Vandesompele J, Hellemans J. 2010. How to do successful gene expression analysis using real-time PCR. Methods 50, 227–230.

Dey S, Corina Vlot A. 2015. Ethylene responsive factors in the orchestration of stress responses in monocotyledonous plants. Frontiers in Plant Science 6, 640.

Dillies M-A, Rau A, Aubert J, *et al.* 2013. A comprehensive evaluation of normalization methods for Illumina high-throughput RNA sequencing data analysis. Briefings in Bioinformatics 14, 671–683.

Dixit AK, Jayabaskaran C. 2012. Phospholipid mediated activation of Calcium Dependent Protein Kinase 1 (CaCDPK1) from chickpea: a new paradigm of regulation. PloS One 7, e51591.

Dorak MT. 2007. *Real-time PCR*. New York, NY: Taylor & Francis.

Eckardt NA. 2008. Role of xyloglucan in primary cell walls. The Plant Cell 20, 1421–1422.

Edel KH, Marchadier E, Brownlee C, Kudla J, Hetherington AM. 2017. The evolution of calcium-based signalling in plants. Current Biology 27, R667–R679.

Ehrenreich IM, Purugganan MD. 2008. Sequence variation of microRNAs and their binding sites in Arabidopsis. Plant Physiology 146, 1974–1982.

Eisman RC, Kaufman TC. 2013. Probing the boundaries of orthology: the unanticipated rapid evolution of *Drosophila* centrosomin. Genetics 194, 903–926.

El Baidouri M, Murat F, Veyssiere M, Molinier M, Flores R, Burlot L, Alaux M, Quesneville H, Pont C, Salse J. 2017. Reconciling the evolutionary origin of bread wheat (*Triticum aestivum*). The New Phytologist 213, 1477–1486.

Ergen NZ, Thimmapuram J, Bohnert HJ, Budak H. 2009. Transcriptome pathways unique to dehydration tolerant relatives of modern wheat. Functional & Integrative Genomics 9, 377–396.

Ernst J, Bar-Joseph Z. 2006. STEM: a tool for the analysis of short time series gene expression data. BMC Bioinformatics 7, 191.

Ernst J, Nau GJ, Bar-Joseph Z. 2005. Clustering short time series gene expression data. Bioinformatics 21 Suppl 1, i159-168.

Ersoz ES, Yu J, Buckler ES. 2007. Applications of Linkage Disequilibrium and Association Mapping in Crop Plants. In: Varshney RK, Tuberosa R, eds. *Genomics-Assisted Crop Improvement*. Dordrecht: Springer Netherlands, 97–119.

Evans C, Hardin J, Stoebel DM. 2018. Selecting between-sample RNA-Seq normalization methods from the perspective of their assumptions. Briefings in Bioinformatics 19, 776–792.

Everaert C, Luypaert M, Maag JLV, Cheng QX, Dinger ME, Hellemans J, Mestdagh P. 2017. Benchmarking of RNA-sequencing analysis workflows using whole-transcriptome RT-qPCR expression data. Scientific Reports 7, 1559.

Faris JD. 2014. Wheat domestication: key to agricultural revolutions past and future. In: Tuberosa R, Graner A, Frison E, eds. *Genomics of plant genetic resources: Volume 1. Managing, sequencing and mining genetic resources*. Dordrecht: Springer Netherlands, 439–464.

Farrow SC, Facchini PJ. 2014. Functional diversity of 2-oxoglutarate/Fe(II)-dependent dioxygenases in plant metabolism. Frontiers in Plant Science 5, 524.

Fassbinder-Orth CA. 2014. Methods for quantifying gene expression in ecoimmunology: from qPCR to RNA-Seq. Integrative and Comparative Biology 54, 396–406.

Feldman M, Levy AA, Fahima T, Korol A. 2012. Genomic asymmetry in allopolyploid plants: wheat as a model. Journal of Experimental Botany 63, 5045–5059.

Feng J, Meyer CA, Wang Q, Liu JS, Shirley Liu X, Zhang Y. 2012. GFOLD: a generalized fold change for ranking differentially expressed genes from RNA-seq data. Bioinformatics 28, 2782–2788.

Floyd SK, Bowman JL. 2018. MicroRNAs: Micro-managing the plant genome. In: Roberts JA, ed. *Annual Plant Reviews Online*. New Jersey: John Wiley & Sons, doi:10.1002/9781119312994.apr0194

Foyer CH. 2018. Reactive oxygen species, oxidative signaling and the regulation of photosynthesis. Environmental and Experimental Botany 154, 134–142.

Frank J, Happeck R, Meier B, Hoang MTT, Stribny J, Hause G, Ding H, Morsomme P, Baginsky S, Peiter E. 2019. Chloroplast-localized BICAT proteins shape stromal calcium signals and are required for efficient photosynthesis. The New Phytologist 221, 866–880.

Fuchs M, Vothknecht U, Chigri F. 2011. Calmodulin and calmodulin-like proteins in *Arabidopsis thaliana*. Journal of Endocytobiosis and Cell Research 21, 114–121.

Gaidatzis D, Burger L, Florescu M, Stadler MB. 2015. Analysis of intronic and exonic reads in RNA-seq data characterizes transcriptional and post-transcriptional regulation. Nature Biotechnology 33, 722–729.

Galon Y, Finkler A, Fromm H. 2010. Calcium-regulated transcription in plants. Molecular Plant 3, 653–669.

Gao L, Zhao G, Huang D, Jia J. 2017. Candidate loci involved in domestication and improvement detected by a published 90K wheat SNP array. Scientific Reports 7, 44530.

Garg G, S Y, Ruchi, G Y. 2015. Key roles of calreticulin and calnexin proteins in plant perception under stress conditions: a review. Advances in Life Sciences 5, 18–26.

Gaupels F, Durner J, Kogel K-H. 2017. Production, amplification and systemic propagation of redox messengers in plants? The phloem can do it all! The New Phytologist 214, 554–560.

Genc Y, Oldach K, Taylor J, Lyons GH. 2016. Uncoupling of sodium and chloride to assist breeding for salinity tolerance in crops. The New Phytologist 210, 145–156.

Gibson G, Powell JE, Marigorta UM. 2015. Expression quantitative trait locus analysis for translational medicine. Genome Medicine 7, 60.

Gilroy S, Białasek M, Suzuki N, Górecka M, Devireddy AR, Karpiński S, Mittler R. 2016. ROS, calcium, and electric signals: key mediators of rapid systemic signaling in plants. Plant Physiology 171, 1606–1615.

Gonçalves AP. 2012. RNA sequencing for the study of gene expression regulation. PhD thesis, University of Cambridge.

González-Prendes R, Quintanilla R, Cánovas A, Manunza A, Figueiredo Cardoso T, Jordana J, Noguera JL, Pena RN, Amills M. 2017. Joint QTL mapping and gene expression analysis identify positional candidate genes influencing pork quality traits. Scientific Reports 7, 39830.

Gornicki P, Faris JD. 2014. Rewiring the wheat reproductive system to harness heterosis for the next wave of yield improvement. Proceedings of the National Academy of Sciences of the United States of America 111, 9024–9025.

Goyal E, Amit SK, Singh RS, Mahato AK, Chand S, Kanika K. 2016. Transcriptome profiling of the salt-stress response in *Triticum aestivum* cv. Kharchia Local. Scientific Reports 6, 27752.

Groß F, Rudolf E-E, Thiele B, Durner J, Astier J. 2017. Copper amine oxidase 8 regulates arginine-dependent nitric oxide production in *Arabidopsis thaliana*. Journal of Experimental Botany 68, 2149–2162.

Gupta B, Huang B. 2014. Mechanism of salinity tolerance in plants: Physiological, biochemical, and molecular characterization. International Journal of Genomics 2014, 701596.

Guzman C, Peña RJ, Singh R, Autrique E, Dreisigacker S, Crossa J, Rutkoski J, Poland J, Battenfield S. 2016. Wheat quality improvement at CIMMYT and the use of genomic selection on it. Applied & Translational Genomics 11, 3–8.

Hall T, Hall TA, Hall TA, *et al.* 1999. BioEdit: a user-friendly biological sequence alignment editor and analysis program for Windows 95/98/NT. Nucleic Acids Symposium Series 41, 95–98.

Hamblin MT, Buckler ES, Jannink J-L. 2011. Population genetics of genomics-based crop improvement methods. Trends in Genetics 27, 98–106.

Hawkesford MJ, Araus J-L, Park R, Calderini D, Miralles D, Shen T, Zhang J, Parry MAJ. 2013. Prospects of doubling global wheat yields. Food and Energy Security 2, 34–48.

Hayat S, Hayat Q, Alyemeni MN, Wani AS, Pichtel J, Ahmad A. 2012. Role of proline under changing environments. Plant Signaling & Behavior 7, 1456–1466.

Heid CA, Stevens J, Livak KJ, Williams PM. 1996. Real time quantitative PCR. Genome Research 6, 986–994.

Hertel TW. 2011. The global supply and demand for agricultural land in 2050: a perfect storm in the making? American Journal of Agricultural Economics 93, 259–275.

Ho HL. 2015. Functional roles of plant protein kinases in signal transduction pathways during abiotic and biotic stress. Journal of Biodiversity, Bioprospecting and Development 2, 1–8.

Howe KL, Contreras-Moreira B, De Silva N, *et al.* 2020. Ensembl Genomes 2020-enabling non-vertebrate genomic research. Nucleic Acids Research 48, D689–D695.

Hrdlickova R, Toloue M, Tian B. 2017. RNA-Seq methods for transcriptome analysis. Wiley Interdisciplinary Reviews. RNA 8, e1364.

Hu C-H, Wei X-Y, Yuan B, *et al.* 2018. Genome-wide identification and functional analysis of NADPH oxidase family genes in wheat during development and environmental stress responses. Frontiers in Plant Science 9, 906.

Hu W, Yan Y, Hou X, He Y, Wei Y, Yang G, He G, Peng M. 2015. *TaPP2C1*, a group F2 protein phosphatase 2C gene, confers resistance to salt stress in transgenic tobacco. PloS One 10, e0129589.

Hussain B, Lucas SJ, Ozturk L, Budak H. 2017. Mapping QTLs conferring salt tolerance and micronutrient concentrations at seedling stage in wheat. Scientific Reports 7, 15662.

Inatsuki T, Sato K, Sakakibara Y. 2016. Prediction of gene structures from RNA-seq data using dual decomposition. IPSJ Transactions on Bioinformatics 9, 1–6.

Ishikawa A. 2017. A strategy for identifying quantitative trait genes using gene expression analysis and causal analysis. Genes 8, 347.

Ismail AM, Horie T. 2017. Genomics, physiology, and molecular breeding approaches for improving salt tolerance. Annual Review of Plant Biology 68, 405–434.

Ismail A, Takeda S, Nick P. 2014. Life and death under salt stress: Same players, different timing? Journal of Experimental Botany 65, 2963–2979.

IWGSC. 2014. A chromosome-based draft sequence of the hexaploid bread wheat (*Triticum aestivum*) genome. Science 345, 1251788.

IWGSC. 2018. Shifting the limits in wheat research and breeding using a fully annotated reference genome. Science 361, eaar7191.

Jafari-Shabestari J, Corke H, Qualset CO. 1995. Field evaluation of tolerance to salinity stress in Iranian hexaploid wheat landrace accessions. Genetic Resources and Crop Evolution 42, 147–156.

James RA, Blake C, Zwart AB, Hare RA, Rathjen AJ, Munns R. 2012. Impact of ancestral wheat sodium exclusion genes *Nax1* and *Nax2* on grain yield of durum wheat on saline soils. Functional Plant Biology 39, 609–618

Jansson L, Hedman J. 2019. Challenging the proposed causes of the PCR plateau phase. Biomolecular Detection and Quantification 17, 100082.

Jewell MC, Campbell BC, Godwin ID. 2010. Chapter 2 – Transgenic Plants for Abiotic Stress Resistance. In: Kole C**,** Michler C**,** Abbott AG, Hall TC, eds. *Transgenic crop plants. Volume 2: Utilization and biosafety.* Berlin, Heidelberg: Springer, 67 – 132.

Jin J, Tian F, Yang D-C, Meng Y-Q, Kong L, Luo J, Gao G. 2017. PlantTFDB 4.0: toward a central hub for transcription factors and regulatory interactions in plants. Nucleic Acids Research 45, D1040–D1045.

Julkowska MM, Testerink C. 2015. Tuning plant signaling and growth to survive salt. Trends in Plant Science 20, 586–594.

Jung H, Chung PJ, Park S-H, Redillas MCFR, Kim YS, Suh J-W, Kim J-K. 2017. Overexpression of *OsERF48* causes regulation of *OsCML16*, a calmodulin-like protein gene that enhances root growth and drought tolerance. Plant Biotechnology Journal 15, 1295–1308.

Kang YJ, Lee T, Lee J, Shim S, Jeong H, Satyawan D, Kim MY, Lee S-H. 2016. Translational genomics for plant breeding with the genome sequence explosion. Plant Biotechnology Journal 14, 1057–1069.

Kang J, Park J, Choi H, Burla B, Kretzschmar T, Lee Y, Martinoia E. 2011. Plant ABC Transporters. The Arabidopsis Book 9, e0153.

Katoh K, Rozewicki J, Yamada K. 2019. MAFFT online service: multiple sequence alignment, interactive sequence choice and visualization. Briefings in Bioinformatics 20, 1160–1166.

Kaya H, Takeda S, Kobayashi MJ, *et al.* 2019. Comparative analysis of the reactive oxygen species-producing enzymatic activity of Arabidopsis NADPH oxidases. The Plant Journal 98, 291–300.

Kendziorski C, Irizarry RA, Chen K-S, Haag JD, Gould MN. 2005. On the utility of pooling biological samples in microarray experiments. Proceedings of the National Academy of Sciences of the United States of America 102, 4252–4257.

Keshtehgar A, Rigi K, Vazirimehr M. 2013. Effects of salt stress in crop plants. International Journal of Agriculture and Crop Sciences 5, 2863-2867.

Khan MIR, Fatma M, Per TS, Anjum NA, Khan NA. 2015. Salicylic acid-induced abiotic stress tolerance and underlying mechanisms in plants. Frontiers in Plant Science 6, 462.

Khraiwesh B, Zhu J-K, Zhu J. 2012. Role of miRNAs and siRNAs in biotic and abiotic stress responses of plants. Biochimica Et Biophysica Acta 1819, 137–148.

Kidrič M, Kos J, Sabotič J. 2014. Proteases and their endogenous inhibitors in the plant response to abiotic stress. Botanica Serbica 38, 139–158.

Kim YY, Jung KW, Yoo KS, Jeung JU, Shin JS. 2011. A stress-responsive caleosin-like protein, AtCLO4, acts as a negative regulator of ABA responses in Arabidopsis. Plant & Cell Physiology 52, 874–884.

Kirik V, Lee MM, Wester K, Herrmann U, Zheng Z, Oppenheimer D, Schiefelbein J, Hulskamp M. 2005. Functional diversification of *MYB23* and *GL1* genes in trichome morphogenesis and initiation. Development 132, 1477–1485.

Klaus B, Huber W. 2016. Analysis of RNA-Seq data: gene-level exploratory analysis and differential expression. https://www.huber.embl.de/users/klaus/Teaching/DESeq2Predoc2014.html

Klepikova AV, Kasianov AS, Chesnokov MS, Lazarevich NL, Penin AA, Logacheva M. 2017. Effect of method of deduplication on estimation of differential gene expression using RNA-seq. PeerJ 5, e3091.

Klug WS, Cummings MR, Spencer CA, Palladino MA, Killian D. 2018. *Concepts of Genetics*. NY, NY: Pearson.

Köster P, Wallrad L, Edel KH, Faisal M, Alatar AA, Kudla J. 2018. The battle of two ions: Ca^{2+} signalling against Na^{+} stress. Plant Biology 21, 39–48.

Kulwal PL. 2018. Trait mapping approaches through linkage mapping in plants. Advances in Biochemical Engineering/Biotechnology 164, 53–82.

Kumar S, Stecher G, Li M, Knyaz C, Tamura K. 2018. MEGA X: Molecular evolutionary genetics analysis across computing platforms. Molecular Biology and Evolution 35, 1547-1549.

Kunert A, Naz AA, Dedeck O, Pillen K, Léon J. 2007. AB-QTL analysis in winter wheat: I. Synthetic hexaploid wheat (*T. turgidum* ssp. *dicoccoides* x *T. tauschii*) as a source of favourable alleles for milling and baking quality traits. Theoretical and Applied Genetics 115, 683–695.

La Verde V, Dominici P, Astegno A. 2018. Towards understanding plant calcium signaling through calmodulin-like proteins: a biochemical and structural perspective. International Journal of Molecular Sciences 19, 1331.

Lange W, Jochemsen G. 1992. Use of the gene pools of *Triticum turgidum* ssp. *dicoccoides* and *Aegilops squarrosa* for the breeding of common wheat (*T. aestivum*), through chromosome-doubled hybrids. Euphytica 59, 213–220.

Lasky JR, Des Marais DL, Lowry DB, Povolotskaya I, McKay JK, Richards JH, Keitt TH, Juenger TE. 2014. Natural variation in abiotic stress responsive gene expression and local adaptation to climate in *Arabidopsis thaliana*. Molecular Biology and Evolution 31, 2283–2296.

Lavarenne J, Guyomarc'h S, Sallaud C, Gantet P, Lucas M. 2018. The spring of systems biology-driven breeding. Trends in Plant Science 23, 706–720.

Le Gall H, Philippe F, Domon J-M, Gillet F, Pelloux J, Rayon C. 2015. Cell wall metabolism in response to abiotic stress. Plants 4, 112–166.

Lehti-Shiu MD, Panchy N, Wang P, Uygun S, Shiu S-H. 2017. Diversity, expansion, and evolutionary novelty of plant DNA-binding transcription factor families. Biochimica Et Biophysica Acta 1860, 3–20.

Li H. 2011. A statistical framework for SNP calling, mutation discovery, association mapping and population genetical parameter estimation from sequencing data. Bioinformatics 27, 2987–2993.

Li H, Handsaker B, Wysoker A, Fennell T, Ruan J, Homer N, Marth G, Abecasis G, Durbin R, 1000 Genome Project Data Processing Subgroup. 2009. The Sequence Alignment/Map format and SAMtools. Bioinformatics 25, 2078–2079.

Li QQ, Skinner J, Bennett JE. 2012. Evaluation of reference genes for real-time quantitative PCR studies in *Candida glabrata* following azole treatment. BMC Molecular Biology 13, 22.

Li Q, Zheng Q, Shen W, Cram D, Fowler DB, Wei Y, Zou J. 2015. Understanding the biochemical basis of temperature-induced lipid pathway adjustments in plants. The Plant Cell 27, 86–103.

Liang G, He H, Yu D. 2012. Identification of nitrogen starvation-responsive microRNAs in *Arabidopsis thaliana*. PloS One 7, e48951.

Liao Y, Smyth GK, Shi W. 2013. The Subread aligner: fast, accurate and scalable read mapping by seed-and-vote. Nucleic Acids Research 41, e108.

Liao Y, Smyth GK, Shi W. 2014. featureCounts: an efficient general purpose program for assigning sequence reads to genomic features. Bioinformatics 30, 923–930.

Liao C, Zheng Y, Guo Y. 2017. MYB30 transcription factor regulates oxidative and heat stress responses through ANNEXIN-mediated cytosolic calcium signaling in Arabidopsis. The New Phytologist 216, 163–177.

Licausi F, Ohme-Takagi M, Perata P. 2013. APETALA2/Ethylene Responsive Factor (AP2/ERF) transcription factors: mediators of stress responses and developmental programs. The New Phytologist 199, 639–649.

Lin Y, Golovnina K, Chen Z-X, Lee HN, Negron YLS, Sultana H, Oliver B, Harbison ST. 2016. Comparison of normalization and differential expression analyses using RNA-Seq data from 726 individual *Drosophila melanogaster*. BMC Genomics 17, 28.

Liu Z, Xin M, Qin J, Peng H, Ni Z, Yao Y, Sun Q. 2015. Temporal transcriptome profiling reveals expression partitioning of homeologous genes contributing to heat and drought acclimation in wheat (*Triticum aestivum* L.). BMC Plant Biology 15, 152.

Livak KJ, Schmittgen TD. 2001. Analysis of relative gene expression data using real-time quantitative PCR and the 2(-Delta Delta C(T)) method. Methods 25, 402–408.

Loginova DB, Silkova OG. 2018. The genome of bread wheat *Triticum aestivum* L.: Unique structural and functional properties. Russian Journal of Genetics 54, 403–414.

Lopez-Maestre H, Brinza L, Marchet C, *et al.* 2016. SNP calling from RNA-seq data without a reference genome: identification, quantification, differential analysis and impact on the protein sequence. Nucleic Acids Research 44, e148.

Lowe R, Shirley N, Bleackley M, Dolan S, Shafee T. 2017. Transcriptomics technologies. PLoS Computational Biology 13, e1005457.

Lu Y, Truman W, Liu X, Bethke G, Zhou M, Myers CL, Katagiri F, Glazebrook J. 2018. Different modes of negative regulation of plant immunity by calmodulin-related genes. Plant Physiology 176, 3046–3061.

Luo Q, Teng W, Fang S, Li H, Li B, Chu J, Li Z, Zheng Q. 2019. Transcriptome analysis of salt-stress response in three seedling tissues of common wheat. The Crop Journal 7, 378–392.

Mahajan MM, Goyal E, Singh AK, Gaikwad K, Kanika K. 2017. Transcriptome dynamics provide insights into long-term salinity stress tolerance in *Triticum aestivum* cv. Kharchia Local. Plant Physiology and Biochemistry 121, 128–139.

Manishankar P, Wang N, Köster P, Alatar AA, Kudla J. 2018. Calcium signaling during salt stress and in the regulation of ion homeostasis. Journal of Experimental Botany 69, 4215–4226.

Manolio TA, Collins FS, Cox NJ, *et al.* 2009. Finding the missing heritability of complex diseases. Nature 461, 747–753.

Mansur YA, Rojano E, Ranea JAG, Perkins JR. 2018. Chapter 7 - Analyzing the effects of genetic variation in noncoding genomic regions. In: Deigner H-P, Kohl M, eds. *Precision Medicine*. Academic Press, 119–144.

Martin M. 2011. CUTADAPT removes adapter sequences from high-throughput sequencing reads. EMBnet.journal 17, 10–12.

Máthé C, Garda T, Freytag C, M-Hamvas M. 2019. The role of serine-threonine protein phosphatase PP2A in plant oxidative stress signaling-facts and hypotheses. International Journal of Molecular Sciences 20, 3028.

Medvedev SS. 2018. Principles of calcium signal generation and transduction in plant cells. Russian Journal of Plant Physiology 65, 771–783.

Miyamoto T, Uemura T, Nemoto K, Daito M, Nozawa A, Sawasaki T, Arimura G-I. 2019. Tyrosine kinase-dependent defense responses against herbivory in Arabidopsis. Frontiers in Plant Science 10, 776.

Mohanta TK, Mohanta N, Mohanta YK, Bae H. 2015. Genome-wide identification of calcium dependent protein kinase gene family in plant lineage shows presence of novel D-x-D and D-E-L motifs in EF-hand domain. Frontiers in Plant Science 6, 1146.

Mohanta TK, Yadav D, Khan AL, Hashem A, Abd Allah EF, Al-Harrasi A. 2019. Molecular players of EF-hand containing calcium signaling event in plants. International Journal of Molecular Sciences 20, 1476.

Moldovan D, Spriggs A, Yang J, Pogson BJ, Dennis ES, Wilson IW. 2010. Hypoxia-responsive microRNAs and trans-acting small interfering RNAs in Arabidopsis. Journal of Experimental Botany 61, 165–177.

Montenegro JD, Golicz AA, Bayer PE, *et al.* 2017. The pangenome of hexaploid bread wheat. The Plant Journal 90, 1007–1013.

Morozova O, Hirst M, Marra MA. 2009. Applications of new sequencing technologies for transcriptome analysis. Annual Review of Genomics and Human Genetics 10, 135–151.

Morton MJL, Awlia M, Al-Tamimi N, Saade S, Pailles Y, Negrão S, Tester M. 2019. Salt stress under the scalpel - dissecting the genetics of salt tolerance. The Plant Journal 97, 148–163.

Munns R, Tester M. 2008. Mechanisms of salinity tolerance. Annual Review of Plant Biology 59, 651–681.

Murata N, Takahashi S, Nishiyama Y, Allakhverdiev SI. 2007. Photoinhibition of photosystem II under environmental stress. Biochimica Et Biophysica Acta 1767, 414–421.

Neill SJ, Desikan R, Clarke A, Hurst RD, Hancock JT. 2002. Hydrogen peroxide and nitric oxide as signalling molecules in plants. Journal of Experimental Botany 53, 1237–1247.

Nie S, Zhang M, Zhang L. 2017. Genome-wide identification and expression analysis of calmodulin-like (CML) genes in Chinese cabbage (*Brassica rapa* L. ssp. *pekinensis*). BMC Genomics 18, 842.

de Oliveira AB, Mendes Alencar NL, Gomes-Filho E. 2013. Comparison between the water and salt stress effects on plant growth and development. In: Akinci S, ed. Responses of organisms to water stress. Rijeka, Croatia: IntechOpen, doi: 10.5772/54223.

Otyama PI, Wilkey A, Kulkarni R, *et al.* 2019. Evaluation of linkage disequilibrium, population structure, and genetic diversity in the U.S. peanut mini core collection. BMC Genomics 20, 481.

Oyiga BC, Ogbonnaya FC, Sharma RC, Baum M, Léon J, Ballvora A. 2019. Genetic and transcriptional variations in *NRAMP-2* and *OPAQUE1* genes are associated with salt stress response in wheat. Theoretical and Applied Genetics 132, 323–346.

Oyiga BC, Sharma RC, Baum M, Ogbonnaya FC, Léon J, Ballvora A. 2018. Allelic variations and differential expressions detected at quantitative trait loci for salt stress tolerance in wheat. Plant, Cell & Environment 41, 919–935.

Ozsolak F, Luzzi V, Watson MA. 2005. mRNA applications. In: Emmert-Buck MR, Gillespie JW, Chuaqui RF, eds. *Dissecting the molecular anatomy of tissue (Principles and practice)*. Berlin, Heidelberg: Springer, 125–144.

Parihar P, Singh S, Singh R, Singh VP, Prasad SM. 2015. Effect of salinity stress on plants and its tolerance strategies: a review. Environmental Science and Pollution Research International 22, 4056–4075.

Pender B, Saddler D, Shea J, Ward D. 2011. 12B: Stationary points and turning points. Cambridge 2 Unit Mathematics Year 11. Sydney: Cambridge University Press, 318.

Pérez-de-Castro AM, Vilanova S, Cañizares J, Pascual L, Blanca JM, Díez MJ, Prohens J, Picó B. 2012. Application of genomic tools in plant breeding. Current Genomics 13, 179–195.

Pérez-Salamó I, Papdi C, Rigó G, *et al.* 2014. The heat shock factor A4A confers salt tolerance and is regulated by oxidative stress and the mitogen-activated protein kinases MPK3 and MPK6. Plant Physiology 165, 319–334.

Pérez-Torres E, Paredes C M, Polanco V, Becerra B V. 2009. Gene expression analysis: a way to study tolerance to abiotic stresses in crops species. Chilean Journal of Agricultural Research 69, 260–269.

Perochon A, Aldon D, Galaud J-P, Ranty B. 2011. Calmodulin and calmodulin-like proteins in plant calcium signaling. Biochimie 93, 2048–2053.

Pessarakli M, Szabolcs I. 2019. Soil salinity and sodicity as particular plant/crop stress factors. In: Pessarakli M, ed. Handbook of plant and crop stress. Boca Raton, FL: CRC Press, Taylor & Francis Group, 3–21.

Pfaffl M. 2004. Quantification strategies in real-time PCR. In: Bustin SA, ed. *A-Z of quantitative PCR*. La Jolla, CA: International University Line, 87 – 112.

Phukan UJ, Jeena GS, Shukla RK. 2016. WRKY transcription factors: molecular regulation and stress responses in plants. Frontiers in Plant Science 7, 760.

Pingault L, Choulet F, Alberti A, Glover N, Wincker P, Feuillet C, Paux E. 2015. Deep transcriptome sequencing provides new insights into the structural and functional organization of the wheat genome. Genome Biology 16, 29.

Queval G, Foyer CH. 2012. Redox regulation of photosynthetic gene expression. Philosophical Transactions of the Royal Society of London. Series B, Biological Sciences 367, 3475–3485.

Rafalski JA. 2010. Association genetics in crop improvement. Current Opinion in Plant Biology 13, 174–180.

Rahman F, Hassan M, Rosli R, Almousally I, Hanano A, Murphy DJ. 2018. Evolutionary and genomic analysis of the caleosin/peroxygenase (CLO/PXG) gene/protein families in the *Viridiplantae*. PloS One 13, e0196669.

Ramírez-González RH, Borrill P, Lang D, *et al.* 2018. The transcriptional landscape of polyploid wheat. Science 361, eaar6089.

Ranty B, Aldon D, Cotelle V, Galaud J-P, Thuleau P, Mazars C. 2016. Calcium sensors as key hubs in plant responses to biotic and abiotic stresses. Frontiers in Plant Science 7, 327.

Rasheed A, Mujeeb-Kazi A, Ogbonnaya FC, He Z, Rajaram S. 2018. Wheat genetic resources in the post-genomics era: promise and challenges. Annals of Botany 121, 603–616.

Rasheed A, Xia X. 2019. From markers to genome-based breeding in wheat. Theoretical and Applied Genetics 132, 767–784.

Rebouças E de L, Costa JJ do N, Passos MJ, Passos JR de S, Hurk R van den, Silva JRV. 2013. Real time PCR and importance of housekeepings genes for normalization and quantification of mRNA expression in different tissues. Brazilian Archives of Biology and Technology 56, 143–154.

Reddy ASN, Ali GS, Celesnik H, Day IS. 2011. Coping with stresses: roles of calcium- and calcium/calmodulin-regulated gene expression. The Plant Cell 23, 2010–2032.

Rengasamy P. 2006. World salinization with emphasis on Australia. Journal of Experimental Botany 57, 1017–1023.

Roberts A, Pimentel H, Trapnell C, Pachter L. 2011. Identification of novel transcripts in annotated genomes using RNA-Seq. Bioinformatics (Oxford, England) 27, 2325–2329.

Robles P, Quesada V. 2019. Transcriptional and post-transcriptional regulation of organellar gene expression (OGE) and its roles in plant salt tolerance. International Journal of Molecular Sciences 20, 1056.

Roy SJ, Negrão S, Tester M. 2014. Salt resistant crop plants. Current Opinion in Biotechnology 26, 115–124.

Saba Rahim M, Sharma H, Parveen A, Roy JK. 2018. Trait mapping approaches through association analysis in plants. Advances in Biochemical Engineering/Biotechnology 164, 83–108.

Sah SK, Reddy KR, Li J. 2016. Abscisic acid and abiotic stress tolerance in crop plants. Frontiers in Plant Science 7, 571.

Sahraeian SME, Mohiyuddin M, Sebra R, *et al*. 2017. Gaining comprehensive biological insight into the transcriptome by performing a broad-spectrum RNA-seq analysis. Nature Communications 8, 1–15.

Saibo NJM, Lourenço T, Oliveira MM. 2009. Transcription factors and regulation of photosynthetic and related metabolism under environmental stresses. Annals of Botany 103, 609–623.

Saijo Y, Loo EP. 2020. Plant immunity in signal integration between biotic and abiotic stress responses. New Phytologist 225, 87–104.

Sakadevan K, Nguyen M-L. 2010. Extent, impact, and response to soil and water salinity in arid and semiarid regions. Advances in Agronomy 109, 55–74.

Sanyal SK, Mahiwal S, Pandey GK. 2019. Calcium signaling: a communication network that regulates cellular processes. In: Sopory S, ed. *Sensory biology of plants*. Singapore: Springer, 279–309.

Schwarte S, Bauwe H. 2007. Identification of the Photorespiratory 2-Phosphoglycolate Phosphatase, *PGLP1*, in Arabidopsis. Plant Physiology 144, 1580–1586.

Seifikalhor M, Aliniaeifard S, Shomali A, Azad N, Hassani B, Lastochkina O, Li T. 2019. Calcium signaling and salt tolerance are diversely entwined in plants. Plant Signaling & Behavior 14, 1665455.

Semagn K, Bjørnstad Å, Ndjiondjop MN. 2006. Principles, requirements and prospects of genetic mapping in plants. African Journal of Biotechnology 5, 2569-2587.

Sha Y, Phan JH, Wang MD. 2015. Effect of low-expression gene filtering on detection of differentially expressed genes in RNA-seq data. Conference Proceedings IEEE Engineering in Medicine and Biology Society 2015, 6461–6464

Shabala S, Wu H, Bose J. 2015. Salt stress sensing and early signalling events in plant roots: Current knowledge and hypothesis. Plant Science 241, 109–119.

Sharma T, Dreyer I, Riedelsberger J. 2013. The role of K^+ channels in uptake and redistribution of potassium in the model plant *Arabidopsis thaliana*. Frontiers in Plant Science 4, 224.

Shewry PR, Hey SJ. 2015. The contribution of wheat to human diet and health. Food and Energy Security 4, 178–202.

Shi S, Li S, Asim M, Mao J, Xu D, Ullah Z, Liu G, Wang Q, Liu H. 2018. The Arabidopsis Calcium-Dependent Protein Kinases (CDPKs) and their roles in plant growth regulation and abiotic stress responses. International Journal of Molecular Sciences 19, 1900.

Shi X, Ling H-Q. 2018. Current advances in genome sequencing of common wheat and its ancestral species. The Crop Journal 6, 15–21.

Silveira JAG, Carvalho FEL. 2016. Proteomics, photosynthesis and salt resistance in crops: An integrative view. Journal of Proteomics 143, 24–35.

Singh AK, Kumar R, Tripathi AK, Gupta BK, Pareek A, Singla-Pareek SL. 2015. Genome-wide investigation and expression analysis of sodium/calcium exchanger gene family in rice and Arabidopsis. Rice 8, 21.

Smith RD, Walker springerJC. 1996. Plant protein phosphatases. Annual Review of Plant Physiology and Plant Molecular Biology 47, 101–125.

Song Q, Liu C, Bachir DG, Chen L, Hu Y-G. 2017. Drought resistance of new synthetic hexaploid wheat accessions evaluated by multiple traits and antioxidant enzyme activity. Field Crops Research 210, 91–103.

Tavakkoli E, Rengasamy P, McDonald GK. 2010. The response of barley to salinity stress differs between hydroponic and soil systems. Functional Plant Biology 37, 621–633.

Teo ZL, Savas P, Loi S. 2016. Gene expression analysis: Current methods. In: Lakhani SR, Fox SB, eds. *Molecular Pathology in Cancer Research*. New York, NY: Springer, 107–136.

The Gene Ontology Consortium. 2019. The Gene Ontology Resource: 20 years and still GOing strong. Nucleic Acids Research 47, D330–D338.

Timmons JA, Szkop KJ, Gallagher IJ. 2015. Multiple sources of bias confound functional enrichment analysis of global-omics data. Genome Biology 16, 186.

Trapnell C, Pachter L, Salzberg SL. 2009. TopHat: discovering splice junctions with RNA-Seq. Bioinformatics (Oxford, England) 25, 1105–1111.

Trapnell C, Roberts A, Goff L, Pertea G, Kim D, Kelley DR, Pimentel H, Salzberg SL, Rinn JL, Pachter L. 2012. Differential gene and transcript expression analysis of RNA-seq experiments with TopHat and Cufflinks. Nature Protocols 7, 562–578.

Tsugama D, Liu S, Fujino K, Takano T. 2018. Calcium signalling regulates the functions of the bZIP protein VIP1 in touch responses in *Arabidopsis thaliana*. Annals of Botany 122, 1219–1229.

Tuteja N. 2007. Mechanisms of high salinity tolerance in plants. Methods in Enzymology 428, 419–438.

Tzfadia O, Bocobza S, Defoort J, *et al.* 2018. The 'TranSeq' 3'-end sequencing method for high-throughput transcriptomics and gene space refinement in plant genomes. The Plant Journal 96, 223–232.

Vadassery J, Reichelt M, Hause B, Gershenzon J, Boland W, Mithöfer A. 2012. CML42-mediated calcium signaling coordinates responses to *Spodoptera* herbivory and abiotic stresses in Arabidopsis. Plant Physiology 159, 1159–1175.

Van den Berge K, Hembach KM, Soneson C, Tiberi S, Clement L, Love MI, Patro R, Robinson MD. 2019. RNA sequencing data: hitchhiker's guide to expression analysis. Annual Review of Biomedical Data Science 2, 139–173.

Vanderbeld B, Snedden WA. 2007. Developmental and stimulus-induced expression patterns of Arabidopsis calmodulin-like genes *CML37*, *CML38* and *CML39*. Plant Molecular Biology 64, 683–697.

Vergauwen D, De Smet I. 2017. From early farmers to Norman Borlaug - the making of modern wheat. Current biology: CB 27, R858–R862.

Verica JA, Chae L, Tong H, Ingmire P, He Z-H. 2003. Tissue-specific and developmentally regulated expression of a cluster of tandemly arrayed cell wall-associated kinase-like kinase genes in Arabidopsis. Plant Physiology 133, 1732–1746.

Virdi AS, Singh S, Singh P. 2015. Abiotic stress responses in plants: roles of calmodulin-regulated proteins. Frontiers in Plant Science 6, 809.

Võsa U, Esko T, Kasela S, Annilo T. 2015. Altered gene expression associated with microRNA binding site polymorphisms. PloS One 10, e0141351.

Voss-Fels K, Frisch M, Qian L, Kontowski S, Friedt W, Gottwald S, Snowdon RJ. 2015. Subgenomic diversity patterns caused by directional selection in bread wheat gene pools. The Plant Genome 8, doi: 10.3835/plantgenome2015.03.0013.

Wan Y, King R, Mitchell RAC, Hassani-Pak K, Hawkesford MJ. 2017. Spatiotemporal expression patterns of wheat amino acid transporters reveal their putative roles in nitrogen transport and responses to abiotic stress. Scientific Reports 7, 5461.

Wan S, Wang W, Zhou T, Zhang Y, Chen J, Xiao B, Yang Y, Yu Y. 2018. Transcriptomic analysis reveals the molecular mechanisms of *Camellia sinensis* in response to salt stress. Plant Growth Regulation 84, 481–492.

Wang J-P, Munyampundu J-P, Xu Y-P, Cai X-Z. 2015. Phylogeny of plant calcium and calmodulin-dependent protein kinases (CCaMKs) and functional analyses of tomato CCaMK in disease resistance. Frontiers in Plant Science 6, 1075.

Wang H, Niu H, Liang M, Zhai Y, Huang W, Ding Q, Du Y, Lu M. 2019*a*. A wall-associated kinase gene *CaWAKL20* from pepper negatively modulates plant thermotolerance by reducing the expression of ABA-responsive genes. Frontiers in Plant Science 10, 591.

Wang B, Sun Y-F, Song N, Wei J-P, Wang X-J, Feng H, Yin Z-Y, Kang Z-S. 2014*a*. MicroRNAs involving in cold, wounding and salt stresses in *Triticum aestivum* L. Plant Physiology and Biochemistry 80, 90–96.

Wang Y, Tiwari VK, Rawat N, Bikram S. Gill, Naxin Huo, You FM, Devin Coleman-Derr, Yong Q. Gu. 2016. GSP: a web-based platform for designing genome-specific primers in polyploids. Bioinformatics 32, 2382–2383.

Wang W, Vinocur B, Altman A. 2003. Plant responses to drought, salinity and extreme temperatures: towards genetic engineering for stress tolerance. Planta 218, 1–14.

Wang M, Wang S, Liang Z, Shi W, Gao C, Xia G. 2018*a*. From Genetic Stock to Genome Editing: Gene Exploitation in Wheat. Trends in Biotechnology 36, 160–172.

Wang Z, Wang Y, Wang N, Wang J, Wang Z, Vallejos CE, Wu R. 2014*b*. Towards a comprehensive picture of the genetic landscape of complex traits. Briefings in Bioinformatics 15, 30–42.

Wang S, Wong D, Forrest K, *et al.* 2014*c*. Characterization of polyploid wheat genomic diversity using a high-density 90,000 single nucleotide polymorphism array. Plant Biotechnology Journal 12, 787–796.

Wang M, Xia G. 2018. The landscape of molecular mechanisms for salt tolerance in wheat. The Crop Journal 6, 42–47.

Wang Z, Yan L, Wan L, Huai D, Kang Y, Shi L, Jiang H, Lei Y, Liao B. 2019*b*. Genome-wide systematic characterization of bZIP transcription factors and their expression profiles during seed development and in response to salt stress in peanut. BMC Genomics 20, 51.

Wang Q, Yang S, Wan S, Li X. 2019*c*. The significance of calcium in photosynthesis. International Journal of Molecular Sciences 20, 1353.

Wang J, Zhu J, Zhang Y, Fan F, Li W, Wang F, Zhong W, Wang C, Yang J. 2018*b*. Comparative transcriptome analysis reveals molecular response to salinity stress of salt-tolerant and sensitive genotypes of indica rice at seedling stage. Scientific Reports 8, 2085.

Wasternack C, Feussner I. 2018. The oxylipin pathways: biochemistry and function. Annual Review of Plant Biology 69, 363–386.

Weirauch MT, Yang A, Albu M, *et al.* 2014. Determination and inference of eukaryotic transcription factor sequence specificity. Cell 158, 1431–1443.

Wicke B, Smeets E, Dornburg V, Vashev B, Gaiser T, Turkenburg W, Faaij A. 2011. The global technical and economic potential of bioenergy from salt-affected soils. Energy & Environmental Science 4, 2669–2681.

Williams EG, Auwerx J. 2015. The convergence of systems and reductionist approaches in complex trait analysis. Cell 162, 23–32.

Wimalasekera R, Villar C, Begum T, Scherer GFE. 2011. *COPPER AMINE OXIDASE1* (*CuAO1*) of *Arabidopsis thaliana* contributes to abscisic acid- and polyamine-induced nitric oxide biosynthesis and abscisic acid signal transduction. Molecular Plant 4, 663–678.

Wingler A, Lea PJ, Quick WP, Leegood RC. 2000. Photorespiration: metabolic pathways and their role in stress protection. Philosophical Transactions of the Royal Society B: Biological Sciences 355, 1517–1529.

Xu Y, Li S, Li L, Zhang X, Xu H, An D. Mapping QTLs for salt tolerance with additive, epistatic and QTL × treatment interaction effects at seedling stage in wheat. Plant Breeding 132, 276–283.

Xu Y, Li P, Yang Z, Xu C. 2017. Genetic mapping of quantitative trait loci in crops. The Crop Journal 5, 175–184.

Xu Z, Song J. 2017. The 2-oxoglutarate-dependent dioxygenase superfamily participates in tanshinone production in *Salvia miltiorrhiza*. Journal of Experimental Botany 68, 2299–2308.

Yadav D, Boyidi P, Ahmed I, Kirti PB. 2018. Plant annexins and their involvement in stress responses. Environmental and Experimental Botany 155, 293–306.

Yang C, Zhao L, Zhang H, Yang Z, Wang H, Wen S, Zhang C, Rustgi S, von Wettstein D, Liu B. 2014. Evolution of physiological responses to salt stress in hexaploid wheat. Proceedings of the National Academy of Sciences of the United States of America 111, 11882–11887.

Yip-Delormel T, Boudsocq M. 2019. Properties and functions of calcium-dependent protein kinases and their relatives in Arabidopsis thaliana. The New Phytologist 224, 585–604.

Zaman M, Shahid SA, Pharis RP. 2016. Salinity a serious threat to food security – Where do we stand? Soils Newsletter 39, 9–10.

Zandalinas SI, Sengupta S, Burks D, Azad RK, Mittler R. 2019. Identification and characterization of a core set of ROS wave-associated transcripts involved in the systemic acquired acclimation response of Arabidopsis to excess light. The Plant Journal 98, 126–141.

Zang D, Wang J, Zhang X, Liu Z, Wang Y. 2019. Arabidopsis heat shock transcription factor HSFA7b positively mediates salt stress tolerance by binding to an E-box-like motif to regulate gene expression. Journal of Experimental Botany 70, 5355–5374.

Zawada AM, Rogacev KS, Müller S, Rotter B, Winter P, Fliser D, Heine GH. 2014. Massive analysis of cDNA ends (MACE) and miRNA expression profiling identifies proatherogenic pathways in chronic kidney disease. Epigenetics 9, 161–172.

Zeng H, Xu L, Singh A, Wang H, Du L, Poovaiah BW. 2015. Involvement of calmodulin and calmodulin-like proteins in plant responses to abiotic stresses. Frontiers in Plant Science 6, 600.

Zhang Y, Liu Z, Khan AA, *et al.* 2016. Expression partitioning of homeologs and tandem duplications contribute to salt tolerance in wheat (*Triticum aestivum* L.). Scientific Reports 6, 21476.

Zhang Q, Liu X, Liu X, Wang J, Yu J, Hu D, Hao Y. 2017. Genome-wide identification, characterization, and expression analysis of calmodulin-like proteins (CMLs) in apple. Horticultural Plant Journal 3, 219–231.

Zhu J-K. 2016. Abiotic stress signaling and responses in plants. Cell 167, 313–324.

Zyprych-Walczak J, Szabelska A, Handschuh L, Górczak K, Klamecka K, Figlerowicz M, Siatkowski I. 2015. The impact of normalization methods on RNA-seq data analysis. BioMed Research International 2015, 621690.

Appendix

Appendix 1. Overview of reads processing and reference genome mapping from all libraries.

a) Osmotic stress libraries

Libraries		Total reads	Filtered reads after QC[b] (%)	Mapped reads	Mapping efficiency (%)	Unique mapped reads (UMR)	Multiple aligned reads	Multiple aligned reads (%)	UMR in reference gene models (GM)
Syn86 Control	0 min	3762527	7.1	2941718	84.2	2088265	853453	29	1757332
	30 min	5040446	6.6	3977669	84.5	3047297	930372	23.4	2589089
	4 h	5706140	9.2	4300722	83	3530248	770474	17.9	2980729
Syn86 Stress	8 min	3854936	5.2	3025224	82.8	2257892	767332	25.4	1861478
	15 min	5049633	7.3	3862225	82.5	3080479	781746	20.2	2582471
	30 min	5262981	7.9	3998840	82.5	3281663	717177	17.9	2765572
	4 h	4255947	7	3291831	83.2	2632432	659399	20	2210856
Zentos Control	0 min	5572114	9.4	4218244	83.6	3287693	930551	22.1	2755152
	30 min	5212469	8.5	4043075	84.7	3200059	843016	20.9	2694845
	4 h	5235429	7.8	4085748	84.7	3136558	949190	23.2	2604404
Zentos Stress	8 min	6068132	9.7	4640926	84.7	3683923	957003	20.6	3104994
	15 min	5460661	9.7	4195570	85.1	3119621	1075949	25.6	2620178
	30 min	4133679	4.6	3299731	83.7	2660847	638884	19.4	2223483
	4 h	5233986	8.8	3867463	81.0	3155938	711525	18.4	2657840
Average		4989220	7.8	3839213.3	83.6	3011636.8	827576.5	21.7	2529173.1
SD[a]		709964.9	1.6	506378.5	1.2	451258.6	128255.651	3.3	386615.0

[a] SD: Standard deviation

[b] QC: Quality control

Libraries		UMR in reference GM (%)	UMR in extended GM + novel transcripts (NT)	UMR in extended GM + NT (%)	UMR after CPM < 2.5 filter	Filtered out UMR after CPM filter (%)
Syn86 Control	0 min	84.2	1970104	94.3	1903870	3.4
	30 min	85.0	2893032	94.9	2822444	2.4
	4 h	84.4	3349358	94.9	3232263	3.5
Syn86 Stress	8 min	82.4	2087307	92.4	2030775	2.7
	15 min	83.8	2909845	94.5	2816758	3.2
	30 min	84.3	3107407	94.7	3012893	3.0
	4 h	84.0	2495707	94.8	2417972	3.1
Zentos Control	0 min	83.8	3093631	94.1	2998533	3.1
	30 min	84.2	3024972	94.5	2932900	3.0
	4 h	83.0	2936801	93.6	2840124	3.3
Zentos Stress	8 min	84.3	3476752	94.4	3370497	3.1
	15 min	84.0	2946499	94.5	2862765	2.8
	30 min	83.6	2507753	94.2	2425364	3.3
	4 h	84.2	2968388	94.1	2861031	3.6
Average		83.9	2840539.7	94.3	2752013.5	3.1
SD		0.6	432525.9	0.6	418200.7	0.3

b) Ionic stress libraries

Libraries		Total reads	Removed after QC (%)	Mapped reads	Mapping efficiency	Unique mapped Reads (UMR)	Multiple aligned reads	Multiple aligned reads (%)	UMR in reference gene models (GM)
Altay2000	**11 days**	8114165	2.47	7388399	93.4	5685325	1703074	23.1	4804455
Control	**24 days**	12148620	2.51	11052250	93.3	8934228	2118022	19.2	7577960
Altay2000	**11 days**	5123752	2.78	4633841	93	3654709	979132	21.1	3083227
Stress	**24 days**	8177854	2.73	7364984	92.6	6005757	1359227	18.5	5079060
Bobur	**11 days**	9681088	2.97	8717906	92.8	7126152	1591754	18.3	6027484
Control	**24 days**	9913293	2.16	9079634	93.6	7376510	1703124	18.8	6260603
Bobur	**11 days**	7204855	2.48	6537136	93	5241318	1295818	19.8	4437689
Stress	**24 days**	11960398	2.42	10846554	92.9	8849873	1996681	18.4	7498109
Average		9040503.1	2.6	8202588	93.1	6609234	1593354	19.7	5596073.4
SD		2380609.1	0.3	2171900.5	0.3	1816597.3	374671.6	1.7	1545664.1

Libraries		UMR in reference GM (%)	UMR in extended GM + novel transcripts (NT)	UMR in extended GM + NT (%)	Reads after deduplication	Reads after (%) deduplication	UMR in extended GM + NT after deduplication
Altay2000	**11 days**	84.5	5350302	94.1	4074424	55.2	2209963
Control	**24 days**	84.8	8394831	94.0	5423626	49.1	3049629
Altay2000	**11 days**	84.4	3426312	93.8	2639730	57.0	1544343
Stress	**24 days**	84.6	5615429	93.5	4260254	57.8	2677389
Bobur	**11 days**	84.6	6709926	94.2	4353254	49.9	2566285
Control	**24 days**	84.9	6934631	94.0	4935428	54.4	3001207
Bobur	**11 days**	84.7	4913937	93.8	3616040	55.3	2149826
Stress	**24 days**	84.7	8301260	93.8	5657327	52.2	3376956
Average		84.6	6205828.5	93.9	4370010.4	53.8	2571949.8
SD		0.2	1708927.2	0.2	981909.7	3.2	590014.8

Libraries		UMR after CPM < 2.5 filter	Filtered out UMR after CPM filter (%)
Altay2000	**11 days**	2136405.0	3.3
Control	**24 days**	2916948.0	4.4
Altay2000	**11 days**	1500433.0	2.8
Stress	**24 days**	2536612.0	5.3
Bobur	**11 days**	2493777.0	2.8
Control	**24 days**	2896362.0	3.5
Bobur	**11 days**	2090544.0	2.8
Stress	**24 days**	3241517.0	4.0
Average		2476574.8	3.6
SD		557644.9	0.9

Appendix 2. . Density plots with the log_{10} normalized expression values of the libraries from the four genotypes studied. a) Zentos, b) Syn86, c) Altay2000 without deduplication, d) Altay2000 deduplicated, e) Bobur without deduplication and f) Bobur deduplicated. C= Control library, S= Stress library.

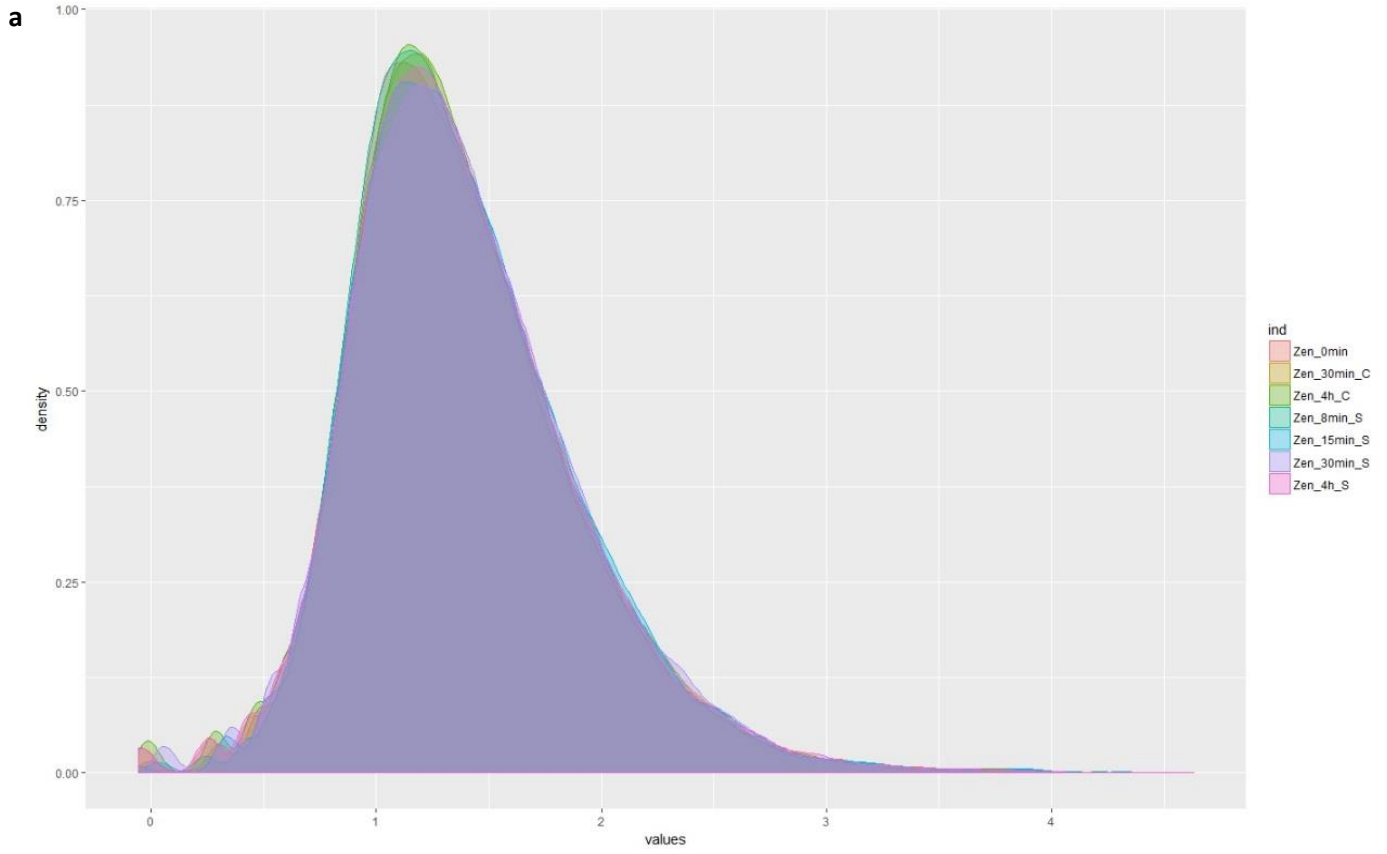

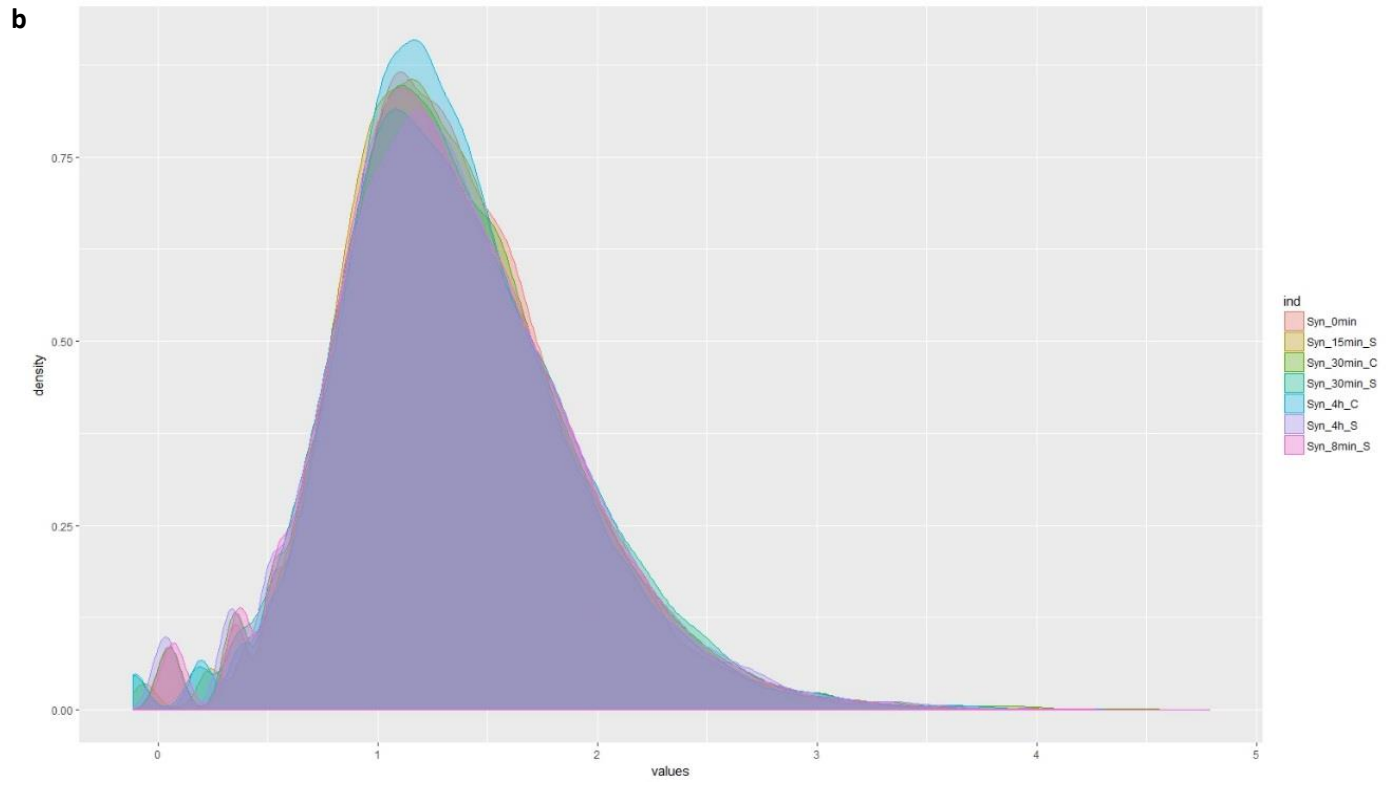

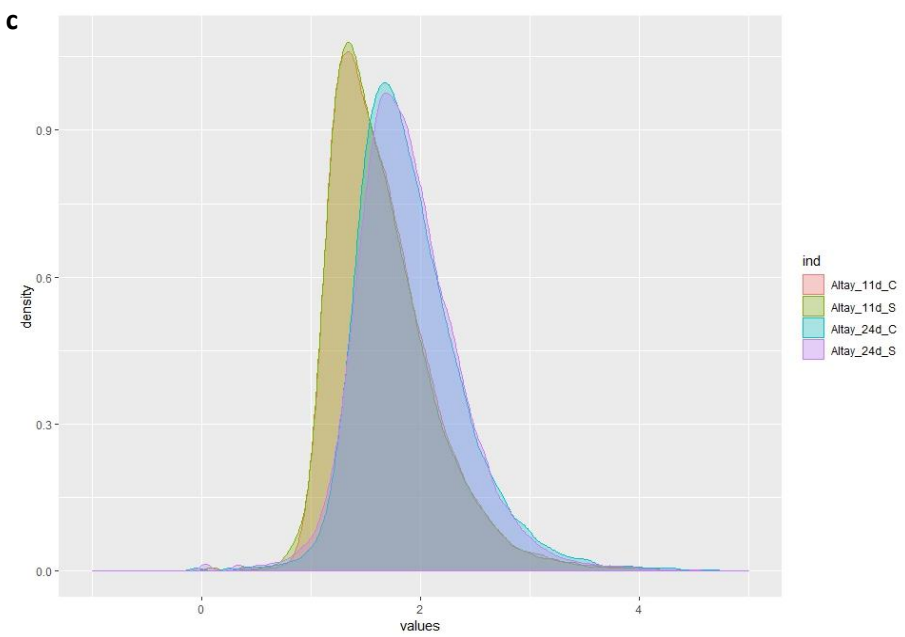
c
density
values
ind
Altay_11d_C
Altay_11d_S
Altay_24d_C
Altay_24d_S

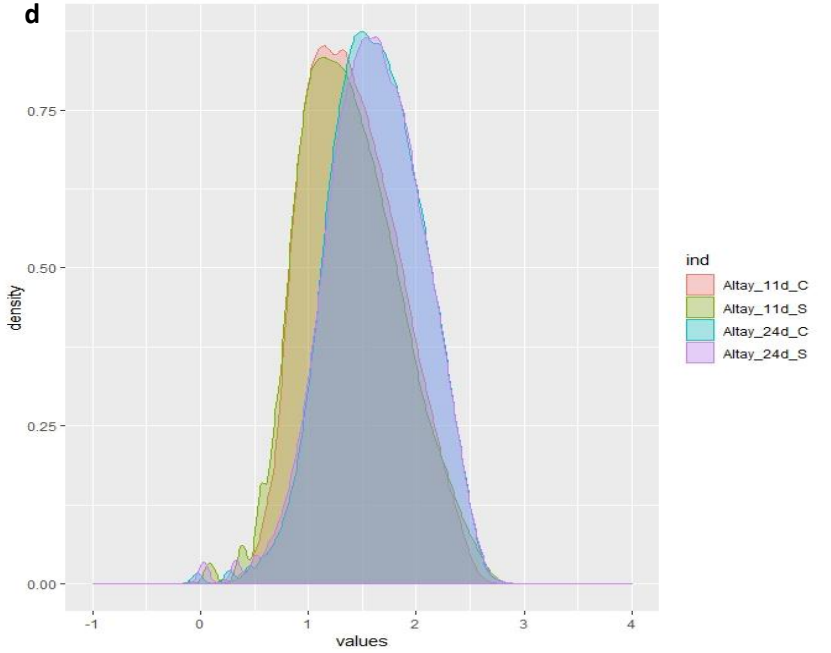
d
density
values
ind
Altay_11d_C
Altay_11d_S
Altay_24d_C
Altay_24d_S

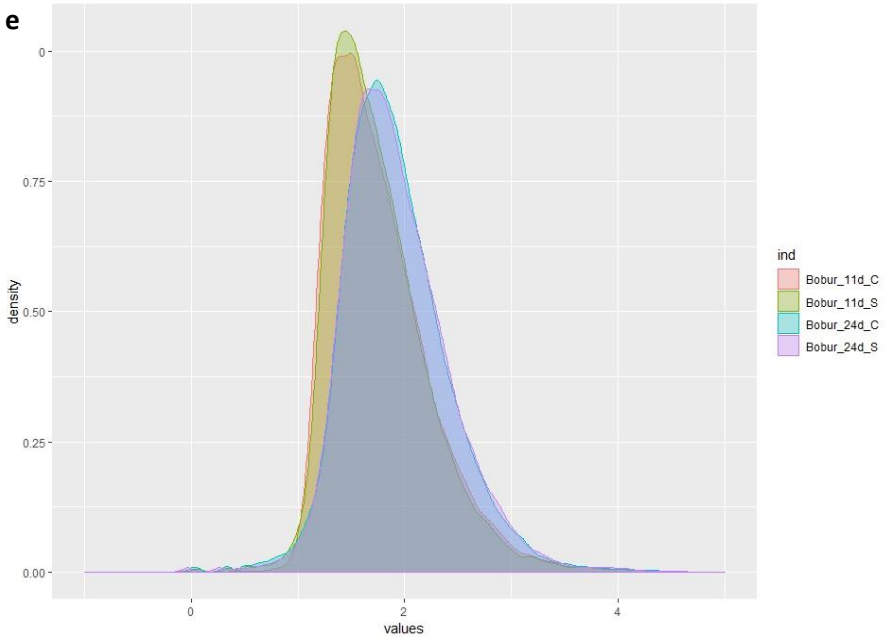
e
density
values
ind
Bobur_11d_C
Bobur_11d_S
Bobur_24d_C
Bobur_24d_S

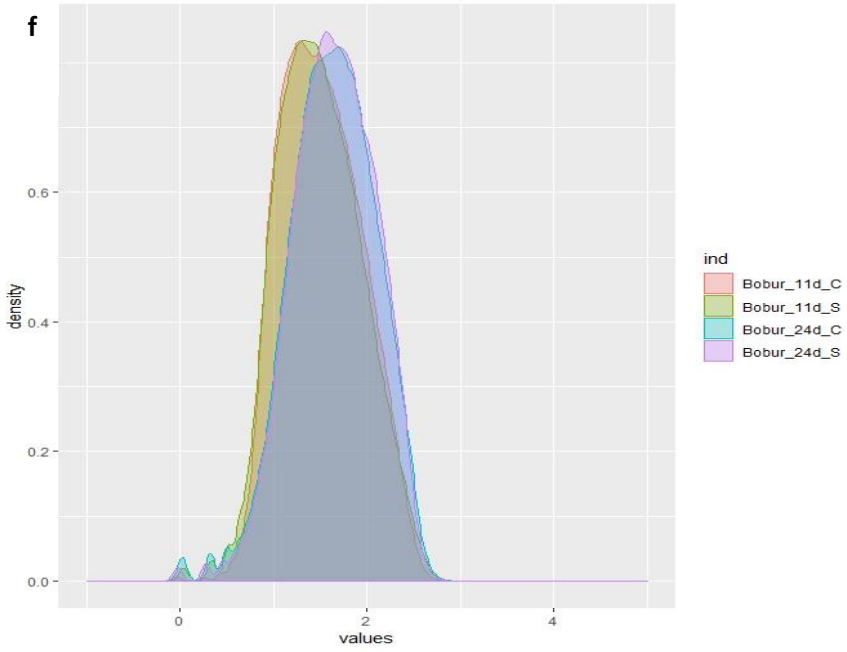
f
density
values
ind
Bobur_11d_C
Bobur_11d_S
Bobur_24d_C
Bobur_24d_S

Appendix 3. Reference genome coordinates from the novel salt-responsive transcripts identified in the four genotypes.

a) Zentos

Novel transcript ID	Chr	Start	End	Length (bp)
Traes7722	chr1A	571738110	571738646	537
Traes7855	chr1A	294136436	294138591	2156
Traes8014	chr1A	2918909	2919478	570
Traes8020	chr1A	316698	316832	135
Traes7267	chr1B	667974971	667975360	390
Traes7288	chr1B	630931945	630932056	112
Traes7289	chr1B	630926476	630926836	361
Traes7294	chr1B	623722417	623722876	460
Traes7339	chr1B	554487349	554487884	536
Traes7352	chr1B	548894526	548895129	604
Traes7358	chr1B	548622175	548622949	775
Traes7375	chr1B	520390543	520391143	601
Traes7525	chr1B	269293975	269294445	471
Traes7659	chr1B	80713246	80713557	312
Traes6997	chr1D	411278015	411278250	236
Traes7003	chr1D	408240724	408241419	696
Traes7005	chr1D	408238354	408239494	1141
Traes7015	chr1D	408072397	408073340	944
Traes7068	chr1D	307419569	307419910	342
Traes7125	chr1D	208091924	208092285	362
Traes7199	chr1D	52115089	52115635	547
Traes7201	chr1D	51769618	51769949	332
Traes7203	chr1D	51623637	51623853	217
Traes6608	chr2A	750364846	750365390	545
Traes6851	chr2A	164305814	164306259	446
Traes6443	chr2B	224214207	224214746	540
Traes6452	chr2B	212115989	212116450	462
Traes6543	chr2B	73989454	73990048	595
Traes5791	chr2D	567569079	567569582	504
Traes5859	chr2D	447831978	447832512	535
Traes6046	chr2D	114646031	114647112	1082
Traes6090	chr2D	46577107	46577676	570
Traes5456	chr3A	593313949	593314305	357
Traes5478	chr3A	546413105	546413578	474
Traes5560	chr3A	359060897	359061610	714
Traes5569	chr3A	354432417	354432898	482
Traes5725	chr3A	12786717	12787350	634
Traes4952	chr3B	810295733	810296148	416
Traes4961	chr3B	804542445	804543022	578
Traes5288	chr3B	119418865	119419461	597
Traes5292	chr3B	109947940	109948349	410

Traes5353	chr3B	6216548	6217193	646
Traes5354	chr3B	6215744	6216216	473
Traes4559	chr3D	597743325	597743702	378
Traes4560	chr3D	597737104	597737748	645
Traes4566	chr3D	594643618	594643948	331
Traes4754	chr3D	274358502	274359124	623
Traes4870	chr3D	74348552	74349319	768
Traes4923	chr3D	7600011	7600723	713
Traes4300	chr4A	585641380	585642190	811
Traes4009	chr4B	357822548	357823240	693
Traes3544	chr4D	471153332	471153861	530
Traes3218	chr5A	680863268	680864106	839
Traes3335	chr5A	437209713	437210296	584
Traes3056	chr5B	254953505	254954187	683
Traes3165	chr5B	58406784	58407927	1144
Traes3173	chr5B	49531223	49532187	965
Traes3187	chr5B	23322984	23324197	1214
Traes2469	chr5D	556372296	556372766	471
Traes2532	chr5D	445644997	445645637	641
Traes2634	chr5D	290394039	290394619	581
Traes2746	chr5D	55591529	55592521	993
Traes2753	chr5D	47856462	47857219	758
Traes2146	chr6A	614491319	614491736	418
Traes2169	chr6A	596381418	596381744	327
Traes2232	chr6A	498540162	498541162	1001
Traes1727	chr6B	658194825	658195116	292
Traes1379	chr6D	471858236	471858588	353
Traes1381	chr6D	471007944	471008809	866
Traes1383	chr6D	469282177	469282776	600
Traes1385	chr6D	469252776	469253180	405
Traes1469	chr6D	372816458	372817612	1155
Traes1229	chr7A	268179081	268179719	639
Traes1250	chr7A	219159372	219160040	669
Traes1259	chr7A	198409311	198409691	381
Traes1261	chr7A	198205874	198206371	498
Traes1004	chr7B	48069144	48069490	347
Traes564	chr7B	716022731	716023200	470
Traes565	chr7B	715479550	715482111	2562
Traes586	chr7B	694920404	694921455	1052
Traes715	chr7B	482681815	482682353	539
Traes821	chr7B	329786246	329786940	695
Traes822	chr7B	329775609	329776185	577
Traes823	chr7B	329694435	329694936	502
Traes897	chr7B	221272783	221273420	638
Traes169	chr7D	619806572	619808038	1467
Traes363	chr7D	277525063	277525532	470
Traes378	chr7D	252534812	252535529	718

Traes418	chr7D	186798577	186799257	681
Traes420	chr7D	186509990	186510510	521
Traes118	chrUn	58456695	58457149	455
Traes14	chrUn	431695763	431695990	228
Traes23	chrUn	411778761	411778925	165
Traes61	chrUn	264884003	264885451	1449

b) Syn86

Novel transcript ID	Chr	Start	End	Length (bp)
Traes7722	chr1A	571738110	571738646	537
Traes7724	chr1A	569447539	569448248	710
Traes7734	chr1A	554056493	554056951	459
Traes7741	chr1A	545762554	545763027	474
Traes7749	chr1A	530159727	530160267	541
Traes7999	chr1A	22559501	22559999	499
Traes8014	chr1A	2918909	2919478	570
Traes7281	chr1B	651560560	651560849	290
Traes7317	chr1B	579610565	579611457	893
Traes7337	chr1B	554587276	554587870	595
Traes7340	chr1B	554040113	554040334	222
Traes7341	chr1B	551768064	551768202	139
Traes7356	chr1B	548625019	548625538	520
Traes7358	chr1B	548622175	548622949	775
Traes7375	chr1B	520390543	520391143	601
Traes7400	chr1B	463562178	463562705	528
Traes7412	chr1B	443001657	443002448	792
Traes7414	chr1B	442105362	442105902	541
Traes7463	chr1B	354917092	354917599	508
Traes7468	chr1B	348904753	348905304	552
Traes7470	chr1B	348491087	348491544	458
Traes7471	chr1B	348419209	348419956	748
Traes7514	chr1B	290864647	290865002	356
Traes7583	chr1B	172420171	172421662	1492
Traes6995	chr1D	411399593	411400078	486
Traes6996	chr1D	411376945	411377620	676
Traes6998	chr1D	411116943	411117403	461
Traes7001	chr1D	408737411	408737881	471
Traes7005	chr1D	408238354	408239494	1141
Traes7010	chr1D	408200084	408200855	772
Traes7060	chr1D	327988653	327989224	572
Traes7063	chr1D	318942521	318944391	1871
Traes7068	chr1D	307419569	307419910	342
Traes7075	chr1D	276770067	276770414	348
Traes7142	chr1D	170649003	170649445	443
Traes7199	chr1D	52115089	52115635	547
Traes7202	chr1D	51728206	51728657	452

Traes7203	chr1D	51623637	51623853	217
Traes7231	chr1D	16279700	16280464	765
Traes6608	chr2A	750364846	750365390	545
Traes6624	chr2A	733634053	733634380	328
Traes6630	chr2A	724976647	724977255	609
Traes6664	chr2A	678897521	678898413	893
Traes6672	chr2A	668049693	668050623	931
Traes6697	chr2A	605000395	605001157	763
Traes6701	chr2A	595216138	595216674	537
Traes6744	chr2A	461977522	461979463	1942
Traes6771	chr2A	391109265	391109855	591
Traes6791	chr2A	343717743	343718645	903
Traes6817	chr2A	241114604	241115602	999
Traes6851	chr2A	164305814	164306259	446
Traes6908	chr2A	50047772	50048201	430
Traes6924	chr2A	30076270	30076454	185
Traes6137	chr2B	793490162	793490401	240
Traes6162	chr2B	757566665	757566898	234
Traes6228	chr2B	637463431	637464280	850
Traes6256	chr2B	571249400	571250028	629
Traes6267	chr2B	548661191	548661430	240
Traes6296	chr2B	474895794	474896104	311
Traes6316	chr2B	435684874	435685328	455
Traes6320	chr2B	422727638	422729414	1777
Traes6328	chr2B	413863560	413864376	817
Traes6408	chr2B	297452538	297454382	1845
Traes6439	chr2B	237159495	237159914	420
Traes6449	chr2B	214819099	214819272	174
Traes6452	chr2B	212115989	212116450	462
Traes6490	chr2B	153967827	153968394	568
Traes6513	chr2B	118320691	118321474	784
Traes6543	chr2B	73989454	73990048	595
Traes5778	chr2D	600086611	600087201	591
Traes5810	chr2D	540485313	540485495	183
Traes5898	chr2D	368794946	368795326	381
Traes5964	chr2D	253620120	253621997	1878
Traes6046	chr2D	114646031	114647112	1082
Traes6090	chr2D	46577107	46577676	570
Traes6110	chr2D	28411438	28411719	282
Traes6122	chr2D	6586596	6587167	572
Traes5382	chr3A	728996595	728997575	981
Traes5385	chr3A	727665455	727665845	391
Traes5386	chr3A	727646220	727646744	525
Traes5387	chr3A	727518631	727519148	518
Traes5391	chr3A	725149941	725150918	978
Traes5394	chr3A	711094256	711094693	438
Traes5398	chr3A	710783682	710784341	660

Traes5431	chr3A	632551147	632551684	538
Traes5433	chr3A	632547975	632549008	1034
Traes5436	chr3A	627924809	627925391	583
Traes5454	chr3A	601371743	601372031	289
Traes5456	chr3A	593313949	593314305	357
Traes5478	chr3A	546413105	546413578	474
Traes5502	chr3A	496223000	496223486	487
Traes5516	chr3A	451666616	451668641	2026
Traes5518	chr3A	444648703	444649171	469
Traes5522	chr3A	431128535	431128999	465
Traes5560	chr3A	359060897	359061610	714
Traes5664	chr3A	108908320	108908789	470
Traes5684	chr3A	66006944	66007088	145
Traes5729	chr3A	9466279	9466918	640
Traes4952	chr3B	810295733	810296148	416
Traes4961	chr3B	804542445	804543022	578
Traes4963	chr3B	802702538	802703263	726
Traes4987	chr3B	759169238	759169902	665
Traes5200	chr3B	304806136	304806573	438
Traes5288	chr3B	119418865	119419461	597
Traes5289	chr3B	119124083	119124727	645
Traes5338	chr3B	22383575	22384134	560
Traes5358	chr3B	5836992	5837595	604
Traes4545	chr3D	603576692	603577512	821
Traes4555	chr3D	598939749	598940772	1024
Traes4557	chr3D	597841545	597842287	743
Traes4558	chr3D	597785125	597785459	335
Traes4560	chr3D	597737104	597737748	645
Traes4566	chr3D	594643618	594643948	331
Traes4754	chr3D	274358502	274359124	623
Traes4765	chr3D	262898051	262898144	94
Traes4768	chr3D	260162923	260163125	203
Traes4832	chr3D	130945998	130946410	413
Traes4870	chr3D	74348552	74349319	768
Traes4923	chr3D	7600011	7600723	713
Traes4925	chr3D	6525175	6525811	637
Traes4932	chr3D	565330	565776	447
Traes4933	chr3D	554505	555083	579
Traes4239	chr4A	702064914	702065698	785
Traes4263	chr4A	670938749	670939279	531
Traes4283	chr4A	615112476	615112893	418
Traes4284	chr4A	615109291	615109990	700
Traes4300	chr4A	585641380	585642190	811
Traes4302	chr4A	585612259	585613283	1025
Traes4335	chr4A	531327096	531328351	1256
Traes4401	chr4A	362904003	362904223	221
Traes4417	chr4A	312727526	312728163	638

Traes4507	chr4A	67034519	67034825	307
Traes3854	chr4B	632402362	632402589	228
Traes3870	chr4B	610830775	610831234	460
Traes3880	chr4B	593347310	593347772	463
Traes4009	chr4B	357822548	357823240	693
Traes4039	chr4B	291663849	291665107	1259
Traes4065	chr4B	245682344	245682736	393
Traes4222	chr4B	11665566	11665829	264
Traes3526	chr4D	500272871	500273418	548
Traes3527	chr4D	500261394	500261895	502
Traes3531	chr4D	491805848	491806816	969
Traes3544	chr4D	471153332	471153861	530
Traes3551	chr4D	461564194	461564577	384
Traes3577	chr4D	423885160	423885508	349
Traes3651	chr4D	268604093	268604472	380
Traes3760	chr4D	91095595	91096019	425
Traes3779	chr4D	58643794	58643923	130
Traes3802	chr4D	20579294	20580468	1175
Traes3202	chr5A	706875113	706875350	238
Traes3218	chr5A	680863268	680864106	839
Traes3252	chr5A	620485808	620486173	366
Traes3294	chr5A	521678656	521679239	584
Traes3335	chr5A	437209713	437210296	584
Traes3377	chr5A	324479259	324480261	1003
Traes3500	chr5A	27518015	27518431	417
Traes3505	chr5A	12976635	12977215	581
Traes3515	chr5A	677094	677535	442
Traes2820	chr5B	686685674	686685829	156
Traes2873	chr5B	595468936	595469226	291
Traes2882	chr5B	573407273	573407810	538
Traes2890	chr5B	550259608	550260308	701
Traes2905	chr5B	521855027	521855661	635
Traes3086	chr5B	212205359	212205971	613
Traes3165	chr5B	58406784	58407927	1144
Traes3173	chr5B	49531223	49532187	965
Traes2482	chr5D	531202424	531202855	432
Traes2556	chr5D	407772873	407772953	81
Traes2573	chr5D	389934564	389935277	714
Traes2580	chr5D	376708309	376708779	471
Traes2608	chr5D	319680939	319681457	519
Traes2634	chr5D	290394039	290394619	581
Traes2697	chr5D	159888029	159888831	803
Traes2746	chr5D	55591529	55592521	993
Traes2753	chr5D	47856462	47857219	758
Traes2248	chr6A	457077858	457078466	609
Traes2278	chr6A	373109313	373110231	919
Traes2285	chr6A	359057802	359060412	2611

Traes2336	chr6A	225112885	225113327	443
Traes2355	chr6A	184815914	184816483	570
Traes2356	chr6A	184814378	184815495	1118
Traes2404	chr6A	106838625	106839504	880
Traes2430	chr6A	61735457	61735608	152
Traes1681	chr6B	715603344	715603786	443
Traes1696	chr6B	695294841	695298675	3835
Traes1700	chr6B	686168847	686169275	429
Traes1741	chr6B	637939468	637939974	507
Traes1752	chr6B	630531430	630531916	487
Traes1777	chr6B	565425353	565425789	437
Traes1827	chr6B	508196995	508197458	464
Traes1831	chr6B	504019975	504020639	665
Traes1881	chr6B	404457181	404459216	2036
Traes1986	chr6B	240543793	240544167	375
Traes2048	chr6B	144274869	144276425	1557
Traes1380	chr6D	471012858	471014052	1195
Traes1381	chr6D	471007944	471008809	866
Traes1382	chr6D	469363737	469364216	480
Traes1383	chr6D	469282177	469282776	600
Traes1386	chr6D	469057040	469057517	478
Traes1387	chr6D	468919835	468920293	459
Traes1412	chr6D	451758668	451759983	1316
Traes1419	chr6D	446002118	446002645	528
Traes1422	chr6D	445720267	445720927	661
Traes1428	chr6D	439913999	439914572	574
Traes1465	chr6D	380440184	380440829	646
Traes1469	chr6D	372816458	372817612	1155
Traes1613	chr6D	88782324	88783025	702
Traes1676	chr6D	752815	753335	521
Traes1087	chr7A	655412738	655413578	841
Traes1090	chr7A	647916524	647916947	424
Traes1099	chr7A	626254370	626254532	163
Traes1141	chr7A	538819130	538819488	359
Traes1143	chr7A	528927955	528928659	705
Traes1166	chr7A	458772836	458773322	487
Traes1205	chr7A	317129734	317130073	340
Traes1240	chr7A	241171525	241172101	577
Traes1256	chr7A	200608778	200610100	1323
Traes1259	chr7A	198409311	198409691	381
Traes1261	chr7A	198205874	198206371	498
Traes1367	chr7A	7831849	7832064	216
Traes1368	chr7A	5692661	5692920	260
Traes1000	chr7B	54222911	54224031	1121
Traes1023	chr7B	22513465	22514408	944
Traes565	chr7B	715479550	715482111	2562
Traes644	chr7B	614293685	614294053	369

Traes715	chr7B	482681815	482682353	539
Traes745	chr7B	413596059	413596644	586
Traes789	chr7B	361981023	361981605	583
Traes821	chr7B	329786246	329786940	695
Traes822	chr7B	329775609	329776185	577
Traes823	chr7B	329694435	329694936	502
Traes869	chr7B	255556192	255556559	368
Traes896	chr7B	223819392	223819774	383
Traes989	chr7B	68197053	68197435	383
Traes169	chr7D	619806572	619808038	1467
Traes174	chr7D	616106917	616107736	820
Traes190	chr7D	591873666	591874148	483
Traes269	chr7D	477409657	477410154	498
Traes371	chr7D	265055751	265056138	388
Traes418	chr7D	186798577	186799257	681
Traes420	chr7D	186509990	186510510	521
Traes452	chr7D	119102523	119103031	509
Traes454	chr7D	116984746	116985164	419
Traes457	chr7D	114483772	114484763	992
Traes473	chr7D	90042972	90043529	558
Traes482	chr7D	73856499	73856764	266
Traes510	chr7D	31566687	31567261	575
Traes512	chr7D	31474747	31475088	342
Traes513	chr7D	31471127	31471492	366
Traes543	chr7D	7187332	7187693	362
Traes130	chrUn	43540875	43541262	388
Traes18	chrUn	422630621	422631023	403
Traes20	chrUn	418283711	418284153	443
Traes21	chrUn	416394355	416394605	251
Traes23	chrUn	411778761	411778925	165
Traes7	chrUn	461463895	461464286	392

c) Altay2000

Novel transcript ID	Chr	Start	End	Length (bp)
Traes7771	chr1A	500076734	500077116	383
Traes7814	chr1A	404473513	404475015	1503
Traes7375	chr1B	520390543	520391143	601
Traes7420	chr1B	431455301	431456975	1675
Traes7583	chr1B	172420171	172421662	1492
Traes6965	chr1D	453269292	453269520	229
Traes7036	chr1D	376983098	376983428	331
Traes6643	chr2A	707040488	707040711	224
Traes6835	chr2A	197674206	197674566	361
Traes6858	chr2A	154135702	154136182	481
Traes6267	chr2B	548661191	548661430	240
Traes6323	chr2B	420610078	420610732	655

Traes6435	chr2B	243781924	243782315	392
Traes6442	chr2B	231630382	231630787	406
Traes6500	chr2B	143636256	143636727	472
Traes5791	chr2D	567569079	567569582	504
Traes5394	chr3A	711094256	711094693	438
Traes4545	chr3D	603576692	603577512	821
Traes4591	chr3D	564477494	564478994	1501
Traes4832	chr3D	130945998	130946410	413
Traes4935	chr3D	512682	513189	508
Traes4386	chr4A	407461604	407462020	417
Traes3966	chr4B	427028606	427029015	410
Traes4003	chr4B	368066287	368066871	585
Traes4199	chr4B	48910164	48910570	407
Traes3252	chr5A	620485808	620486173	366
Traes3085	chr5B	213322330	213323729	1400
Traes3173	chr5B	49531223	49532187	965
Traes2532	chr5D	445644997	445645637	641
Traes2634	chr5D	290394039	290394619	581
Traes2753	chr5D	47856462	47857219	758
Traes2175	chr6A	588597759	588598146	388
Traes2205	chr6A	553757049	553757390	342
Traes2232	chr6A	498540162	498541162	1001
Traes2237	chr6A	490997038	490997808	771
Traes2307	chr6A	305127623	305127971	349
Traes2352	chr6A	194722360	194722946	587
Traes2362	chr6A	169628325	169629338	1014
Traes2404	chr6A	106838625	106839504	880
Traes1831	chr6B	504019975	504020639	665
Traes1918	chr6B	356478519	356478899	381
Traes1493	chr6D	317122260	317122503	244
Traes1105	chr7A	621330133	621330647	515
Traes1106	chr7A	621325410	621325667	258
Traes1108	chr7A	621320416	621320963	548
Traes1232	chr7A	261583786	261584563	778
Traes1344	chr7A	36799119	36799564	446
Traes1011	chr7B	40659560	40660223	664
Traes667	chr7B	583115896	583116849	954
Traes715	chr7B	482681815	482682353	539
Traes745	chr7B	413596059	413596644	586
Traes750	chr7B	408954468	408954728	261
Traes833	chr7B	324639455	324639820	366
Traes897	chr7B	221272783	221273420	638
Traes966	chr7B	112123773	112124134	362
Traes348	chr7D	310507312	310507685	374
Traes383	chr7D	245335539	245335790	252

d) Bobur

Novel transcript ID	Chr	Start	End	Length (bp)
Traes7918	chr1A	171597573	171598137	565
Traes7323	chr1B	566038078	566040531	2454
Traes7396	chr1B	473527734	473529577	1844
Traes7199	chr1D	52115089	52115635	547
Traes6664	chr2A	678897521	678898413	893
Traes6670	chr2A	674001983	674002293	311
Traes6835	chr2A	197674206	197674566	361
Traes6170	chr2B	733858845	733859028	184
Traes6228	chr2B	637463431	637464280	850
Traes6355	chr2B	374236457	374237796	1340
Traes5509	chr3A	477795453	477796666	1214
Traes4952	chr3B	810295733	810296148	416
Traes5049	chr3B	606379558	606379993	436
Traes5234	chr3B	227845303	227845574	272
Traes5320	chr3B	60741588	60742120	533
Traes5353	chr3B	6216548	6217193	646
Traes5354	chr3B	6215744	6216216	473
Traes4545	chr3D	603576692	603577512	821
Traes4695	chr3D	395646358	395646874	517
Traes4832	chr3D	130945998	130946410	413
Traes4870	chr3D	74348552	74349319	768
Traes4925	chr3D	6525175	6525811	637
Traes4239	chr4A	702064914	702065698	785
Traes4252	chr4A	684076582	684077046	465
Traes3965	chr4B	427034911	427035401	491
Traes3966	chr4B	427028606	427029015	410
Traes3534	chr4D	488427310	488427553	244
Traes3252	chr5A	620485808	620486173	366
Traes3472	chr5A	65985622	65986151	530
Traes2805	chr5B	705123672	705124022	351
Traes2882	chr5B	573407273	573407810	538
Traes3080	chr5B	217627191	217627825	635
Traes3165	chr5B	58406784	58407927	1144
Traes3173	chr5B	49531223	49532187	965
Traes2494	chr5D	512907742	512908236	495
Traes2532	chr5D	445644997	445645637	641
Traes2634	chr5D	290394039	290394619	581
Traes2697	chr5D	159888029	159888831	803
Traes2746	chr5D	55591529	55592521	993
Traes2753	chr5D	47856462	47857219	758
Traes2346	chr6A	201359465	201359891	427
Traes1683	chr6B	713501014	713501216	203
Traes1810	chr6B	526859760	526860070	311
Traes1827	chr6B	508196995	508197458	464
Traes1831	chr6B	504019975	504020639	665

Traes1386	chr6D	469057040	469057517	478
Traes1644	chr6D	43192524	43193110	587
Traes1108	chr7A	621320416	621320963	548
Traes1139	chr7A	539451089	539451467	379
Traes1222	chr7A	291199812	291200241	430
Traes1261	chr7A	198205874	198206371	498
Traes586	chr7B	694920404	694921455	1052
Traes667	chr7B	583115896	583116849	954
Traes715	chr7B	482681815	482682353	539
Traes805	chr7B	352721310	352721832	523
Traes917	chr7B	194927795	194928300	506
Traes918	chr7B	194316615	194317236	622
Traes182	chr7D	603270743	603271163	421
Traes193	chr7D	584233016	584233479	464
Traes348	chr7D	310507312	310507685	374
Traes40	chrUn	346827214	346827904	691
Traes7	chrUn	461463895	461464286	392

Appendix 4. Clusters of expression profiles of Syn86 (red) and Zentos (green) with the number of genes indicated in each one. In each expression profile frame, the gray lines show the time course expression pattern of each gene and the red or green lines are LOESS (locally estimated scatterplot smoothing) curves that represents the expression tendency of the clusters of genes

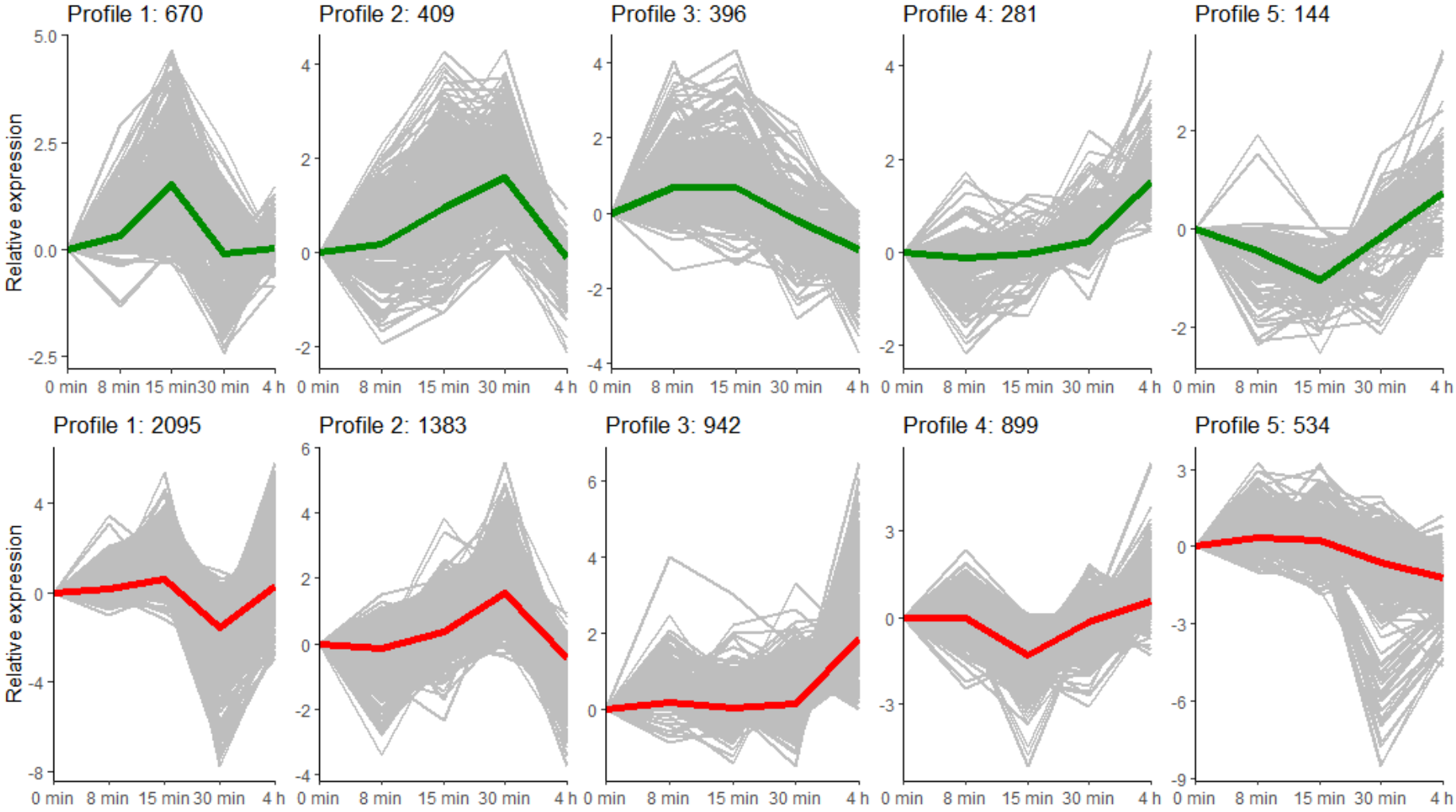

Appendix 5. GO terms over-represented in the gene clusters from Syn86 and Zentos.

a) **Zentos**

Profile 1

Category ID	Category Name	Genes Category	Genes Assigned	Corrected p-value
GO:0003700	transcription factor activity, sequence-specific DNA binding	492	33	0.00000025
GO:0006869	lipid transport	28	9	0.0000012
GO:0004672	protein kinase activity	1404	57	0.000027
GO:0006468	protein phosphorylation	1407	57	0.000029
GO:0009415	response to water	12	6	0.000033
GO:0005509	calcium ion binding	432	26	0.00017
GO:0006355	regulation of transcription, DNA-templated	881	39	0.00057

Profile 2

Category ID	Category Name	Genes Category	Genes Assigned	Corrected p-value
GO:0043565	sequence-specific DNA binding	318	39	1.5^{-25}
GO:0003700	transcription factor activity, sequence-specific DNA binding	492	46	2.7^{-25}
GO:0006355	regulation of transcription, DNA-templated	881	56	9^{-23}
GO:0016702	oxidoreductase activity, acting on single donors with incorporation of two atoms of oxygen	38	8	0.0000088
GO:0046872	metal ion binding	512	22	0.00011
GO:0004601	peroxidase activity	118	10	0.00097

Profile 3

Category ID	Category Name	Genes Category	Genes Assigned	Corrected p-value
GO:0048046	apoplast	33	14	1.8^{-16}
GO:0016762	xyloglucan:xyloglucosyl transferase activity	30	13	2.5^{-15}
GO:0006073	cellular glucan metabolic process	30	13	2.5^{-15}

GO:0004553	hydrolase activity, hydrolyzing O-glycosyl compounds	272	27	4.7^{-15}
GO:0005618	cell wall	34	13	1.9^{-14}
GO:0010411	xyloglucan metabolic process	26	10	9.6^{-11}
GO:0005975	carbohydrate metabolic process	491	28	1.4^{-9}
GO:0042546	cell wall biogenesis	34	10	2.2^{-9}
GO:0003700	transcription factor activity, sequence-specific DNA binding	492	23	0.0000067
GO:0003677	DNA binding	1152	34	0.00018
GO:0006355	regulation of transcription, DNA-templated	881	28	0.00055

Profile 4

Category ID	Category Name	Genes Category	Genes Assigned	Corrected p-value
GO:0050832	defense response to fungus	11	8	1.9^{-12}
GO:0042742	defense response to bacterium	11	8	1.9^{-12}
GO:0004332	fructose-bisphosphate aldolase activity	19	6	0.0000051
GO:0016998	cell wall macromolecule catabolic process	33	7	0.0000055
GO:0006032	chitin catabolic process	33	7	0.0000055
GO:0004568	chitinase activity	33	7	0.0000055
GO:0016705	oxidoreductase activity, acting on paired donors, with incorporation or reduction of molecular oxygen	251	14	0.000012
GO:0005975	carbohydrate metabolic process	491	19	0.000012
GO:0055114	oxidation-reduction process	1551	35	0.000016
GO:0020037	heme binding	386	16	0.000069
GO:0008061	chitin binding	18	5	0.00021
GO:0005506	iron ion binding	317	14	0.00022

Profile 5

Category ID	Category Name	Genes Category	Genes Assigned	Corrected p-value
GO:0005576	extracellular region	51	10	7.7^{-12}
GO:0004867	serine-type endopeptidase inhibitor activity	23	6	0.00000034

b) **Syn86**

Profile 1

Category ID	Category Name	Genes Category	Genes Assigned	Corrected p-value
GO:0015979	photosynthesis	136	82	5.5^{-62}
GO:0009523	photosystem II	81	44	1^{-29}
GO:0009522	photosystem I	33	27	4.4^{-25}
GO:0055114	oxidation-reduction process	1652	205	1.8^{-21}
GO:0009654	photosystem II oxygen evolving complex	64	31	1.7^{-18}
GO:0009538	photosystem I reaction center	16	15	5.3^{-15}
GO:0019898	extrinsic component of membrane	52	25	1.7^{-14}
GO:0006869	lipid transport	25	15	6.5^{-10}
GO:0048046	apoplast	39	17	0.000000018
GO:0016655	oxidoreductase activity, acting on NAD(P)H, quinone or similar compound as acceptor	12	10	0.00000003
GO:0016747	transferase activity, transferring acyl groups other than amino-acyl groups	154	33	0.000000087
GO:0015995	chlorophyll biosynthetic process	20	12	0.00000014
GO:0005975	carbohydrate metabolic process	513	69	0.00000016
GO:0016760	cellulose synthase (UDP-forming) activity	46	17	0.00000041
GO:0008152	metabolic process	1043	112	0.00000071
GO:0016702	oxidoreductase activity, acting on single donors with incorporation of two atoms of oxygen	48	17	0.00000088
GO:0016762	xyloglucan:xyloglucosyl transferase activity	37	15	0.00000095
GO:0006073	cellular glucan metabolic process	37	15	0.00000095
GO:0005840	ribosome	606	74	0.0000029
GO:0016491	oxidoreductase activity	957	103	0.000003
GO:0005618	cell wall	41	15	0.0000051
GO:0020037	heme binding	435	58	0.0000063
GO:0030244	cellulose biosynthetic process	56	17	0.000013
GO:0006412	translation	630	74	0.000015

GO:0010411	xyloglucan metabolic process	33	13	0.000019
GO:0005506	iron ion binding	374	50	0.000062
GO:0003735	structural constituent of ribosome	630	71	0.00015
GO:0008289	lipid binding	74	18	0.00021
GO:0008171	O-methyltransferase activity	35	12	0.0004
GO:0042546	cell wall biogenesis	42	13	0.00051
GO:0010333	terpene synthase activity	31	11	0.00083
GO:0016020	membrane	1269	117	0.001
GO:0015986	ATP synthesis coupled proton transport	45	13	0.001

Profile 2

Category ID	Category Name	Genes Category	Genes Assigned	Corrected p-value
GO:0003735	structural constituent of ribosome	630	170	1^{-90}
GO:0005840	ribosome	606	165	1.4^{-88}
GO:0006412	translation	630	166	1.1^{-86}
GO:0005622	intracellular	709	128	9.1^{-46}
GO:0016998	cell wall macromolecule catabolic process	38	19	2.6^{-14}
GO:0006032	chitin catabolic process	38	19	2.6^{-14}
GO:0004568	chitinase activity	38	19	2.6^{-14}
GO:0020037	heme binding	435	58	3.5^{-13}
GO:0015935	small ribosomal subunit	51	18	3.2^{-10}
GO:0003700	transcription factor activity, sequence-specific DNA binding	536	58	3.1^{-9}
GO:0015934	large ribosomal subunit	48	16	0.000000018
GO:0043565	sequence-specific DNA binding	346	43	0.000000024
GO:0006414	translational elongation	59	17	0.000000059
GO:0004672	protein kinase activity	1471	107	0.00000047
GO:0006468	protein phosphorylation	1473	107	0.00000051
GO:0008061	chitin binding	19	10	0.00000052
GO:0006979	response to oxidative stress	137	24	0.00000066
GO:0004867	serine-type endopeptidase inhibitor activity	44	14	0.00000067

GO:0009611	response to wounding	20	10	0.000001
GO:0004601	peroxidase activity	124	22	0.0000026
GO:0005975	carbohydrate metabolic process	513	50	0.0000035
GO:0016705	oxidoreductase activity, acting on single donors with incorporation of two atoms of oxygen	295	33	0.000065
GO:0003746	translation elongation factor activity	55	13	0.00014
GO:0010333	terpene synthase activity	31	10	0.00016
GO:0016758	transferase activity, transferring hexosyl groups	148	21	0.00032
GO:0004553	hydrolase activity, hydrolyzing O-glycosyl compounds	286	31	0.00033
GO:0006952	defense response	34	10	0.00043
GO:0048544	recognition of pollen	54	12	0.00088

Profile 3

Category ID	Category Name	Genes Category	Genes Assigned	Corrected p-value
GO:0008152	metabolic process	1043	78	2.7^{-13}
GO:0003824	catalytic activity	1463	91	5.8^{-11}
GO:0009415	response to water	19	9	0.00000046
GO:0004867	serine-type endopeptidase inhibitor activity	44	12	0.0000011
GO:0055114	oxidation-reduction process	1652	87	0.0000011
GO:0004350	glutamate-5-semialdehyde dehydrogenase activity	5	5	0.000013
GO:0016491	oxidoreductase activity	957	57	0.000016
GO:0043169	cation binding	97	15	0.000042
GO:0006950	response to stress	143	17	0.00028
GO:0030170	pyridoxal phosphate binding	141	16	0.001

Profile 4

Category ID	Category Name	Genes Category	Genes Assigned	Corrected p-value
GO:0055085	transmembrane transport	669	52	1.2^{-9}
GO:0004014	adenosylmethionine decarboxylase activity	5	5	0.00001

GO:0006597	spermine biosynthetic process	5	5	0.00001
GO:0006814	sodium ion transport	25	8	0.00012
GO:0008295	spermidine biosynthetic process	8	5	0.00054
GO:0006355	regulation of transcription, DNA-templated	919	49	0.001

Profile 5

Category ID	Category Name	Genes Category	Genes Assigned	Corrected p-value
GO:0045735	nutrient reservoir activity	35	17	2.8^{-19}
GO:0030145	manganese ion binding	46	17	9.4^{-17}
GO:0000786	nucleosome	121	17	4.2^{-9}
GO:0003700	transcription factor activity, sequence-specific DNA binding	536	31	0.00000024
GO:0003677	DNA binding	1139	47	0.0000006
GO:0006334	nucleosome assembly	64	11	0.0000029
GO:0006355	regulation of transcription, DNA-templated	919	36	0.00023

Appendix 6. Amplification efficiency estimations among target and reference genes by the estimation of the slope of linear regression models based on the ΔCt values and the cDNA input from serial dilutions. Bold values indicate the reference gene selected for each gene and tissue studied.

Gene	Efficiency (slope)	
	Ef1.1 **(leaves/roots)**	***Ef1.2*** **(leaves/roots)**
TraesCS2D02G173600	-0.104/**0.089**	**0.043**/0.113
TraesCS5D02G238700	**-0.043**/**-0.006**	-0.167/0.064

Appendix 7. Melting curves of some PCR products derived from the amplification of reference and target genes. Left column shows curves from leaves and right column from roots.

a) ***TraesCS2D02G173600***

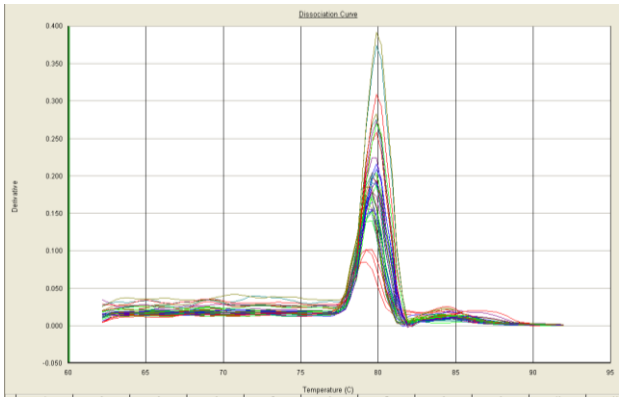

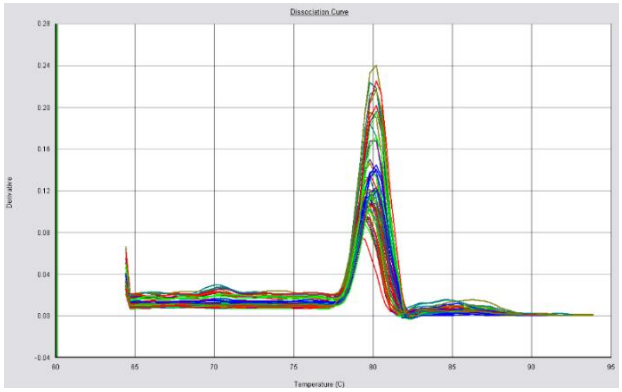

b) ***TraesCS5D02G238700***

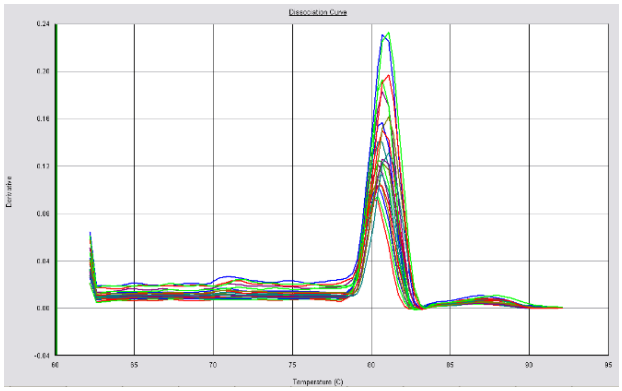

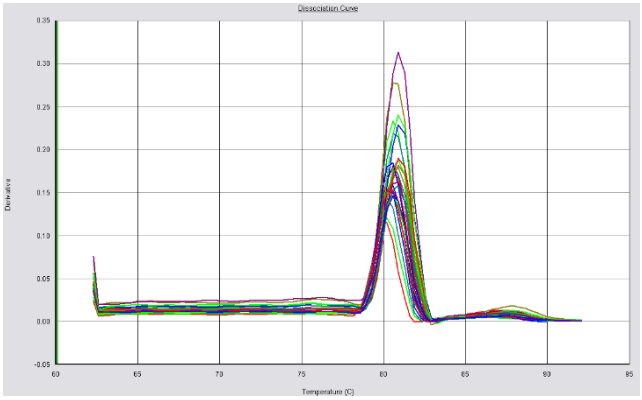

c) ***Ef1.1***

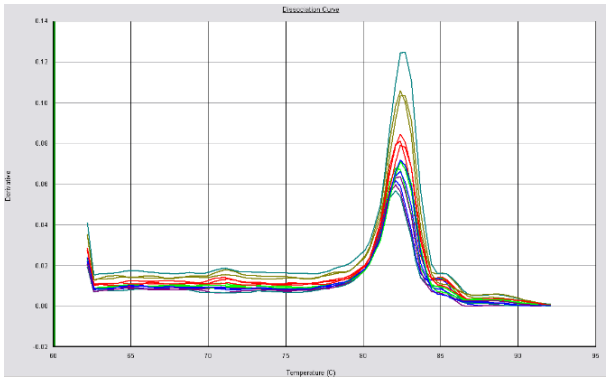

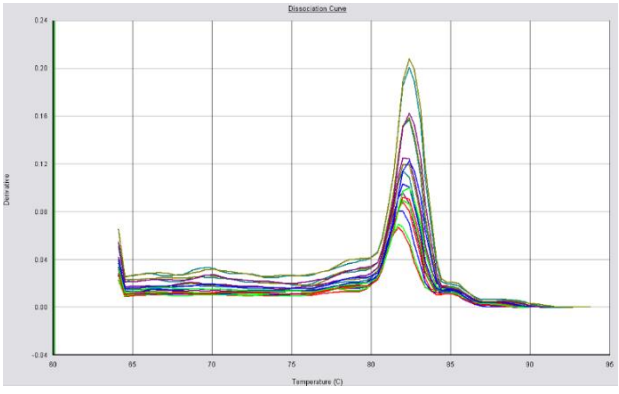

d) ***Ef1.2***

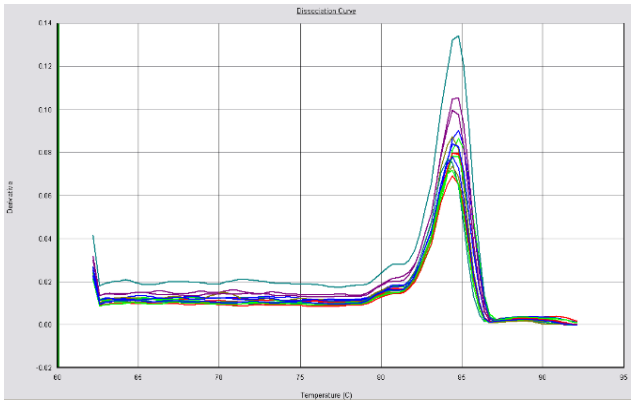
Dissociation Curve
Temperature (C)

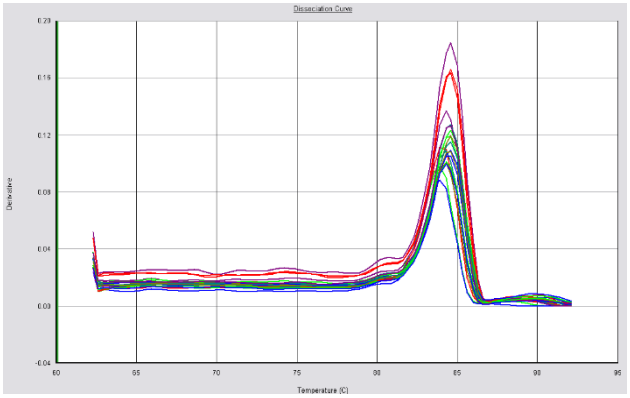
Dissociation Curve
Temperature (C)

Appendix 8. Comparison of GFOLD values and ΔΔCt values of studied genes

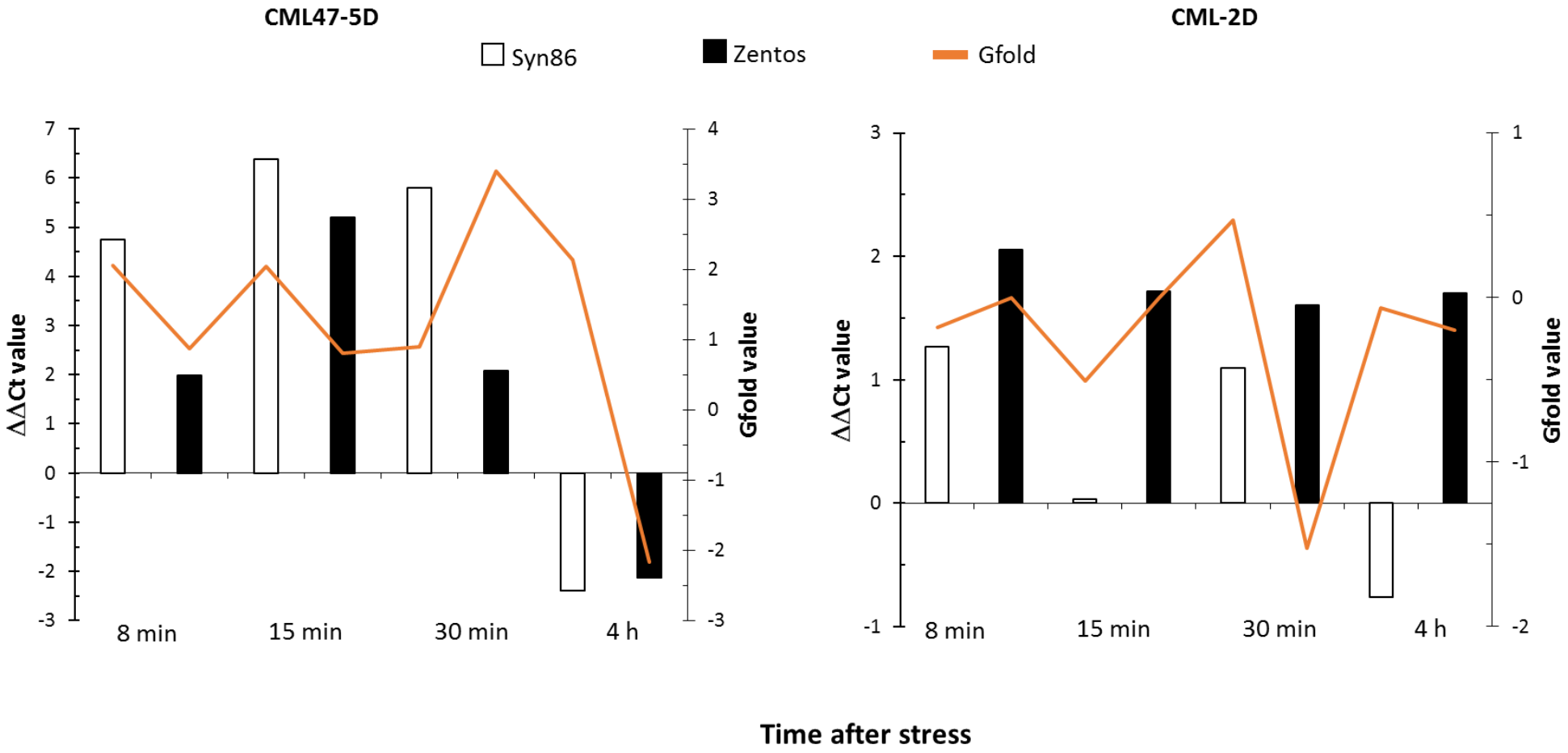

Appendix 9. Promotor sequences of the calcium-binding genes studied with the polymorphisms identified in the contrasting genotypes in bold letters. The start of the gene sequence is represented in italics.

a) Promotor *TraesCS2D02G173600*

chr2D:117219829..117222419

TGAGATGAAATAAAATTGGTGAATCCCGACAATGCTTGGGACTCATAAGTAATTTCCAATGGA
GCATAAATACTATGTTGTAAAAGGTCTACAAGGTCAATGTGACTCCAAAAGAAATATGTAAAG
GTGTAAAGCGCGACTTGAATCGAAAGATTTTGTGCAAAGAGAATGAACAAATTACAATGAGTG
TTAGTGTCACATCATGACCGACATCATGATCTGAGTTACATCAGATGAATGTAAAGAACACAAG
GGATACTGCTTCAAGAAATTTTTTATGGACTAGAGCAAGTCTCTAGATAGTTGCATTTAAAGTT
TAAAGAATCAGATGATATTTTGGGTTAAAGAAAATGGAAGGACAATTGTATTCATGCAAAGTT
ATAGAATGGGAAATTCATTTCCCAATCTTGTGCATGTGGATGACGTCCTACTTGCTAGTGGTGA
TGTCAATCTACTTCAGGAGGAGAAAAGAAGTTCTTGTCCTCAAAGTTCGAAATTGCATTTCTCA
GAGTGTCTCTCGTTATAAATATCGAGATTCATCAAGAAAAGAATAAAATAGGGTATTAGGAAT
GTCACATGGACATGCTAACAAAGGTCTCTAAAGTATGGATGCGAGAAAACCTACGCCTGTTCTT
ATAGTCAAGGGTAATGGAACTGGAAACTATGGTGTTCCAAAAGTTGATGAGAAAAGATTGAAA
ACGGATATGGTACCATATGCTTCAGCTGTTGGAAGCTCACTATATTACC**[C/T]**TGA**[CACAATT]**C
ACGTATCCGGGTTGTTTTGGCAATATCCAGTCCATATATAGATCACTGGAATGGAGTCAAAGAT
ATCGGCCTCGTGCTGAAAGAAATAAGTGCTCTCAAAAGATTGTGAGTACAAAGACAGGACTTG
TGAAATGTATAGCGAAATCCACAATTGTCGCTAACTTTCATACTTGGAGATTTTTGTGTGGAAA
AGCTCCAAAGAATGAAACAATTATCATCAATGTGATGCAAAGATATTTTATAGCTTGATATGAG
GCTGAGGGACAGGCAAAATGGTTAAGGAGACCTGTACCCGGAGTTAATAATGGTTGACAACAG
CGATAACCATTTTAAGTTGTTCGCTCCTATGACAACGAGTCAAGTGTTGATGCCAAACAAACTG
ACACAGAGTTATGCGTTGTAAAGGAGAAAGTCCGGAATTATGTAGAAATGCTTGAAGCATAAA
AGCAACAGACAAGTGTTTGCAGATCTGCTTATTAAAGGCTTACCGCCCAGTGTGTTCGGAGAAC
ACACAGTCGACATGGGTTTTATGGTATAGTCTAAGATTTCCGGACAATAAAAGGGCCCAAGGTT
AAAGAATTTGTTTCAAAACAGAAAGGTACGTTGTGGCTGTCTGATTCTATCGGCAATTGAGCTG
TGACGATGAAACATGTTCTATGTATTGATCTATTATGAAACGAGTAAAGTAAAAGTATAAGGTC
AAAAGTAAAAGTTGAGATCAAGGGGGAGAATGTTAGGATGATCTCCACCGTGTGGGCCCAACG
GCCCACCGGGCCCTTAGATCT**[A/G]**CGCCCTGATTGAGGGCGCGGTTGACGGGCCCCTGTCACC
TGCACTATATAAAGAGGTGGGGGCCGGCGGCTCGCATCACGAGGTTCGTCGCGACGCCGTACA
CCCCACCTACATCCCCTACCGATCTAGAGTTAGTGCAGTGCTGACGGGAAGCACCGCCACCGCT
ACTCTGCCATTACCGGCCACCGTCACCATGGCCGGCA**[T/C]**CGGGAGCTCCTCGAGCCACAAGA
AGAAGGTAATACCTACCACCACTGTTGCCGGAATCCTAGCCTAACCGATCCACAGAATCTATCA
CCTTCAACATCTTAGCCCAACTGTTAGCTCTGAATGAATGGATGCAGGCATGGTTAACCCTGCA
TATTTTCTCTGAGAAATGAAGTTGGTAACAAAACCATGGCAGAACCAAATCAAATAAGCGGTTT
GGCAGGTTGGCATTCTTGAGGGAAGAACTTTCAGCATTCTTGGGCAACTACGGTAGAATCTCGT
CCCTTTTTGTTCCCCTTTTGGATTGGTCTTTCAACGGAGAATCTCCTTCATCCAGGCCCTACCACT
TCCCCCACTAGGAATTTATCCCCACGCCTCGTTGCTGCAAGCAAGCATCGGAATATAATCTGGC
AGTAGTAGTAGTGGTACGAAAATAACCACACACCTACGCGGCTACACCAAACATCAGAAAAAA
TGCAGGCGATGCATGATTTATTAGGAAATGTCAGGCAAAGACTAAGAATCGAACAATGCGATA
AGTCTCTCGAGAAAGAAATCGCAACGTGATACACATAACCTTATTCGTCAGAGAATGTGACAC
GCACTTGCTGACTAGCGTGTAGATGCCTGAAAATTCAGCTCGCCCTCCACCAAGAAGAAGATA
AGATTCAGATCAGCGCCCCCTCGCAGCCTGCAGATGAAGACGAATAAAGCCACGAGATGCTGC
GCAGATCGGATCGACTATAAAAGGAGGCGCAGCCGCGAGAGGCCCTT*ACACCATCCATCACCTT*
AGCTAGCATAGCATCCCGTCTCTGCGTCCTGAGCTTGCGAACGCGGCCGGACAT

b) Promotor *TraesCS5D02G238700*

chr5D:346689406..346690887

TTTGTCTGTGCCTGTTTCCTCTGCTCTTGTTGCCTTGGTGCTTGCTTCTTGATCGTCTCTGAGATGAGA
*ATTGTCGCTGCGTGCTGGAT*GCTATTTGCCGAGCCCGAAGGCTCGGGATATATAGTCCCGGGTTG
CCTCGCGAGAAGGAGGGAAAGAAGTTGGAAGGGGGGACGGACGACGGCCGGGACTTGGGAAG
AAAGCCGGGAGCGAGGAAGGTTCCCGGAAGCAGGGAGGCCTGGTGGAAACGCCGGACCGACG
GAGCGGTCGCCGGTTCGTGCCTTGTGAGAGCGATGGAATTGTCGCGCGCGCGCGAGCGGGT
TTCGAGGGAGCTTCGCGGCGTGGAAACATGGGCGGGTCGACGTCGGTCGTCTCGTCACGGCGC
ACCGGCGACCCGACCGTATTCT**[C/T]**GGTTGGGGTTGGCGTTGGAATTCCACGCAGCCTCGCCTG
CTACTCTTTCCGTTGTCGGGTTCCTCCTGGTTGATTTTCCTTCTGCGACTGAATTTTGATTTGATT
TCGATAGATATATGTACGGTGGTGGACTGGCCGCACGGACCTGGTGGTATACGTGTTCAAGAA
AAATTAGACATCGTGTGTGTTTGTGTGTGACCTGGTGGTATACGGCCACTGGCGTGAAGGAAGG
TTGGTGAGTTGGCTAGCGAGCTCTTGACCCGATTTCGTGGTGGACTCGACCAAACCAAACCAAA
CCAAGCAGTGGTGTAGGTCTTCGCGCCAGCGGACGTGAGAGAATGCTTGATAATGCTTTTTTCC
CAGCAAATTTCCAATCTATTCATCTTCAATCATGATAATACCATGAATATAAAAAATAATAAAA
AATACATTCAGATTCATAAACCACCTAGTGACGACTATAAGCACTGAAGCATGCTGAAGGCGC**[**
G/A]CCGCCGTCATCGCCCCTCTGTTGCCGAAGTTGGGCACAACTTGTTAGTGAGAAAGTCGTCG
TGCTAAATCTCCATAAGACGAGCGCACCAGAGCAACAACCGCCGCTGATGAAAAAAAAACGTA
AATCGAAAGGATTCAACTTGAAGACACACGATCGTAGACGAACAACGACGAGATCCGAGCAA
ATCCATCAAAGATAGATTCGCCGGAGACACACCTCCACATGTCCATCAATGATGCTAGGCACAC
CGCCAGAACGGGCGCTAAACAGGAAAACCTTTATTTCATCTTCAGGGACCGCCGCCGTCTCGCT
TTAATGAGCAGGACATAAACCATAACAAAACCGAAAGGGACGACTAAAATCGGAGCTCTCCCG
CTAGCCCTTGCGAGGATCCACCACGCTCTCATGACCCTAGGCCCACTGAAGATGAGGCGGACCT
ACGACAACACCGATGAGAGACATGAACCCTAGCCTTTTTTAAGAAGGAGGCGGCTATACATGA
TCGTGCTTCCACCACCGTCCACTATGACTGA**[G]**GGTGTTTACACGCGACTAATGTGCTAATTAT
GTGTGCGAGCGGGTGCATATA

Appendix 10. SNPs identified in salt-responsive genes with calcium-binding domain. The reference allele is represented by 0 and the alternative allele by 1.

Gene	Position	Alternative allele	Syn86	Zentos	SNP location in gene	Salt responsive
TraesCS1A02G239600	426881024	T	0/0	1/1	UTR	Syn86
	426881030	A	1/1	0/0	UTR	
TraesCS1B02G251900	444688564	T	1/1	0/0	UTR	Syn86
TraesCS1B02G370900	600605115	A	1/1	0/0	UTR	Syn86
TraesCS2A02G215000	202042541	C	0/0	1/1	UTR	Syn86
TraesCS2A02G545600	754357893	A	1/1	0/0	UTR	Syn86
TraesCS2B02G113800	77170854	C	0/0	1/1	UTR	Syn86
	77170975	A	1/1	0/0	UTR	
	77170544	C	0/0	1/1	exon	
	77170646	T	0/0	1/1	exon	
TraesCS2B02G376700	539651338	G	0/0	1/1	UTR	Syn86
TraesCS2B02G576100	765069399	T	0/0	1/1	UTR	Syn86
	765069719	G	1/1	0/0	exon	
TraesCS3A02G335000	581276075	C	1/1	0/0	UTR	Syn86
TraesCS3A02G454900	692961935	G	1/1	0/0	UTR	Syn86
TraesCS3B02G362600	574267558	G	1/1	0/0	UTR	Syn86

	574267731	G	1/1	0/0	UTR	
TraesCS3D02G499700	589417216	C	1/1	0/0	UTR	Syn86
TraesCS4A02G310100	603038176	G	1/1	0/0	unpredicted UTR	Syn86
TraesCS4A02G310600	603372837	G	1/1	0/0	UTR	Syn86
	603372858	T	1/1	0/0	exon	
	603372757	T	1/1	0/0	UTR	
TraesCS4D02G003600	1415905	G	1/1	0/0	UTR	Syn86
TraesCS4D02G174400	302399810	C	1/1	0/0	intron	Syn86
TraesCS5A02G261200	475269281	T	1/1	0/0	exon	Syn86
TraesCS5A02G461500	641733968	A	1/1	0/0	UTR	Syn86
TraesCS5B02G063600	71521277	A	1/1	0/0	unpredicted UTR	Syn86
TraesCS5B02G247400	429093157	A	1/1	0/0	unpredicted UTR	Syn86
TraesCS5B02G462600	638124329	C	0/0	1/1	UTR	Syn86
	638124438	G	1/1	0/0	exon	
TraesCS5D02G474200	513978818	C	1/1	0/0	exon	Syn86
TraesCS6A02G101800	70573375	C	0/0	1/1	UTR	Syn86
	70573390	T	0/0	1/1	UTR	
TraesCS6B02G037600	22105419	A	1/1	0/0	unpredicted UTR	Syn86
	22105468	G	1/1	0/0	unpredicted UTR	
	22105558	G	1/1	0/0	unpredicted UTR	
TraesCS6B02G129800	126220744	A	0/0	1/1	exon	Syn86
	126220872	C	0/0	1/1	UTR	
TraesCS6B02G227900	354955972	G	1/1	0/0	intron	Syn86
TraesCS6D02G090400	56277741	A	1/1	0/0	UTR	Syn86
TraesCS7A02G245300	223472910	A	0/0	1/1	UTR	Syn86
	223472964	C	1/1	0/0	UTR	
TraesCS7A02G248600	230566681	T	1/1	0/0	exon	Syn86
TraesCS7A02G483700	675232270	C	1/1	0/0	exon	Syn86
	675232271	G	1/1	0/0	exon	
TraesCS3A02G038300	20589880	A	0/0	1/1	UTR	Zentos
	20589932	G	0/0	1/1	UTR	
	20590267	A	0/0	1/1	exon	
	20590404	G	0/0	1/1	exon	
	20590405	C	0/0	1/1	exon	
TraesCS2A02G166200	118488650	G	0/0	1/1	UTR	Zentos
	118488839	T	1/1	0/0	UTR	
TraesCS3D02G041400	15937155	T	1/1	0/0	UTR	Zentos
TraesCS5A02G426500	611567227	A	1/1	0/0	intron	Zentos
	611567555	A	1/1	0/0	exon	
TraesCS3D02G041500	15943904	T	1/1	0/0	UTR	Zentos
	15943959	C	1/1	0/0	UTR	
TraesCS5B02G428400	604067961	T	1/1	0/0	UTR	Zentos
	604067974	G	1/1	0/0	UTR	
	604068106	G	1/1	0/0	UTR	
	604068120	A	1/1	0/0	UTR	
	604068263	G	1/1	0/0	UTR	
TraesCS2B02G181800	156606159	C	1/1	0/0	UTR	Zentos

	156606173	G	1/1	0/0	UTR	
	156606246	G	1/1	0/0	UTR	
	156606294	C	1/1	0/0	UTR	
TraesCS7D02G439800	559393803	G	1/1	0/0	UTR	Both
TraesCS2A02G156400	103139824	T	0/0	1/1	UTR	Both
	103139852	A	0/0	1/1	UTR	
	103139965	G	0/0	1/1	UTR	
	103140100	C	0/0	1/1	exon	
TraesCS2B02G182000	157040899	A	1/1	0/0	UTR	Both
TraesCS4A02G123100	153779965	A	1/1	0/0	exon	Both
	153780078	G	1/1	0/0	UTR	
TraesCS4B02G121300	142928707	C	1/1	0/0	UTR	Both
TraesCS5A02G229000	444891521	T	0/0	1/1	exon	Both
	444891771	G	1/1	0/0	UTR	
TraesCS5B02G227700	404184046	C	0/0	1/1	exon	Both
	404184096	A	0/0	1/1	UTR	
TraesCS5B02G396400	573226206	T	1/1	0/0	UTR	Both
TraesCS7A02G450400	644104500	T	1/1	0/0	exon	Both
TraesCS7B02G350200	607529797	G	0/0	1/1	exon	Both